UNIVERSIDAD DE LA FRONTERA

Facultad de Ingeniería, Ciencias y Administración
Programa Doctorado y Magíster en Recursos Naturales

"CATALYTIC ACTIVITY OF IRON OR COPPER OXIDE-SUPPORTED ALLOPHANE NANOPARTICLES FOR PHENOL AND ATRAZINE OXIDATION BY FENTON-LIKE REACTION AND HETEROGENEOUS ELECTRO-FENTON PROCESS"

TESIS PARA OPTAR AL GRADO DE DOCTOR
EN CIENCIAS DE RECURSOS NATURALES

ELIZABETH GARRIDO RAMIREZ

TEMUCO-CHILE

2011

CATALYTIC ACTIVITY OF IRON OR COPPER OXIDE-SUPPORTED ALLOPHANE NANOPARTICLED FOR PHENOL AND ATRAZINE OXIDATION BY FENTON-LIKE REACTION AND HETEROGENEOUS ELECTRO-FENTON PROCESS

Esta tesis fue realizada bajo la supervisión de la Directora de Tesis, Dra. MARIA DE LA LUZ MORA GIL, Departamento de Ciencias Químicas, Universidad de La Frontera y por la Co-Directora de Tesis, Dra. MARIA SOLEDAD URETA ZAÑARTU, Departamento de Ciencias del Ambiente, Universidad de Santiago de Chile y ha sido aprobada por los miembros de la comisión examinadora

ELIZABETH GARRIDO RAMIREZ

- -

DIRECTOR PROGRAMA DE POSTGRADO EN CIENCIAS DE RECURSOS NATURALES

- -

DIRECCIÓN DE POSTGRADO UNIVERSIDAD DE LA FRONTERA

- -

Dra. MARIA DE LA LUZ MORA

- -

Dra. MARIA SOLEDAD URETA

- -

Dra. MARIA CRISTINA DIEZ

- -

Dra. GRACIELA PALMA

- -

Dr. GERARDO GALINDO

- -

Dr. PATRICIO REYES

Esta tesis esta dedicada a Dios
Porque cuando estuve afligida y necesitada…
Él pensó en mí

Agradecimientos / Acknowledgments

Agradezco a mi tutora, la Dra. María de La Luz Mora por permitirme desarrollar mi tema de tesis en su laboratorio, y por contribuir a mi formación científica mediante su preocupación por generar instancias que me han permitido establecer redes de cooperación con otros investigadores.

Agradezco a mi co-tutora, la Dra. María Soledad Ureta y a su grupo de trabajo (Cristhian Berrios, Francisco Fernández, Ricardo Salazar y Daniela Báez) por haberme recibido en su laboratorio, guiarme en mis primeros acercamientos en electroquímica y hacerme sentir parte de su grupo de trabajo.

My gratefully to Dr. Jöel Barrault and his research groups (Sabine Valande and M. Sivahia) for give me the opportunity to do a research stay in the laboratory “catalysis by oxide” of Poitiers University, France.

Agradezco a la Comisión Nacional Científica y Tecnológica (CONICYT) por la beca de doctorado D-21070269, beca de apoyo a la realización de tesis doctoral AT-24100139, beca de asistencia a congresos en Chile y beca de asistencia a congresos internacionales.

Agradezco al proyecto MECESUP FRO0601 por la beca de pasantía doctoral y a la Dirección de Postgrado de la Universidad de La Frontera por las ayudas económicas otorgadas para la asistencia a congresos internacionales.

Agradezco a mis padres (Eduardo y Ginette) y hermanas (Ximena y Jacqueline) por su continuo apoyo, por sus oraciones y por compartir conmigo las penas y alegrías que han conllevado el desarrollo de esta tesis.

Finalmente quiero agradecer a Gonzalo, mi esposo y eterno compañero, gracias por creer en mí, por apoyarme y animarme en los momentos difíciles, por darme soporte cuando el computador no respondía y sobre todo por la comprensión que has tenido durante las innumerables veces que te he dejado solo por sacar adelante mi tesis.

Abstract

Phenol and atrazine are recalcitrant organic pollutant considered harmful to human and aquatic life. Therefore, the developments of new technologies that allow their effective degradation are necessaries. In this context, the heterogeneous processes based on the Fenton reaction, such as, Fenton-like reaction and electro-Fenton process, are promissory for the degradation of a wide range of organic pollutant, including phenol-like compounds and atrazine. In the Fenton-like reaction solid catalysts containing iron or copper oxide are used as Fenton reagent for generate $^{\bullet}OH$ radical from the reaction with hydrogen peroxide. In electro-Fenton process, hydrogen peroxide is electro-generated by oxygen reduction in the cathode, while, the iron (Fe^{3+}/Fe^{2+}) or copper (Cu^{2+}/Cu^{+}) species are continuously electro-regenerated. The use of clays or iron minerals as solid catalyst in the heterogeneous Fenton processes is a promissory alternative due their abundance, low cost and friendly environmental nature. Allophane is a clay mineral found mainly in volcanic ash soils. Some properties such as, unique morphology in the nano-scale range, large surface area and high thermal stability make their use as iron or copper-oxide support suitable for be used as solid catalyst in heterogeneous Fenton process. The aim of this work is to study the catalytic properties of iron/or copper oxide-supported allophane nanoparticles with different SiO_2/Al_2O_3 ratio for phenol and atrazine oxidation by heterogeneous Fenton processes. Iron or copper oxide was deposited on synthetic allophane with SiO_2/Al_2O_3 of 1.0 (AlSi1) and 2.2 (AlSi2). The structural and surface properties of modified and unmodified allophane were determined by N_2 adsorption-desorption at 77 K, electrophoretic mobility measurements, infrared spectroscopy, transmission and scanning electronic microscopy, thermo-gravimetric analysis, and X-ray diffractometry. AlSi1 was similar to Al-rich soil allophane, while AlSi2 was typical of hydrous feldspathoid allophane. The catalytic activity of iron or copper-oxide supported

allophane was studied in the phenol oxidation by Fenton-like reaction. It was found that the catalytic activity of iron or copper-supported allophane was markedly influenced by their SiO_2/Al_2O_3 ratio and by their respective structure. The iron/or copper oxide deposited on AlSi2 catalyst with tail-like structure and high surface area was more active for phenol oxidation than its AlSi1 counterpart. Large differences in terms of catalytic efficiency (conversion rates) and stability were observed for the copper oxide-supported allophane counterparts, indicating that the iron oxide supported-allophanes with a hydrous feldspathoid structure are highly active and stable in the Fenton-like reaction.

Iron oxide-supported AlSi2 allophane was also used for to study the atrazine (ATZ) oxidation in a high concentration (46-92 μM) by Fenton-like reaction and heterogeneous electro-Fenton process. The effects of the initial pH, hydrogen peroxide concentration and amount of iron oxide-supported allophane deposited on electrode-based carbon were studied. Both processes were efficient for ATZ degradation under acidic conditions. However, it was possible to carry out the reaction at more neutral pH (pH ~6) achieving 68% ATZ oxidation in the Fenton-like reaction and 76% in the heterogeneous electro-Fenton process. Heterogeneous electro-Fenton process was more efficient than Fenton-like reaction; due to continuous electro-regeneration of iron species (Fe^{3+}/Fe^{2+}). ATZ degradation by heterogeneous electro-Fenton process occurs by dealkylation of ethylamino side chain for producing desethylatrazine (DEA) and desethyldeisopropyl atrazine (DEIA) as main degradation products. In this work, it is concluded that allophane nanoparticles with SiO_2/Al_2O_3 of 2.2 and similar structure of hydrous feldspathoid allophane are promissory materials for be used as transition metals (iron or copper oxide) support for organic pollutant degradation by heterogeneous Fenton processes.

Table of contents

Abstract **i**

Table of contents **iii**

Figure Index **vii**

Table Index **xi**

Chapter 1 - Introduction and Objectives

1.1. Introduction **1**

1.2. Hypotheses **4**

1.3. General objective **4**

1.4. Specific objectives **5**

1.5. References **6**

Chapter 2 - Theoretical background

Clays and oxide minerals as catalysts and nanocatalysts in Fenton-like reactions – A review

2.1. Abstract **11**

2.1. Introduction **12**

2.2.Heterogeneous solid catalysts **17**

2.3.1. Transition metal-exchanged zeolites **17**

2.3.2. Pillared interlayered clays **22**

2.3.3. Iron-oxide minerals **26**

2.3.4. Nanocatalysts **34**

2.4. Iron-oxide-coated allophane nanocatalysts in Fenton-like reactions **36**

2.5. Conclusions **42**

2.6. References **44**

Chapter 3

Catalytic oxidation of phenol by the Fenton-like reaction over iron or copper oxide-supported allophane clays materials: influence of catalyst SiO_2/Al_2O_3 ratio

3.1. Abstract **58**

3.2. Introduction **59**

3.3. Experimental **62**

3.3.1. Supports preparation **62**

3.3.2. Iron or copper oxide-supported allophane **63**

3.3.3. Characterization of the catalysts **64**

3.3.4. Catalytic oxidation of phenol **65**

3.4. Results and Discussion **66**

3.4.1. Characterization **66**

3.4.1.1. Allophane clays materials **66**

3.4.1.2. Iron or copper oxide-supported allophanes **75**

3.4.2. Catalytic activity **78**

3.4.2.1. Phenol oxidation over iron supported allophane **78**

3.4.2.2. Phenol oxidation over copper supported allophane **84**

3.5. Conclusion **89**

3.6. Acknowledgments **90**

3.7. References **91**

Chapter 4

Oxidation of a high Concentration of Atrazine by Fenton-like reaction and heterogeneous electro-Fenton process using an iron oxide-supported allophane

4.1. Abstract **96**

4.2. Introduction **97**

4.3. Materials and Methods **102**

4.3.1. Chemicals **102**

4.3.2. Catalyst preparation **103**

4.3.3. X-ray photoelectron spectroscopy **104**

4.3.4. Electrodes preparation **104**

4.3.5. Electrochemical characterization **105**

4.3.6. Fenton-like reaction and heterogeneous electro-Fenton process **105**

4.3.7. Analytical methods **106**

4.4. Results and discussion **108**

4.4.1. X-ray photoelectron spectroscopy **108**

4.4.2. Atrazine degradation by Fenton-like reaction **111**

4.4.3. Voltametric behaviour of carbon paste electrode modified with AlSi2Fe6 **115**

4.4.4. ATZ oxidation by heterogeneous electro-Fenton reaction: bulk electrolysis **122**

4.4.5. Atrazine degradation products **126**

4.5. Conclusions **131**

4.6. Acknowledges **131**

4.7. References **132**

Chapter 5

General discussion and conclusions

5.1. General discussions **136**

5.2. General conclusions **139**

5.3. References **141**

Chapter 6 Appendix

6.1. List of original papers of this thesis **142**

6.2. List of papers in collaboration **142**

Figure Index

2.1. ^{57}Fe Mösbauer spectrum (at 300K) of synthetic allophane coated with iron oxide (adapted from Mora et al., 1994) **39**

2.2. Transmission electron micrographs of synthetic allophane, Top (a): adapted from Mora et al., (1994); bottom (b): unpublished data **40**

3.1. Structure of hydrous feldspathoid-like AlSi2 allophane (a) and Al-rich imogolite-like SiAl1 allophane (b). **69**

3.2. Proposed aggregation state for AlSi1 allophane (a) and AlSi2 allophane (b), induced by heating **70**

3.3. Scanning electron micrographs of the parent AlSi1 (a) and AlSi2 (b) allophane materials. **70**

3.4. Transmission electron micrographs of the synthesized parent AlSi1 (a) and AlSi2 (b) allophane materials. **71**

3.5. X-ray diffraction patterns of the parent AlSi1 and AlSi2 allophanes and of the corresponding AlSi2 samples impregnated with iron or copper oxide. **72**

3.6. Thermogravimetry curves (a) and differential thermal analysis curves (b) for AlSi1 and AlSi2 allophane samples before and after impregnated with iron or copper oxide. **73**

3.7. Fourier-transform infrared (FTIR) spectra for the synthesized parent AlSi1 and AlSi2 allophane samples and for their corresponding iron/copper oxide-supported and calcined (at 300°C) counterparts. **75**

3.8. Phenol oxidation (a) and total organic carbon (TOC) decay (b) over 4 h of reaction catalysed by AlSi1 and AlSi2 allophane samples before and after **79**

impregnated with iron oxide: AlSi1 (●); AlSi2 (Δ); AlSi1Fe6 (▲); AlSi2Fe2 (□); AlSi2Fe6 (■); and $AlSi2Fe6_{(T300)}$ (✯).

3.9. Surface area, mineralization efficiency (TOC/Phenol) and iron oxide content (% wt. Fe_2O_3) for parental AlSi1 and AlSi2 allophane samples and for their corresponding iron/copper oxide-supported and calcined (at 300ºC) counterparts. **82**

3.10 Influence of the reaction temperature on the phenol oxidation and TOC decay rates for $AlSi2Fe6_{(T300)}$ allophane catalyst at pH = 3.7: Phenol/25 ºC (□); TOC/25 ºC (○); Phenol/40 ºC (■); TOC/40 ºC (●). **84**

3.11 Phenol and TOC decay after 8 h of reaction over copper oxide-supported AlSi2 allophane catalyst before and after calcination at 300 ^{o}C: Phenol, AlSi2Cu6 (Δ); TOC, AlSi2Cu6 (○); Phenol, $AlSi2Cu6_{(T300)}$ (▲); TOC, $AlSi2Cu6_{(T300)}$ (●). **86**

3.12 Influence of the reaction temperature on the phenol oxidation and TOC decay rates for AlSi2Cu6 allophane catalyst at pH = 5.0: Phenol/25 ºC (Δ); TOC/25 ºC (○); Phenol/40 ºC (▲); TOC/40 ºC (●) **89**

4.1. Chemical structure of atrazine (2-chloro-4-ethylamino-6-isopropylamine-1,3,5-triazine) **97**

4.2. XP spectrum of iron oxide-supported allophane. Inset. XPS data obtained from the fit of the Fe 2p spectra **108**

4.3. Rate of ATZ oxidation at different initial pHs and hydrogen peroxide concentrations by Fenton-like reaction: (a) $[H_2O_2]$ = 0.2 M; (b) $[H_2O_2]$ = 0.3 M. Symbols: adsorption at pH 3 (○); Fenton-like reaction at: pH = 3(▲); pH = 4 (■); pH = 6 (●). For all experiments $[ATZ]_0$ = 92 μM, 25ºC. Straight **112**

lines corresponding to a linear regression

4.4. Cyclic voltammograms at 0.1 V s^{-1} of CPE (solid line) and AlSi2Fe6-CPE (dash line). Voltamogramms recorded in [Na_2SO_4] = 0.5 M and initial pH ~3 **117**

4.5. (a) Cyclic voltammograms of AlSi2Fe6-CPE at different scan rate (01-0.35 V s^{-1}). [Na_2SO_4] = 0.5 M, pH 3.0; (b) I_{1c} *vs*. $\nu^{1/2}$ plot; (c) normalized current ($Ip/\nu^{1/2}$) *vs*. scan rate for peak 1C; (d) Dependence of peak potential Ep with potential scan rate(ν) for peak 1C. **119**

4.6. Cyclic voltamogramms at 0.1 V s^{-1} for AlSi2Fe6-CPE under N_2 saturated solution, using 0.5 M Na_2SO_4 as support electrolyte adjusted at pH 3.0. CV performed in presence (dashed line) and absence (solid line) of ATZ (96 μM) **120**

4.7. Cyclic voltammetry at 0.3 V s^{-1} for AlSi2Fe6-CPE in O_2 saturated 0.5 M Na_2SO_4 at pH 3.0, in the presence (dashed line) and the absence (solid line) of ATZ (96 μM). **122**

4.8. Rate of ATZ oxidation by heterogeneous electro-Fenton process using different AlSi2Fe6 / graphite ratios deposited on GC electrode: blank GC (○); AlSi2Fe6 / graphite ratio= 0.2 (■);AlSi2F6 /graphite ratio= 0.6 (□);AlSi2Fe6 /graphite ratio =1.0 (Δ). $[ATZ]_0$ = 46 μM, room temperature, oxygen saturated solution, E= -1.04 V. Straight lines corresponding to a linear regression and were adjusted after the induction time **123**

4.9. Rate ATZ oxidation by heterogeneous electro-Fenton process using 0.6 AlSi2Fe6 / graphite rate deposited on GC electrode, at different initial pH: pH ~ 6 (○); pH ~ 4 (▲); pH ~3 (★). For all experiments, [ATZ] = 46 μM; room temperature; oxygen solution saturated; -1.04 V. Straight lines corresponding to a linear regression, adjusted after induction time **126**

4.10. Mineralization pathway for ATZ degradation by •OH generated by electro-Fenton reaction (Modified from Balci et al., 2009), Black arrows indicate the ATZ degradation by heterogeneous electro-Fenton process using AlSi2Fe6-MGC electrodes **129**

4.11. Concentration of atrazine and its aromatic intermediates detected during the heterogeneous electro-Fenton process: ATZ (•); DEA (■); DEIA (▲) ($[ATZ]_0$ = 46 μM; AlSi2Fe6-GC electrode with AlSi2Fe6/graphite rate of 0.3 at pH 3.0) **130**

Table Index

2.1.	Catalytic degradation of organic compounds over iron- or copper-exchanged zeolites through different Fenton-like processes	**19**
2.2.	Pillared interlayered clays (PILC) as heterogeneous catalysts for the decomposition of various organic compounds via Fenton-like reactions	**24**
2.3.	Oxidation of various organic compounds by iron-oxide minerals through Fenton-like processes	**28**
2.4.	Mechanisms proposed for the oxidation of organic compounds on the surface or iron-oxide catalysts through a Fenton-like reaction	**29**
2.5.	Nanocatalysts used in the degradation of various organic compounds	**35**
3.1.	Chemical composition, textural properties and isoelectric point value of the parent synthesized allophanes and of their corresponding iron or copper oxide-supported counterparts, before or after thermal treatment.	**67**
3.2.	Structural formula of the synthesized parent allophanes (AlSi1 and AlSi2) determined from chemical composition and thermogravimetric analysis	**73**
3.3.	Phenol conversion, total organic carbon (TOC) decay, mineralization efficiency and Fe leaching for the synthesized parent and iron oxide-supported AlSi2 allophane samples, as well as for their corresponding calcined counterparts.	**80**
3.4.	Phenol conversion, total organic carbon (TOC) decay, mineralization efficiency and Cu leaching for the synthesized parent AlSi2 allophane sample impregnated with copper oxide and their corresponding calcined counterparts.	**87**
4.1.	Atrazine physicochemical properties	**98**

4.2. Chemical composition and textural/charge properties of iron oxide-supported allophane (Garrido-Ramírez et al., 2011 submitted). **103**

4.3. XPS data obtained from the fit of the Fe 2p spectra of iron oxide-supported allophane **110**

4.4. ATZ conversion and Fe leaching for iron oxide-supported allophane (AlSi2Fe6) at different hydrogen peroxide concentrations and pHs **113**

4.5. Apparent rate constant (k10) and regression coefficient for ATZ oxidation by Fenton-like reaction at different hydrogen peroxide concentrations and pHs **113**

4.6. Apparent rate constant (k) and regression coefficient for ATZ oxidation using different AlSi2Fe6/graphite ratio deposited on GC electrode by heterogeneous electro-Fenton process **124**

1

Introduction and objectives

1.1. Introduction

Numerous wastewater streams containing recalcitrant organic pollutants are continuously generated by many industrial processes, and agricultural and domestic activities. Among organic pollutants, phenol and atrazine are considered dangerous to human and aquatic organisms (USEPA 2000; Bankovic et al., 2010; Lin et al., 2002). Phenol and its derivates have been widely used as raw material in many chemical, pharmaceutical, petrochemical or chemical industries (Lin et al., 2002). Atrazine is a selective herbicide used worldwide for controlling broadleaf and grassy weeds in corn and forestry plantations. Conventional wastewater treatments (biological or physicochemical) are not able to degrade phenol-like compounds or atrazine, which are bio-resistant pollutants (Botas et al., 2010; Lin et al 2002). It is common that the treatment consists only of separation processes without achieving a complete mineralization Therefore, it is necessary to develop new technologies that allow the efficient degradation of recalcitrant organic pollutants in a friendly way.

Advanced oxidation processes (AOP) have been widely studied for the degradation of many recalcitrant organic compounds (Badawi et al., 2006; Gültekin and Ince 2007; Klavarioti et al., 2009). AOP are based on the generation of $^{\bullet}OH$ radicals, which are highly reactive species (E^0 = 2.8 V versus normal hydrogen electrode (NHE), Siedlecka et al., 2007), that can oxidize most organic substances rapidly (Zeep et al., 1992). Some examples include $^{\bullet}OH$ production by O_3/UV, H_2O_2/UV, TiO_2/O_3, H_2O_2/O_3 and those based on the Fenton reaction (Pérez-Estrada et al., 2007; Propiel et al., 2008; Primo et al., 2008a).

In the Fenton reaction the generation of $^{\bullet}OH$ radicals is due to the reaction of hydrogen peroxide and ferrous salts under strong acid conditions (pH ~ 3.0). Beside iron salts, other transition

metals, such as copper, cerium, and manganese can also promote the generation of $^{\bullet}OH$ radicals from hydrogen peroxide (Barrault et al., 2000b; Carriazo et al., 2005a,b; Aravindham et al., 2006). Fenton reaction has been effective in the degradation of a wide variety of organic pollutants (Tekin et al., 2006; Núñez et al., 2007; Ay and Kargi, 2010), including, phenol-like compounds (Kang et al., 2002; Zimbron and Reardon 2009) and atrazine (Arnolds et al., 1995; Gallard and De Laat, 2000; Chan and Chu, 2005). Fenton reaction is a simple process that can be carried out under ambient conditions of temperature and pressure, and does not required especially equipment. The main drawback of this process is the acid medium necessary for avoid the Fe(III) oxy-hydroxide precipitation at higher pH (Sum et al., 2005; Martínez et al., 2007; Bobu et al., 2008). In addition, high concentrations of iron soluble and hydrogen peroxide usually are required in the homogeneous Fenton process (Navalon et al., 2010). For overcome these drawbacks, some modifications at the homogeneous Fenton reaction have been proposed, such as, the heterogeneous Fenton reaction (Barrault et al., 2000a,b; Barreiro et al., 2007; Hanna et al., 2008; Navalon et al., 2010) and the electro-Fenton process (Ventura et al., 2002; Balci et al., 2009).

In the heterogeneous Fenton reaction (Fenton-like reaction) solid catalyst are used as Fenton reagent. In these catalysts it is possible to perform the reaction in a wide pH range, as iron or copper species are “inmobilized” on the surface of the catalyst avoiding their precipitation. Therefore, in the Fenton-like reaction negligible iron dissolution is expected. Some solid catalysts that have been studied include: copper or iron interchanged zeolites (Centi et al., 2000; Noorjahan et al., 2005; Chen et al., 2008), pillared interlayered clays (Barrault et al., 2000a,b; Catrinescu et al., 2003; Carriazo et al., 2005a,b; Sanabria et al., 2008) and iron oxide minerals (Huang et al., 2001; Baldrian et al., 2006; Barreiro et al., 2007; Hanna et al., 2008).

The electro-Fenton process (EF) is based on the electro-generation of hydrogen peroxide by oxygen reduction on the cathode and/or electro-regeneration of iron species (Fe(II)/Fe(III)). The iron species can be used as iron soluble (Ventura et al., 2002) or as solid catalyst (heterogeneous electro-Fenton process). The solid catalyst can be added into the solution (Sanchez-Sanchez et al., 2007) or incorporated on the electrode (Balci et al., 2009).

The use of clays or iron minerals as solid catalyst in the heterogeneous Fenton processes (Fenton-like reaction and electro-Fenton process) is a promissory alternative due to their abundance, low cost and friendly environment nature. In addition, catalysts in the nano-cale range can accelerate the Fenton-like reaction due to its large surface area, in which, the catalytically active sites are exposed and are more accessible to the substrate molecule (Valdes-Solis et al., 2007a,b).

Allophane is clay mineral found mainly in volcanic ash soils. The unit particle of allophane is a hollow spherule in the nano-scale range (Wada and Wada 1977; Calaby-Floody et al., 2009; 2011). Different structures of allophane have been reported according to SiO_2/Al_2O_3 ratio (Parffit 2009). In Chilean soils (Andisols) allophane to be in association with iron oxide, mainly ferrhydrite-like materials, which are found as coating of allophane particles (Escudey and Galindo 1983; Mora et al., 1994). This natural association together some properties, such as, unique morphology, large surface and high thermal stability make the use of iron or copper oxide-supported allophane nanoparticles suitable as heterogeneous catalyst in the heterogeneous Fenton processes. The properties of iron oxide supported allophane have widely been studied (Mora et al 1994; Mora and Canales 1995; Violante et al., 1996; Jara et al., 2005) showing that the coating of allophane with iron oxide increases the acidity of the active surface sites, because iron atoms are bounded to Si-O structure of allophane nanoparticles. However, the determination of properties of copper oxide-supported allophane remains unexplored.

Iron oxide-supported allophane has been used as adsorbent of organic pollutant (Diez et al 1999; Espinoza et al 2009), as modifying agent of glassy carbon electrode in chlorophenol electro-oxidation (Ureta-Zañartu et al., 2002) and as enzymatic support (Menezes-Blackburn *et* al., 2011). However, the catalytic properties of iron/or copper-oxide supported allophane for heterogeneous Fenton processes have not been reported.

The aim of this work is to study the catalytic properties of iron/or copper oxide-supported allophane nanoparticles with different SiO_2/Al_2O_3 ratio for phenol and atrazine oxidation by Fenton-like reaction and electro-Fenton process.

1.2 Hypothesis

Iron or copper oxide-supported allophane nanoparticles can be used as solid catalyst for phenol and atrazine oxidation by Fenton-like reaction and heterogeneous electro-Fenton process.

1.3. General Objective

To study the catalytic properties of iron/or copper oxide-supported allophane nanoparticles with different SiO_2/Al_2O_3 ratio for phenol and atrazine oxidation by Fenton-like reaction and heterogeneous electro-Fenton process.

1.4. Specific Objectives

1. To study the structural, chemical and physicochemical properties of synthetic allophane nanoparticles with different SiO_2/Al_2O_3 ratio before and after coating with iron or copper-oxide.
2. To study the catalytic activity of iron or copper oxide-supported allophane nanoparticles with different SiO_2/Al_2O_3 for phenol oxidation by Fenton-like reaction.

3. To study the atrazine oxidation by Fenton-like reaction and heterogeneous electro-Fenton process using an iron oxide-supported on allophane nanoparticles.

1.5. References

Aravindhan R., Fathima N.N., Rao, J.R.; Nair, B.U., 2006. Wet oxidation of acid brown dye by hydrogen peroxide using heterogeneous catalyst Mn-salen-Y zeolite: A potential catalyst. J. Hazard. Mater. 138, 152–159.

Arnold, S.M., Hickey, W.J., Harris, R.F., 1995. Degradation of atrazine by Fenton`s reagent: condition optimization and product quantification. Environ. Sci. Technol. 29, 2083–2089.

Ay, F., Kargi, F. 2010. Advanced oxidation of amoxicillin by Fenton´s reagent treatment. . J. Hazard. Mater. 179 (1-3), 622-627.

Badawy, M.I., Ghaly, M.Y., Gad-Allah, T.A. 2006. Advanced oxidation processes for the removal of organophosphorus pesticides from wastewater. Desalination. 194 (1-3), 166-175.

Balci, B., Oturan, N., Cherrier, R., Oturan, M. 2009. Degradation of atrazine in aqueous medium by electrocatalytically generated hydroxyl radicals. A kinetic and mechanistic study. Water Res.. 43, 1924-1934.

Baldrian, P., Merhautová, V., Gabriel, J., Nerud, F., Stopka, P., Hrubý,M., Benes, M.J., 2006. Decolorization of synthetic dyes by hydrogen peroxide with heterogeneous catalysis by mixed iron oxides. Appl. Catal. B: Environ. 66, 258–264.

Banković, P., Mojović, Z., Milutinović-Nikolić, N., Marinović, S., Jovanović, D. 2010. Mixed pillared bentonite for electrooxidation of phenol. Appl. Clay Sci. 49, 84-89.

Barrault, J., Abdellaoui, M., Bouchoule, C., Majesté, A., Tatibouët, J.M., Louloudi, A., Papayannakos, N., Gangas, N.H. 2000a. Catalytic wet peroxide oxidation over mixed (Al-Fe) pillared clays. Appl. Catal. B: Environ. 27, 225−230.

Barrault, J., Tatibouët, J.M., Papayannakos, N. 2000b. Catalytic wet peroxide oxidation of phenol over pillared clays containing iron or copper species. C.R. Acad. Sci. Paris, Sér. II C, Chem. 3, 777–783.

Barreiro, C., Capelato, M.D., Martin-Neto, L., Bruun Hansen, H. 2007. Oxidative decomposition of atrazine by a Fenton-like reaction in a H_2O_2/ferrihydrite system. Water Res. 41, 55-62.

Bobu, M., Yediler, A., Siminiceanu, I., Schulte-Hostede, S., 2008. Degradation studies of ciprofloxacin on a pillared iron catalyst. Appl. Catal. B: Environ. 83, 15–23.

Botas, J.A., Melero, J.A., Martínez, F., Pariente, M.I. 2010. Assessment of Fe2O3/SiO2 catalysts for the continuous treatment of phenol aqueous solutions in a fixed bed reactor. Catal. Today.149, 334-340.

Calabi-Floody, M., Theng, B.K.G., Reyes, P., Mora, M.L. 2009. Natural nanoclays: applications and future trends – a Chilean perspective. Clay Miner. 44, 161–176.

Calabi-Floody, M., Bendall, J.S., Jara, A.A., Welland, M.E., Theng, B.K.G., Rumpel, C., Mora, M.L. 2011. Nanoclays from an Andisol: extraction, properties and carbon stabilization. Geoderma 16, 159–167. Carriazo, J., Guelou, E., Barrault, J., Tatibouët, J.M., Moreno, S. 2003. Catalytic wet peroxide oxidation of phenol over Al–Cu or Al–Fe modified clays. Appl. Clay Sci. 22, 303–308.

Carriazo, J., Guélou, E., Barrault, J., Tatibouët, J.M., Molina, R., Moreno, S. 2005a. Synthesis of pillared clays containing Al, Al–Fe or Al–Ce–Fe from a bentonite: characterization and catalytic activity. Catal. Today. 107–108, 126–132.

Carriazo, J., Guélou, E., Barrault, J., Tatibouët, J.M., Molina, R., Moreno, S. 2005b. Catalytic wet peroxide oxidation of phenol by pillared clays containing Al–Ce–Fe. Water Res. 39, 3891–3899.

Centi, G., Perathoner, S., Torre, T., Verduna, M.G., 2000. Catalytic wet oxidation with H_2O_2 of carboxylic acids on homogeneous and heterogeneous Fenton-type catalysts. Catal. Today 55, 61–69.

Chan, K.H., Chu, W., 2005. Model applications and mechanism study on the degradation of atrazine by Fenton's system. J. Hazard. Mater. 118, 227–237.

Chen, A., Ma, X., Sun, H., 2008. Decolorization of KN-R catalyzed by Fe-containing Y and ZSM-5 zeolites. J. Hazard. Mater. 156, 568–575.

Diez, M.C., Mora, M.L., Videla, S. 1999. Adsorption of phenolic compounds and color from bleached kraft mill effluent using allophanic compounds. Water Res. 33, 125–130.

Escudey, M., Galindo, G. 1983. Effect of iron oxide coatings on electrophoretic mobility and dispersion of allophane. J. Colloid Interface Sci. 93, 78−83.

Espinoza, J., Fuentes, E., Baéz, M. 2009. Sorption behaviour of bensulfuron-methyl on andisols and ultisols volcanic ash derived soils: Contribution of humic fractions and mineral–organic complexes. Environ. Pollut. 157, 3387−3395.

Gallard, H., De Laat, J., 2000. Kinetic modelling of Fe(III)/H_2O_2 oxidation reactions in dilute aqueous solution using atrazine as a model organic compound. Water Res. 34, 3107–3116.

Gültekin, I., Ince, N.H. 2007. Synthetic endocrine disruptors in the environment and water remediation by advanced oxidation processes. J. Environ. Manage. 85 (4), 816-832.

Hanna, K., Kone, T., Medjahdi, G. 2008. Synthesis of the mixed oxides of iron and quartz and their catalytic activities for the Fenton-like oxidation. Catal. Commun. 9, 955–959.

Huang, H-H., Lu, M-C., Chen, J-N. 2001. Catalytic decomposition of hydrogen peroxide and 2-chlorophenol with iron oxides. Water Res. 35, 2291–2299.

Jara, A.A., Goldberg, S., Mora, M.L. 2005. Studies of the surface charge of amorphous aluminosilicates using surface complexation models. J. Colloid Interface Sci. 292,160–170.

Kang, N., Lee, D.S., Yoon, J. 2002. Kinetic modeling of Fenton oxidation of phenol and monochlorophenols. Chemosphere. 47 (9), 915-924.

Klavarioti, M., Mantzavinos, D., Kassinos, D. 2009. Removal of residual pharmaceuticals from aqueous systems by advanced oxidation processes. Environ. Int. 35, 402–417.

Lin, S.S, Chen, C.L., b, Chang, D.J., Chena, C.C. 2002. Catalytic wet air oxidation of phenol by various CeO2 catalysts. Water Res. 36, 3009-3014.

Martínez, F., Calleja, G., Melero, J.A., Molina, R. 2007. Iron species incorporated over different silica support for the heterogeneous photo-Fenton oxidation of phenol. Appl. Catal. B: Environ. 70, 452-460.

Menezes-Blackburn, D., Jorquera, M., Gianfreda, L., Rao, M., Greiner, R., Garrido, E., Mora, M.L. 2011. Activity stabilization of *Aspergillus niger* and *Escherichia coli* phytases immobilized on allophanic synthetic compounds and montmorillonite nanoclays. Bioresource Technol. 102, 9360−9367.

Mora, M.L., Escudey, M., Galindo, G. 1994. Síntesis y caracterización de suelos alofánicos. Bol. Soc. Chil.Quim. 39, 237–243.

Mora, M.L., Canales, J. 1995. Interaction of humic substances with allophanic compounds. Commun. Soil. Sci. Plant. Anal. 26, 2805−2817.

Navalon, S., Alvaro, M., Garcia, H. 2010. Heterogeneous Fenton catalysts based on clays, silicas and zeolites. Appl. Catal. B: Environ. 99, 1–26.

Noorjahan, M., Kumari, V.D., Subrahmanyam, M., Panda, L., 2005. Immobilized Fe(III)-HY: an efficient and stable photo-Fenton catalyst. Appl. Catal. B: Environ. 57, 291–298.

Núñez, L., García-Hortal, J.A., Torrades, F., 2007. Study of kinetic parameters related to the decolourization and mineralization of reactive dyes from textile dyeing using Fenton and photo-Fenton processes. Dyes Pigm. 75, 647–652.

Parffit, R.L. 2009. Allophane and imogolite: role in soil biogeochemical processes. Clay Miner. 44, 135–155.

Pérez-Estrada, L.A., Malato, S., Agüera, A., Fernández-Alba, A.R., 2007. Degradation of dipyrone and its main intermediates by solar AOPs Identification of intermediate products and toxicity assessment. Catal. Today 129, 207–214.

Popiel, S., Witkiewicz, Z., Chrzanowski, M., 2008. Sulfur mustard destruction using ozone, UV, hydrogen peroxide and their combination. J. Hazard. Mater. 153, 37–43.

Primo, O., Rivero, M.J., Ortiz, I., 2008a. Photo-Fenton process as an efficient alternative to the treatment of landfill leachates. J. Hazard. Mater. 153, 834–842.

Sanabria, N., Álvarez, A., Molina, R., Moreno, S., 2008. Synthesis of pillared bentonite starting from the Al–Fe polymeric precursor in solid state, and its catalytic evaluation in the phenol oxidation reaction. Catal. Today 133–135, 530–533.

Sánchez-Sánchez, C., Expósito, E., Casado, J., Montiel, V. 2007. Goethite as a more effective iron dosage source for mineralization of organic pollutants by electro-Fenton process. Electrochem. Commun. 9, 19 - 24.

Siedlecka, E.M., Wieckowska, A., Stepnowski, P., 2007. Influence of inorganic ions on MTBE degradation by Fenton's reagent. J. Hazard. Mater. 147, 497–502.

Sum, O.S.N., Feng, J., Hu, X., Yue, P.L., 2005. Photo-assisted Fenton mineralization of an azo-dye black 1 using a modified laponite clay-based Fe nanocomposite as a heterogeneous catalyst. Top. Catal. 33, 233–242

Tekin, H., Bilkay, O., Ataberk, S.S., Balta, T.H., Ceribasi, H., Sanin, F.D., Dilek, F.B., Yetis, U. 2006. Use of Fenton oxidation to improve the biodegradability of a pharmaceutical wastewater. J. Hazard. Mater. 136 (2), 258-265.

Ureta-Zañartu, M.S., Mora, M.L., Diez, M.C., Berríos, C., Ojeda, J., Gutiérrez, C. 2002. Chlorophenol electrooxidation on iron oxide-covered aluminosilicates deposited on glassy carbon. J. Appl. Electrochem. 32, 1211–1218.

USEPA(2000)"http://www.epa.gov/pesticides/cumulative/common_mech_groups.htm#triazine.Ventura, A., Jacquet, G., Bermond, A. Camel, V. 2002. Electrochemical generation of the Fenton`s reagent: application to atrazine degradation. Water Res. 36, 3517-3522.

Valdés-Solís, T.P., Valle-Vigón, P., Sevilla, M., Fuertes, A.B., 2007a. Encapsulation of nanosized catalysts in the hollow core of a mesoporous carbon capsule. J. Catal. 251, 239–243.

Valdés-Solís, T.P., Valle-Vigón, P., Álvarez, S., Marbán, G., Fuertes, A.B., 2007b. Manganese ferrite nanoparticles synthesized through a nanocasting route as a highly active Fenton catalyst. Catal. Commun. 8, 2037–2042.

Ventura, A., Jacquet, G., Bermond, A. Camel, V. 2002. Electrochemical generation of the Fenton`s reagent: application to atrazine degradation. Water Res. 36, 3517-3522

Violante, A., Rao, M.A., De Chiara, A., Gianfreda, L. 1996. Sorption of phosphate and oxalate by a synthetic aluminium hydroxysulphate complex. Eur. J. Soil Sci. 47, 241–247.

Wada, S.-I., Wada, K. 1977. Density and structure of allophane. Clay Miner. 12, 289–298.

Zeep, R.G., Faust, B.C., Hoigne, J., 1992. Hydroxyl radical formation in aqueous reactions (pH 3-8) of iron(II) with hydrogen peroxide: the photo-Fenton reaction Environ. Sci. Technol. 26, 313–319.

Zimbron, J.A., Reardon, K. 2009. Fenton's oxidation of pentachlorophenol. Water Res. 43 (7), 1831-1840.

2

Theoretical Background

Clays and oxide minerals as catalysts and nanocatalysts in Fenton-like reactions – A review

E.G. Garrido-Ramírez[a], B.K.G Theng[b,*], M.L. Mora[c]

[a]*Programa de Doctorado en Ciencias de Recursos Naturales Universidad de La Frontera, Av. Francisco Salazar 01145, Casilla 54-D, Temuco, Chile*

[b]*Landcare Research, Private Bag 11052, Palmerston North 4442, New Zealand*

[c]*Scientific and Technological Bioresources Nucleus, Departamento de Ciencias Químicas, Universidad de La Frontera, Av. Francisco Salazar 01145, Casilla 54-D, Temuco, Chile*

2.1. Abstract

Advanced oxidation processes (AOP), involving the generation of highly oxidizing radical species, have attracted much attention because of their potential in eliminating recalcitrant organic pollutants from different environmental matrices. Among the most investigated AOP is the Fenton reaction in which hydroxyl radicals ($^{\bullet}OH$) are generated through the catalytic reaction of Fe(II)/Fe(III) in the presence of hydrogen peroxide. The use of clays and iron oxide minerals as catalysts of Fenton-like reactions is a promising alternative for the decontamination of soils, groundwaters, sediments, and industrial effluents. The low cost, abundance, and environmentally friendly nature of clay minerals and iron oxides are an added advantage. Additionally, the introduction of nanoparticles in heterogeneous catalytic processes has led to appreciable improvements in catalytic efficiency. Here we review the application of clays and iron oxide minerals as supports or active catalysts in Fenton-like reactions, and summarize the latest advances in nanocatalyst development. We also evaluate the potential use of allophane nanoparticles, coated with iron oxides, as catalysts of Fenton-like reaction.

Keywords: allophane, catalysts, clays, Fenton-like reaction, oxide minerals, zeolites

2.2. Introduction

The development of processes, such as advanced oxidation, for the efficient degradation of persistent organic pollutants in the environment has attracted a great deal of interest. Advanced oxidation processes involve the generation of reactive radicals, notably hydroxyl radicals ($HO^{\bullet}$) that are highly oxidative and capable of decomposing a wide range and variety of organic compounds (Ramírez et al., 2007a). Depending on the structure of the organic compound in question, different reactions may occur including hydrogen atom abstraction, electrophilic addition, electronic transfer, and radical-radical interactions (Nogueira et al., 2007).

Advanced oxidation processes (AOP) use a combination of strong oxidants such as ozone, oxygen, or hydrogen peroxide and catalysts (e.g., transition metals, iron), semiconductor solids together with sources of radiation or ultrasound (Primo et al., 2008a). Typical AOP include O_3/UV, H_2O_2/UV, TiO_2/UV, H_2O_2/O_3 (Pérez-Estrada et al., 2007; Popiel et al., 2008) and those based on the Fenton reaction. Initially developed by Fenton (1894) for the oxidation of tartaric acid, this reaction has been used for the decomposition and removal of hydrocarbons (Kong et al., 1998; Kanel et al., 2004; Ferrarese et al., 2008), organic dyes (Núñez et al., 2007; Cheng et al., 2008), antibiotics (Bobu et al., 2008), pesticides (Arnold et al., 1995; Balmer and Sulzberger, 1999; Gallard and De Laat, 2000; Saltmiras and Lemley, 2002; Ventura et al., 2002; Chan and Chu, 2005; Barreiro et al., 2007; Oller et al., 2007b), landfill leachates (Deng and Englehardt, 2006; Deng, 2007; Primo et al., 2008a, 2008b), explosives (Liou and Lu, 2008), phenols (Barrault et al., 1998; Fajerwerg et al., 2000; Barrault et al., 2000b; Catrinescu et a12l., 2003; Carriazo et

al., 2005b; Araña et al., 2007; El-Hamshary et al., 2007) as well as for microbial decontamination (Rincón and Pulgarin, 2007; Shah et al., 2007).

The Fenton process involves the reaction of Fe(II) with hydrogen peroxide, giving rise to hydroxyl radicals as shown in equation [2.1]. This catalytic reaction is propagated by the reduction of Fe(III) to Fe(II) as shown in equation [2.2] with the generation of more radicals as depicted by equations [2.3], [2.4] and [2.5].

$$Fe^{2+} + H_2O_2 \longrightarrow Fe^{3+} + OH^- + HO^{\bullet} \qquad E_a = 39.5 \text{ kJ mol}^{-1} \qquad k_1 = 76 \text{ M}^{-1}\text{s}^{-1} \qquad [2.1]$$

$$Fe^{3+} + H_2O_2 \longrightarrow Fe^{2+} + HO_2^{\bullet} + H^+ \qquad E_a = 126 \text{ kJ mol}^{-1} \qquad k_2 = 0.001\text{–}0.01 \text{ M}^{-1}\text{s}^{-1} \qquad [2.2]$$

$$Fe^{2+} + HO_2^{\bullet} \longrightarrow Fe^{3+} + HO_2^- \qquad E_a = 42 \text{ kJ mol}^{-1} \qquad k_3 = 1.3 \text{ x } 10^6 \text{ M}^{-1}\text{s}^{-}1 \qquad [2.3]$$

$$Fe^{3+} + HO_2^{\bullet} \longrightarrow Fe^{2+} + O_2 + H^+ \qquad E_a = 33 \text{ kJ mol}^{-} \qquad k_4 = 1.2 \text{ x } 10^6 \text{ M}^{-}1\text{s}^{-1} \qquad [2.4]$$

$$H_2O_2 + HO^{\bullet} \longrightarrow HO_2^{\bullet} + H_2O \qquad E_a = 14 \text{ kJ mol}^{-1} \qquad k_5 = 2.7 \text{ x } 10^7 \text{ M}^{-}1 \text{ s}^{-1} \qquad [2.5]$$

Typical values of the activation energy (E_a), and apparent rate constant (k) for these reactions are taken from Lee and Yoon (2004) and Nogueira et al. (2007), respectively.

The generation of hydroxyl radicals in the Fenton reaction has been used in a variety of processes: (1) homogeneous Fenton process, involving iron(II) salts dissolved in an acid medium, (2), heterogeneous catalysis ('Fenton-like reaction'), (3) photo-reduction of Fe(III) to Fe(II) through the use of ultraviolet radiation ('photo Fenton process') (Zeep et al., 1992; Feng et al.; 2003a, 2003b, 2004c, 2009; Farré et al., 2007; Malato et al., 2007; Schwingel de Oliveira et al., 2007; Oller et al., 2007a), (4) electro-oxidation and photo-electro-oxidation (Ventura et al., 2002; Andrade et al., 2007; Kurt et al., 2007; Sirés et al., 2007; Ting et al., 2007), and (5) nanocatalysis (Kwon et al., 2007; Valdés-Solís et al., 2007b; Joo and Zhao, 2008).

The homogeneous Fenton process has been widely investigated (Pignatello, 1992; Arnold et al., 1995; Lee et al., 2001; Chan and Chu, 2005; Barros et al., 2006; Deng and Englehardt, 2006; Deng, 2007; Li et al., 2007; Nogueira et al., 2007; Núñez et al., 2007; Schwingel de Oliveira et al., 2007; Siedlecka et al., 2007; Ferrarese et al., 2008). This simple process uses conventional equipment and operates at ambient temperatures and pressures. The process, however, has some drawbacks due mainly to the formation of different Fe(III) complexes as solution pH changes.

The optimum pH for the homogeneous Fenton process is about 2.8 when the iron in solution occurs partly as Fe(III) and partly as $Fe(III)(OH)^{2+}$, representing the photo-active species. Below this pH, the hydroxyls radicals are scavenged by protons and the concentration of $Fe(III)(OH)^{2+}$ declines while above this pH, Fe(III) precipitates as an oxyhydroxide (Pignatello, 1992; Sum et al., 2005; Li et al., 2007; Martínez et al., 2007; Bobu et al., 2008). In order to maintain a pH of ~ 3, large amounts of acid (usually sulphuric acid) must be added to the reaction medium (Valdés-Solís et al., 2007b). Thus, it is impractical to apply the homogeneous Fenton process to *in situ* environmental remediation because (without pH adjustment) large amounts of ferric hydroxide sludges would be produced, creating disposal and other environmental problems (Catrinescu et al., 2003; Feng et al., 2004c; Hanna et al., 2008).

On the other hand, heterogeneous solid catalysts can mediate Fenton-like reactions over a wide range of pH values (Caudo et al., 2007; Cheng et al., 2008). This is because the Fe(III) species in such catalysts is "immobilized" within the structure and in the pore/interlayer space of the catalyst. As a result, the catalyst can maintain its ability to generate hydroxyl radicals from H_2O_2 and iron hydroxide precipitation is prevented (Catrinescu et al., 2003; Chen and Zhu, 2006; 2007). Besides showing limited leaching of iron ions, the catalysts can be recovered after the

reaction, and remain active during successive operations (Centi et al., 2000; Sum et al., 2005; Kasiri et al., 2008).

A range of heterogeneous solid catalysts, including activated carbon impregnated with iron and copper oxide metals have been used to degrade recalcitrant organic compounds through the Fenton-like reaction (Georgi and Kopinke, 2005; Ramírez et al., 2007b). Some examples are Nafion film or Nafion (Fernandez et al., 1998, 1999; Gumy et al., 2005), resin-supported Fe(II) or Fe (III) (Cheng et al., 2004; Liou et al., 2005), iron-containing ashes (Flores et al., 2008), iron-coated pumice particles (Kitis and Kaplan, 2007), and iron-immobilized aluminates (Muthuvel and Swaminathan, 2008).

Clays and oxide minerals, either as such or as supports of iron and other metal species, can also serve as heterogeneous catalysts in the Fenton-like reaction (Halász et al., 1999; Barrault et al., 2000b; Chirchi and Ghorbel, 2002; Carriazo et al., 2005b; Baldrian et al., 2006; Matta et al., 2007; Bobu et al., 2008; Chen et al., 2008; Ortíz de la Plata et al., 2008). Indeed, these materials provide an attractive alternative for the decontamination of soils, underground waters, sediments, and industrial effluents because they are natural, abundant, inexpensive, and environmentally friendly (Watts et al., 1994, 2002; Watts and Dilly, 1996; Andreozzi et al., 2002a; Carriazo et al., 2005b; Aravindhan et al., 2006; Mecozzi et al., 2008). Examples of solid catalysts are natural and synthetic zeolites exchanged with iron or copper ions (Pulgarin et al., 1995; Fajerwerg and Debellefontaine, 1996; Larachi et al., 1998; Kusic et al., 2006; Chen et al., 2008; Kasiri et al., 2008), pillared interlayered clays (Barrault et al., 1998; Guélou et al., 2003; Li et al., 2006; Giordano et al., 2007; De León et al., 2008; Sanabria et al., 2008) and iron oxide minerals (Lin and Gurol, 1998; Kwan and Voelker, 2002, 2003; Wu et al., 2006; Matta et al., 2007; Hanna et al., 2008; Liou and Lu, 2008).

However, these catalysts, especially those containing iron(III) oxides, need ultraviolet radiation to accelerate the reduction of Fe(III) to Fe(II). This is because the reaction, depicted in equation [2], is much slower than the decomposition of H_2O_2 in the presence of Fe(II) (equation.[1]) as used in the photo-Fenton process (Kwan and Voelker, 2003; Nogueira et al., 2007). The photo-Fenton or photo-Fenton-like process is generally more efficient than its normal (non-irradiated) Fenton or Fenton-like counterpart but the operating cost of the former is quite high in terms of energy and UV-lamp consumption (Centi et al., 2000). Additionally, the photo-Fenton process requires that the whole catalyst be accessible to light.

Valdés-Solís et al. (2007a, 2007b) have developed a new catalyst using nanosize particles with a high surface area that can accelerate the Fenton-like reaction without requiring UV radiation. These nanocatalysts are very reactive because the active sites are located on the surface. As such, they have a low diffusional resistance, and are easily accessible, to the substrate molecules. Nanocatalysis is but one of the many practical applications of nanotechnology which is concerned with the synthesis and functions of materials at the nanoscale range (<100 nm) (Mamalis, 2007; Miyazaki and Islam, 2007; Lines, 2008). An important feature of nanomaterials is that their surface properties can be very different from those shown by their macroscopic or bulk counterparts (Theng and Yuan, 2008). As the term suggests, 'nanocatalysis' uses nanoparticles and nanosize porous supports with controlled shapes and sizes (Bell, 2003).

This review describes the use of clays and iron oxide minerals as supports or active catalysts in the Fenton-like reaction, and summarizes recent advances in the development of nanocatalysts with improved catalytic efficiency. We also evaluate the potential of allophane nanoparticles, coated with iron oxides, to serve as catalysts in the Fenton-like reaction.

2.3. Heterogeneous solid catalysts

A wide range of solid materials, such as transition metal-exchanged zeolites (Pulgarin et al., 1995; Fajerwerg and Debellefontaine, 1996; Larachi et al., 1998; Kušić et al., 2006; Chen et al., 2008; Kasiri et al., 2008), pillared interlayered clays containing iron or copper species (Barrault et al., 1998; Guélou et al., 2003; Li et al., 2006; Giordano et al., 2007; De León et al., 2008; Sanabria et al., 2008) and iron oxide minerals (Lin and Gurol, 1998; Kwan and Voelker, 2002, 2003; Wu et al., 2006; Matta et al., 2007; Hanna et al., 2008; Liou and Lu, 2008) have been proposed as heterogeneous catalysts for the oxidative degradation of organic compounds through the Fenton-like reaction. By combining the efficiency of the homogeneous Fenton process with the advantages of heterogeneous catalysis, these materials show great promise for the treatment of highly recalcitrant organic pollutants.

Solid catalysts must fulfill a number of requirements, such as high activity in terms of pollutant removal, marginal leaching of active cations, stability over a wide range of pH and temperature, and a high hydrogen peroxide conversion with minimum decomposition (Larachi et al., 1998). For practical applications, these materials should also be available at a reasonable cost.

2.3.1. Transition metal-exchanged zeolites

Zeolites are hydrated aluminosilicates with a cage-like structure. Their internal and external surface areas may extend to several hundred square meters per gram, while their cation exchange capacities are up to several milliequivalents per kilogram. At least 41 types of natural zeolites have been identified, and many others have been synthesized. Zeolites have an open porous structure capable of accommodating a wide variety of exchangeable cations, including iron (Kušić et al., 2006; Tekbas et al., 2008).

Zeolites are ideal catalysts because the dimension of their pores is similar to that of the reacting molecules (Neamtu et al., 2004b; Aravindhan et al., 2006; Tekbas et al., 2008). Thus, zeolites can function as both selective adsorbents and '*in-situ*' oxidation catalysts (Doocey et al., 2004). The size and shape of the nanopores in synthetic zeolites can vary according to the experimental conditions as do their macroscopic properties (Ovejero et al., 2001b; Neamtu et al., 2004b; Tekbas et al., 2008). Being strongly bound to exchange sites within the pore structure, transition metals (e.g., iron, copper) are not prone to leach out or precipitate during the process (Neamtu et al., 2004b).

Zeolites containing transition metal ions have been shown to be efficient catalysts in the oxidation of a range of organic pollutants through the Fenton-like reaction (Ovejero et al., 2001b; Doocey et al., 2004; Makhotkina et al., 2006; Kuznetsova et al., 2008), the photo-Fenton process (Rios-Enriquez et al., 2004; Noorjahan et al., 2005; Kasiri et al., 2008; Muthuvel and Swaminathan, 2008; Tekbas et al., 2008), and the wet oxidation process using hydrogen peroxide (Larachi et al., 1998; Centi et al., 2000; Fajerwerg et al., 2000; Huu Phu et al., 2001; Ovejero et al., 2001a; Neamtu et al., 2004a, 2004b; Zrnčević and Gomzi, 2005; Aravindhan et al., 2006).

Neamtu et al. (2004a) have proposed that Fe-exchanged zeolites degrade organic pollutants through the Fenton reaction (Eq. 1) by generating $HO^{\bullet}$ radicals that can diffuse into the bulk solution. This implies that the pollutants are decomposed in the external medium as well as within the zeolite framework. Kušić et al. (2006) have proposed a similar mechanism for the degradation of phenol by Fe-ZSM-5 zeolite, while Noorjahan et al. (2005) concluded that the enhanced activity of a Fe(III)-HY zeolite system was due to the synergistic effect of pollutant adsorption and $HO^{\bullet}$ radical diffusion.

In common with the homogeneous Fenton process, the efficiency of heterogeneous Fenton-like catalysis is influenced by several operating parameters, such as iron concentration, type of iron catalyst, H_2O_2 concentration, iron catalyst/hydrogen peroxide ratio, temperature, pH and treatment time (Doocey et al.. 2004; Kušić et al.. 2006). Data on the degradation of recalcitrant organic compounds through the Fenton reaction, using Fe- and Cu-exchanged zeolites, are summarized in Table 2.1.

Table 2.1. Catalytic degradation of organic compounds over iron- or copper-exchanged zeolites through different Fenton-like processes

Compound	Catalyst/Support	Process	Reference
Remazol Brilliant Orange 3C	Fe(III)-exchanged natural zeolite	Photo-Fenton	Tekbas et al. (2008)
Indigoid dye C.I. Acid Blue 74	Fe-ZSM-5 synthetic zeolite	Photo-Fenton	Kasiri et al. (2008)
Reactive Brilliant Blue KN-R	Fe-NaY and Fe-ZSM-5	Fenton-like reaction	Chen et al. (2008)
Azo dye Acid Violet 7	Fe(III) immobilized Al_2O_3 catalyst	Photo-Fenton	Muthuvel and Swaminathan (2008)
Azo dye Porción Marine H-EXL	Fe-exchanged Y zeolite	Wet hydrogen peroxide oxidation	Neamtu et al. (2004b)
Acid brown	Mn-exchanged Na-Y zeolite	Wet hydrogen peroxide oxidation	Aravindhan et al. (2006)
C.I. Reactive Yellow 84 (RY84)	Fe-Y zeolite	Wet hydrogen peroxide oxidation	Neamtu et al. (2004a)
Phenol	Fe-ZSM-5 zeolite	Wet hydrogen peroxide oxidation	Huu Phu et al. (2001)
Phenol model wastewater	Fe-ZSM-5	Fenton-like reaction and Photo-Fenton	Kušić et al. (2006)

Phenol	Cu-Y-5	Wet hydrogen peroxide oxidation	Zrnčević and Gomzi (2005)
Chlorinated phenols	Fe-Beta zeolite Fe-4A zeolite	Fenton-like reaction	Doocey et al. (2004)
Phenolic solutions	Fe-NaY, Fe-USY, and Fe-ZSM-5	Fenton-like reaction	Ovejero et al. (2001b)
Phenol	Fe(III)-HY catalyst	Photo-Fenton	Noorjahan et al. (2005)
Phenol	MFI zeolite	Wet hydrogen peroxide oxidation	Ovejero et al. (2001a)
Phenol	Fe-ZSM-5	Wet hydrogen peroxide oxidation	Fajerwerg et al. (2000)
Phenolic aqueous wastes	Fe-ZSM-5	Wet hydrogen peroxide oxidation	Fajerwerg and Debellefontaine (1996)
Phenolic aqueous wastes	Fe-ZSM-5	Wet hydrogen peroxide oxidation	Fajerwerg et al. (1997)
4-nitrophenol	Fe-ZSM-5	Photo-Fenton	Pulgarin et al. (1995)
Phenol	Cu-ZSM-5	Wet hydrogen peroxide oxidation	Valkaj et al. (2007)
1,1-dimethylhydrazine and ethanol	Fe-MF1 zeolite catalyst	Fenton-like reaction	Kuznetsova et al. (2008)
1,1-dimethylhydrazine	Fe-ZSM-5 zeolite	Fenton-like reaction	Makhotkina et al. (2006)
Carboxylic acids	Fe-ZSM-5	Wet hydrogen peroxide oxidation	Centi et al. (2000)
Acetic acid	Cu-NaY zeolite	Wet hydrogen peroxide oxidation	Larachi et al. (1998)
2,4-xylidine	Fe(III)-zeolite Y	Fenton-like reaction	Rios-Enríquez et al. (2004)

These studies show that the catalytic efficiency and stability against leaching of Fe-exchanged zeolites are related to their iron content. For example, Doocey et al. (2004) found that the rate of hydrogen peroxide decomposition was higher for Fe-4A zeolite (3.4% w/w iron) than Fe-Beta zeolite (1.25% w/w iron). At the same time, the former was slightly more stable in the cation leaching test. The catalytic efficiency and stability of Fe-exchanged zeolites are also affected by pH and temperature. Using Fe-Beta and Fe-4A zeolites as catalysts, Doocey et al. (2004) observed optimal hydrogen peroxide decomposition at pH 3.5. Neamtu et al. (2004b) reported that the degradation of the Azo dye *Procion Marine H-EXL* by Fe-Y zeolite was higher at pH 3 (97%) than at pH 5 (53%) in 10 minutes of operation, while increasing the time of operation to 30 minutes resulted in 97% removal at pH 5. For the reaction at pH 3, this (initial) value did not change throughout the treatment. During the reaction at pH 5, however, the pH decreases to about 3.5. This might be because the dye molecules fragment into organic acids as the reaction proceeds. As a result, solution pH decreases and the degradation process is accelerated (neamtu et al., 2004b). Similar results were obtained by Kasiri et al. (2008) for the photo-degradation of Acid Blue 74 using Fe-ZSM-5 zeolite. Thus, Fe-exchanged zeolites can effectively operate at near neutral pH as cation leaching is limites, and zeolite stability is maintained (Doocey et al., 2004; Neamtu et al., 2004a, 2004b).

Although a rise in temperature increases catalytic efficiency, it also enhances cation leaching and decomposition of hydrogen peroxide to oxygen and water. Neamtu et al. (2004a) found an optimal temperature of 50 ºC for the degradation of the azo dye C.I. Reactive Yellow 84 (RY84) by wet hydrogen peroxide oxidation using a Fe-exchanged Y zeolite catalyst.

The preparation of metal-exchanged zeolites also influences catalytic activity. Valkai et al. (2007), for example, reported that the activity of a Cu-ZSM-5 catalyst prepared by direct

hydrothermal synthesis (DHS) was higher than that of a catalyst obtained by the ion exchange (IE) method in terms of phenol oxidation and hydrogen peroxide decomposition. The stability of the DHS catalyst was also superior to that of the IE material because leaching of the active ingredient was relatively low in the former instance.

Using a Fe-exchanged zeolite, Centi et al. (2000) compared the catalytic efficiency of the homogeneous Fenton process with that of the (heterogeneous) Fenton-like reaction. The Fe-ZSM-5 catalyst was more efficient in degrading propionic acid (72%) than the homogeneous Fenton process (43%). The heterogeneous process was also less sensitive to changes in pH.

2.3.2. Pillared interlayered clays

Pillared interlayered clays (PILC) are low-cost, microporous solid catalysts with unique properties and structures (Li et al., 2006; Ramírez et al., 2007a; Mishra et al., 2008), formed by intercalation of metal polycations into swelling clay minerals, notably smectites. On heating at high temperatures (≈500 ^{o}C), the intercalated polycations are converted into the corresponding metal oxide clusters through dehydration and dehydroxylation. By propping the silicate layers apart, these oxides act as “pillars”, creating interlayer meso- and micro-pores (Mishra et al., 1996; Kloprogge, 1998; Bergaya et al., 2006; Bobu et al., 2008; Pan et al., 2008). The intercalation of metal oxocations increases the basal spacing of the parent clays. The increase in basal spacing is higher for Fe-supported Al-PILC catalysts (Fe-Al-PILC) than for their Fe-PILC counterparts. Li et al. (2006) reported a basal spacing increment of 0.62 nm for Fe-Al-PILC and 0.51 nm for Fe-PILC with respect to the original bentonite clay, while Chen and Zhu (2007) reported an increment of 3.93 nm for Fe-PILC. Sanabria et al. (2008) found a basal spacing

increment of 0.38 nm for Al-Fe-PILC, while Pan et al. (2008) observed an increment of 0.64 nm for Al-PILC prepared from Na-montmorillonite.

The surface area of PILC, determined by adsorption of N_2 gas at 77 K and applying the Brunauer-Emmett-Teller (BET) equation, is invariably much larger than the corresponding starting clay or clay mineral. For example, Pan et al. (2008) measured a surface area of 176 m^2 g^{-1} for Al-PILC as against 43 m^2 g^{-1} for the original Na-montmorillonite. Similarly, Li et al. (2006) obtained a BET surface area of 114.6 m^2 g^{-1} for Fe-PILC and 194.2 m^2 g^{-1} for Al-Fe-PILC as compared with 31.8 m^2 g^{-1} for the original bentonite clay. In addition, pillaring greatly increases the accessibility of interlayer catalytic sites to the reactant molecules (Kloprogge, 1998; Carriazo et al., 2003; Sanabria et al., 2008).

Pillared interlayered clays containing oxocations of copper (Cu-PILC) or iron (Fe-PILC) together with Al-PILC supporting iron and copper ions, have been widely used as catalysts for the degradation of recalcitrant organic compounds via Fenton-like reactions, photo-Fenton reactions, and wet hydrogen peroxide oxidation (Table 2.2). Pillared interlayered clay catalysts are also very stable, showing minimal leaching of interlayer metal species to the external solution (Caudo et al., 2007; Chen and Zhu, 2007; Giordano et al., 2007; Ramírez et al., 2007a; Bobu et al., 2008; Caudo et al., 2008; Pan et al., 2008; Sanabria et al., 2008). These materials can therefore be used repeatedly with little loss of catalytic activity, while problems associated with water contamination by soluble metals and waste disposal are avoided. The relatively short periods of operation are an added advantage of using PILCs catalysts.

Table 2.2. Pillared interlayered clays (PILC) as heterogeneous catalysts for the decomposition of various organic compounds via Fenton-like reactions

Compound	Catalyst/Support	Clay	Process	Reference
Azo dye X-3B	Fe-PILC Al-Fe-PILC	Bentonite	Photo-Fenton	Li et al. (2006)
Methylene blue	Fe-PILC	Natural montmorillonite	Photo-Fenton	De León et al. (2008)
Orange II	Hydroxyl-Fe-PILC	Bentonite	Photo-Fenton	Chen and Zhu (2006)
Acid Light Yellow G	Fe-PILC (catalyst)	Natural bentonite	Photo-Fenton	Chen and Zhu (2007)
Azo dye Orange II solution	Al-PILC impregnated with Fe	Natural saponite	Fenton-like reaction	Ramírez et al. (2007a)
Ciprofloxacin (fluoroquinolones)	Fe-PILC nanocomposite	Laponite (synthetic hectorite)	Photo-Fenton	Bobu et al. (2008)
Phenol	Mixed (Al-Fe)-PILC	Commercial Greek bentonite	Catalytic wet oxidation with H_2O_2	Barrault et al. (2000a)
Phenol	Al-Cu-PILC Al-Fe-PILC	Commercial Greek bentonite	Catalytic wet oxidation with H_2O_2	Barrault et al. (2000b)
Phenol	Al- or mixed Al-Fe-complexes PILC	Commercial Greek bentonite	Catalytic wet oxidation with H_2O_2	Guélou et al. (2003)
Phenol	Fe-PILC	Laponite	Photo-Fenton	Iurascu et al. (2009)
4-nitrophenol	Fe(III)-exchanged PILC	Montmorillonite	Fenton-like reaction	Chirchi and Ghorbel (2002)
Phenol	Al-Cu-, Al-Fe- and Fe-PILC	Natural sodium bentonite and natural sodium montmorillonite	Catalytic wet oxidation with H_2O_2	Carriazo et al. (2003)
Phenol	Fe-exchanged Al-PILC	Synthetic beidellite	Catalytic wet oxidation with H_2O_2	Catrinescu et al. (2003)

Phenol	Al-, Al-Fe- and Al-Ce-Fe-PILC	Natural Colombian bentonite	Catalytic wet oxidation with H_2O_2	Carriazo et al. (2005a)
Phenol	Al-Fe PILC Al-Ce-Fe PILC	Natural Colombian bentonite	Fenton-like reaction	Carriazo et al. (2005b)
Phenol	Al-Fe-PILC	Natural bentonite	Catalytic wet oxidation with H_2O_2	Sanabria et al. (2008)
Benzene	Al-PILC as supports for Cu, V, Fe	Natural sodium montmorillonite	Fenton-like reaction	Pan et al. (2008)
p-coumaric acid and *p*-hydroxybenzoic acid Olive oil mill wastewater	Cu-PILC Fe-PILC	Commercial bentonite	Catalytic wet oxidation with H_2O_2	Caudo et al. (2007)
Polyphenols Olive oil mill wastewater	Cu-based zeolite Cu-PILC	Zeolite and commercial bentonite	Catalytic wet oxidation with H_2O_2	Giordano et al. (2007)
Wastewater from agro-food production	Cu-PILC	Commercial bentonite	Catalytic wet oxidation with H_2O_2	Caudo et al. (2008)

In investigating the wet acid oxidation by H_2O_2 of *p*-coumaric acid and *p*-hydroxybenzoic acid using Cu-PILC with different Cu loadings (0.5, 1.0 and 2.0% Cu), Caudo et al. (2008), for example, found that 76–82% of total organic carbon (TOC) was removed within four hours of operation. Similarly, Sanabria et al. (2008) observed 100% removal of phenol in two hours of operation by a Fenton-like reaction, using Fe-PILC in an aqueous medium, while Giordando et al. (2007) were able to remove 97% of polyphenols from olive oil mill wastewater within three hours, using Cu-PILC in a wet oxidation process with H_2O_2. Although the optimal pH for the

Fenton and photo-Fenton processes is around 3 (Ramírez et al., 2007a; Bobu et al., 2008; Sanabria et al., 2008), Fe-PILC are active over a wide range of pH (De León et al., 2008), and offer the potential to operate at near neutral pH without significant loss of activity (Chen and Zhu, 2007; Bobu et al., 2008; Caudo et al., 2008).

As already remarked on, this is because the Fe(III) species is largely "immobilized" in the interlayer space of the clay mineral. As such, the iron in PILC is stable against changes in solution pH and shows only limited leaching. Further, the strong surface acidity of some Fe-PILC allows catalytic activity to be maintained over a wide range of pH values (Chen and Zhu, 2006, 2007; De Leon et al., 2008). In using Fe-PILC as heterogeneous catalyst, H_2O_2 is often added to the solution at near neutral pH. As the reaction proceeds, however, the solution pH decreases due to formation of acidic intermediates (e.g., acetic acid, oxalic acid). These acids can capture any Fe ions that are released from the catalyst, giving rise to soluble complexes and promoting a homogeneous Fenton process. The concentration of Fe in solution is proportional to that of the pollutant. When the acidic intermediated are mineralized (oxidized) to CO_2 and H_2O, the Fe ions can be re-adsorbed to the PILC surface, forming an Fe(III) cycle (Bobu et al., 2008)

2.3.3. Iron oxide minerals

The ability and potential of iron oxide minerals to catalyze the oxidation of organic compounds through the Fenton-like reaction have been well documented (Lin and Gurol, 1998; Huang et al., 2001; Kwan and Voelker, 2002, 2003; Baldrian et al., 2006; Wu et al., 2006; Matta et al., 2007; Hanna et al., 2008; Liou and Lu, 2008; Ortiz de la Plata et al., 2008). The iron oxide minerals that have been investigated include goethite (Kong et al., 1998; Lin and Gurol, 1998; Huang et al., 2001; Kwan and Voelker, 2003; Wu et al., 2006; Liou and Lu, 2008), hematite (Huang et al.,

2001; Matta et al., 2007), magnetite (Kong et al., 1998), ferrihydrite (Huang et al., 2001; Kwan and Voelker, 2002; Barreiro et al., 2007), pyrite (Matta et al., 2007) and lepidocrocite (Matta et al., 2007).

Iron oxides, used for wastewater decontamination, can be recovered and reused because they are practically insoluble in water. Since iron minerals are widespread in the soil environment, they can also be used for the *in situ* remediation of soils and groundwaters through the Fenton-like reaction in the presence of H_2O_2 (Kanel et al., 2004; Yeh et al., 2008). Furthermore, the operation does not require strict control of pH as is the case in the homogeneous Fenton process (Andreozzi et al., 2002a). Several authors, for example have reported that the iron/hydrogen peroxide system can catalyze the oxidation of pollutants at pH values between 3 and 7 through a Fenton-like reaction (Table 2.3). The process apparently involves hydroxyl radicals, generated by decomposition of hydrogen peroxide on the surface of iron oxide particles through a chain reaction mechanism (Lin and Gurol, 1998; Huang et al., 2001; Kwan and Voelker, 2003) although Andreozzi et al. (2002a) have suggested that the oxidation of organic compounds can occur through a non-radical mechanism (Table 2.4).

Table 2.3. Oxidation of various organic compounds catalyzed by iron oxide minerals through Fenton-like processes

Compound	Catalyst	Process	Reference
Bromophenol Blue, Chicago Sky Blue, Cu Phthalocyanine, Eosin Yellowish, Evans Blue, Naphthol Blue Black, Phenol Red, Poly B-411, Reactive Orange 16	Magnetic mixed iron oxides ($MO-Fe_2O_3$); M=Fe, Co, Cu, Mn	Fenton-like reaction	Baldrian et al. (2006)
Methyl red (MR)	Quartz/amorphous iron(III) oxide, quartz/maghemite, quartz/magnetite, quartz/goethite	Fenton-like reaction	Hanna et al. (2008)
2,4,6-trinitrophenol and ammonium picrate	Goethite	Fenton-like reaction	Liou and Lu (2008)
2,4,6-trinitrotoluene	Ferrihydrite, hematite, goethite, lepidocrocite, magnetite and pyrite	Fenton-like reaction	Matta et al. (2007)
2-chlorophenol	Ferrihydrite, goethite and hematite	Fenton-like reaction	Huang et al. (2001)
2-chlorophenol	Goethite	Fenton-like reaction	Lu et al. (2002)
Benzoic acid	[gamma]-FeOOH	Fenton-like reaction	Chou and Huang (1999)
3,4-dihydroxybenzoic acid	Goethite	Hydrogen peroxide in aqueous slurry	Andreozzi et al. (2002a)
Petroleum-contaminated soils (diesel and kerosene)	Goethite and magnetite	Fenton-like reaction	Kong et al. (1998)
Aromatic hydrocarbons and chloroethylenes	Goethite	Fenton-like reaction	Yeh et al. (2008)
Atrazine	Ferrihydrite	Fenton-like reaction	Barreiro et al. (2007)
Aromatic substrates	Goethite	Hydrogen peroxide in aqueous slurry	Andreozzi et al. (2002b)

Dimethyl sulphoxide	Goethite	Fenton-like reaction (aqueous solution)	Wu et al. (2006)

Table 2.4. Mechanisms proposed for the oxidation of organic compounds on the surface of iron oxide catalysts through a Fenton-like reaction

1. Radical mechanism proposed by Lin and Gurol (1998)

$$\equiv Fe(III)-OH + H_2O_2 \Leftrightarrow (H_2O_2)_s \quad (2.6)$$

$$(H_2O_2)_s \Leftrightarrow (\equiv Fe(II)^{*}O_2H) + H_2O \quad (2.7)$$

$$\equiv Fe(II)^{*}O_2H) \Leftrightarrow Fe(II) + HO_2^{*} \quad (2.8)$$

$$\equiv Fe(II) + H_2O_2 \xrightarrow{K_4} \equiv Fe(III)-OH + {}^{*}OH + H_2O \quad (2.9)$$

$$\equiv Fe(II) + O_2 \xrightarrow{K_{4a}} Fe(III)-OH + HO_2^{*} \quad (2.9a)$$

$$HO_2^{*} \Leftrightarrow H^{+} + O_2^{*-} \qquad \text{pKa} = 4.8 \quad (2.10)$$

$$\equiv Fe(III)-OH + HO_2^{*}/O_2^{*-} \xrightarrow{K_6} \equiv Fe(II) + H_2O/OH^{-} + O_2 \quad (2.11)$$

$${}^{*}OH + \equiv Fe(II) \xrightarrow{K_7} \equiv Fe(III)-OH \quad (2.12)$$

$${}^{*}OH + (H_2O_2)_s \xrightarrow{K_8} Fe(III)-OH + HO_2^{*} + H_2O \quad (2.13)$$

$$(H_2O_2)_s + HO_2^{*}/O_2^{*-} \xrightarrow{K_9} \equiv Fe(III)-OH + H_2O/OH^{-} + {}^{*}OH + O_2 \quad (2.14)$$

$$HO_2^{*} + HO_2^{*} \xrightarrow{K_{10}} (H_2O_2)_s + O_2 \quad (2.15)$$

$${}^{*}OH + HO_2^{*}/O_2^{*-} \xrightarrow{K_{11}} H_2O_2 + O_2 \quad (2.16)$$

2. Radical mechanism proposed by Kwan and Voelker (2003)

$$\equiv Fe(III) + H_2O_2 \rightarrow \equiv Fe(HO_2)^{2+} + H^{+} \quad (2.17)$$

$$\equiv Fe(HO_2)^{2+} \rightarrow \equiv Fe(II) + HO_2^{*} \quad (2.18)$$

$$\equiv Fe(II) + H_2O_2 \rightarrow Fe(III) + {}^{*}OH + OH^{-} \quad (2.19)$$

$${}^{*}OH + H_2O_2 \rightarrow H_2O + HO_2^{*} \quad (2.20)$$

$$\equiv Fe(II) + O_2^{*-} \rightarrow \equiv Fe(III) + O_2 \quad (2.21)$$

$\equiv Fe(III) + HO_2^* \rightarrow \equiv Fe(II) + HO_2^-$	(2.22)
$\equiv Fe(II) + HO_2^- \rightarrow \equiv Fe(III) + HO_2^*$	(2.23)
3. Non-radical mechanism proposed by Andreozzi et al. (2002a) for the oxidation of 3,4-dihydroxybenzoic acid in a goethite/H_2O_2 system	
≡Fe(III)-OH (catalytically active sites on goethite)	(2.24)
≡Fe(III)-OH +H^+ →≡Fe(III)-OH_2^+	(2.25)
≡Fe(III)-OH→Fe(III)-O^- + H^+	(2.26)
$H_2O_2 + (*) \xleftrightarrow{K_h} H_2O_2^* \qquad K_h = \frac{[H_2O_2^*]}{H_2O_2C_I}$	(2.27)
$S + (*) \xrightarrow{K_1} S^*$	(2.28)
$S + H_2O_2^* \xrightarrow{K_2} products + 2(*)$	(2.29)

According to the radical mechanism proposed by Lin and Gurol (1998), the reaction is initiated by the formation of an inner-sphere complex between hydrogen peroxide (H_2O_2) and ≡Fe(III)-OH groups at the oxide surface (Table 2.4, equation 2.6). The surface complex may be regarded as a ground-state (equation 2.7), mediating a reversible electronic transfer from ligand to metal. The electronically excited state can be deactivated through dissociation of the peroxide radical ("successor complex"), as shown by equation 2.8. Being very active, the peroxide radical can immediately react with other compounds. Therefore, the reverse reaction of equation 2.8 may be assumed to be negligible ($K_3 >> K_{3a}$). The reduced iron can react with either hydrogen peroxide or oxygen, as shown by reactions 2.9 and 2.9a. Reaction 2.9a, however, is slower than reaction 2.9. The hydrogen and peroxide radicals produced can react with Fe(II) and Fe(III), exposed on surface sites, according to reactions 2.11 and 2.12. These free radicals can also react with H_2O_2

(reactions 2.13 and 2.14). Finally, the radicals can react with themselves, terminating the reactions (2.15 and 2.16).

On the other hand, Andreozzi et al. (2002a) have suggested a non-radical mechanism for the degradation of 3,4-dihydroxybenzoic acid as shown by equations 2.27 and 2.28 (Table 2.4) where (*) denotes the active sites on the catalyst and C_I is their concentration (mol dm^{-3}). The adsorbed substrate (*S*) and hydrogen peroxide react on the catalyst surface, giving rise to reaction products and the regeneration of active sites (equation 2.29).

The efficiency of iron oxide minerals in catalyzing the decompostion of organic pollutants through the Fenton-like reaction is influenced by several parameters, such as hydrogen peroxide concentration, type and surface area of the iron mineral, solution pH (and ionic strength), and pollutant characteristics (Matta et al., 2007; Yeh et al., 2008). Kwan and Voelker (2003) have described a method for determining the rate of formation of hydroxyl radicals ($V_{OH\bullet}$) in iron oxide/hydrogen peroxide systems. $V_{OH\bullet}$ is proportional to the product of the concentrations of surface area of the iron oxide and hydrogen peroxide, with a different coefficient of proportionality for each iron oxide.

Since the concentration of hydrogen peroxide is directly related to the amount of hydroxyl radicals produced in the catalytic reaction, this parameter influences degradation efficiency. In investigating the oxidation of dimethyl sulphoxide (DMSO) by hydrogen peroxide with goethite as catalyst, Wu et al. (2006) found that when the H_2O_2 concentration was increased from 2.5 to 10 g/L, more hydroxyl radicals were generated, and the rate of degradation increased. However, when the dosage of H_2O_2 was further increased from 10 to 15 g/L, the rate of decomposition declined. This was ascribed to scavenging of H_2O_2 by hydroxyl radicals resulting in the formation

of hydroperoxide radicals that were much less active and did not contribute to the oxidation of DMSO.

As regards mineral type, Fe(III) oxides are catalytically less active than their Fe(II) counterparts (Kwan and Voelker, 2003). In evaluating the activity of different iron minerals in catalyzing the degradation of 2,4,6-trinitrotoluene (TNT) through a Fenton-like reaction in aqueous solution at pH 3, Matta et al. (2007) found that iron(III) oxides (hematite, goethite, lepidocrocite, ferrihydrite) were less effective than Fe(II) minerals, such as magnetite and pyrite.

The surface area of iron oxide minerals is also an important factor influencing the degradation of organic pollutants by the Fenton-like reaction. Hanna et al. (2008), for example, observed that the efficiency of four quartz-iron oxide mixtures in degrading methyl red (MR) at pH 5 decreased in the order quartz-goethite (Q_4) > quartz/amorphous iron(III) oxide (Q_1) > quartz-maghemite (Q_2) > quartz-magnetite (Q_3). This was also the order by which the surface area of the mineral mixtures decreased: Q_4 (148 $m^2\,g^{-1}$) > Q_1 (121 $m^2\,g^{-1}$) > Q_2 (11.5 $m^2\,g^{-1}$) > Q_3 (8.6 $m^2\,g^{-1}$).

Other factors influencing the degradation of organic compounds by iron oxides are medium pH and chemical properties of the pollutant. At acid pH values, the degradation process is mainly due to dissolution of iron oxides in solution, promoting the homogeneous Fenton-like reaction. Liou et al. (2008) studied the degradation of explosives (2,4,6-trinitrophenol and ammonium picrate) by hydrogen peroxide at pH 2.8, using goethite as catalyst. Here again, the underlying mechanism involves dissolution of goethite and the generation of ferrous ions which react with H_2O_2 to produce $HO^{\bullet}$, according to the homogeneous Fenton process. In studying the oxidation of atrazine using ferrihydrite as catalyst, Barreiro et al. (2007) found that the rate of oxidation strongly depended on pH. A high degradation rate was observed at pH 3–4 when ferrihydrite

dissolution strongly increased. The increase in oxidation rate at low pH was attributed to the enhanced solubility of iron (III) species at acid pH, promoting the homogeneous Fenton reaction. Fe(III) can also be solubilized by forming complex es with organic acid intermediates produced during pollutant degradation (Feng et al., 2006; Martínez et al., 2007; Bobu et al., 2008)

At near neutral pH values, the solubility of iron oxide minerals decreases, and hence the degradation of organic compounds (on the catalyst surface) is mediated by the heterogeneous Fenton reaction which controls the efficiency of the process. Under these conditions, the electrostatic interactions between the catalyst surface and the organic compounds become important. Kwan and Voelker (2004) investigated the effect of electrostatic interaction between catalyst (goethite) surface and several probe molecules (formic acid, nitrobenzene and 2-chlorophenol) on their oxidization by H_2O_2. At pH 4, formic acid was negatively charged and interacted with the positively charged iron oxide surface where $HO^{\bullet}$ species were generated. As a result, the oxidation rate of formic acid increased by a factor of 50 relative to that of the neutral molecule. This observation provides strong support for the hypothesis that surface-adsorbed organic compounds are readily accessible to oxidation by $HO^{\bullet}$ radicals.

Hanna et al. (2008) evaluated the catalytic efficiency of four iron-quartz oxide mixtures in degrading methyl red (MR) at pH 5 and 7. The high catalytic activity at pH 5 was ascribed to electrostatic interactions between the carboxylate group of MR (pKa = 5.1) and the partially protonated oxide surface (PZC > 6). Since the soluble iron concentration at both pH values was below the limit of detection, adsorption of MR to the solid oxide surface had a determining influence on the degradation of MR through the heterogeneous Fenton reaction. Wu et al. (2006) found that the goethite-catalyzed degradation of dimethyl sulphoxide (DMSO) decreased in the order: pH 5 > pH 3 > pH 7 ≈ pH 10. They suggested that electrostatic interactions between the

partial negative charge on the oxygen atom of DMSO and the partially protonated goethite surface at pH 5 favoured degradation.

2.3.4. Nanocatalysts

An important feature of nanoparticles is that their surface properties can deviate markedly from those of their macroscopic (bulk) counterparts (Theng and Yuan, 2008). In terms of catalysis, the activity and selectivity of nanocatalysts are strongly dependent on their size, shape, and surface structure, as well as on their bulk composition (Bell, 2003; Perez, 2007). The synthesis, development, and practical applications of nanoparticulate catalysts have been decribed by Bell (2003), Perez (2007), Bach et al. (2008), and Dhakshinamoorthy and Pitchumani (2008). Examples of the use of nanocatalysts in the degradation of recalcitrant organic compounds are given in Table 2.5. Liu (2006) have proposed that nanoparticles are potentially useful for remediating polluted sites because they can reach or penetrate into zones that are inaccessible to microsize solid catalysts.

Table 2.5. Nanocatalysts used in the degradation of various organic compounds

Compound	Nanocatalyst	Process	Reference
Orange II	Composite of iron oxide and silicate nanoparticles (Fe-nanocomposite	Photo-Fenton reaction	Feng et al. (2003a)
Orange II	Fe^{3+}-doped TiO_2 and bentonite clay-based Fe nanocatalyst	Photo-Fenton reaction	Feng et al. (2004a)
Orange II	Bentonite clay-based Fe-nanocomposite	Photo-Fenton reaction	Feng et al. (2004b)
Trichloroethene	Pd-on-Au	Aqueous-phase hydrodechlorination	Nutt et al. (2006)
Butachlor	Immobilized TiO_2 nanoparticles	Photocatalysis in aqueous solution	Mahmoodi et al. (2007)
Nonylphenyl poly(oxyethylene)ethers (NPE-10)	Au-doped nano-TiO_2	Photodegradation	Du et al. (2008)
Orange G	Iron-nickel bimetallic nanoparticles	Degradation in aqueous solution	Bokare et al. (2008)
Phenol	Chain-like Ru nanoparticle arrays	Hydrogenation in aqueous media	Lu et al. (2008)
Lindane and atrazine	Fe-Pd bimetallic nanoparticles	Aerobic and anaerobic degradation	Joo and Zhao (2008)
Cango red	Selenium nanoparticles	Photocatalytic decolorization	Yang et al. (2008)

The application of nanoparticles as catalysts of the Fenton-like and photo-Fenton reactions has been described by several investigators (Feng et al., 2004a, 2004b, 2006; Valdés-Solís et al., 2007a, 2007b; Zelmanov and Semiat, 2008). In comparison with their microsize counterparts, nanoparticles show a higher catalytic activity because of their large specific surface where

catalytically active sites are exposed (Nurmi et al., 2005). The advantage of using nanoparticles as catalysts for Fenton-like reactions would more than offset the disadvantage (associated with the use of iron(III) catalysts) of requiring ultraviolet radiation to accelerate the reaction.

In investigating the catalytic degradation of ethylene glycol and phenol by iron(III) oxide nanoparticles in the absence of ultraviolet radiation, Zelmanov and Semiat (2008) found that the rate of degradation was 2–4 and 35 times higher, respectively, than the values reported in the literature using Fenton's reagent/H_2O_2/UV. Kwon et al. (2007) evaluated two iron oxide catalysts for the oxidation of carbon monoxide and methane at low temperatures. One of the materials (NANOCAT®) had an average particle size of 3 nm and a specific surface area of 250 $m^2\ g^{-1}$, while the other material (Fe_2O_3PVS) had an average particle size of 300 nm and a surface area of 4 $m^2\ g^{-1}$. Although both catalysts were effective, the nanocatalyst showed superior activity because of its high surface area. Using a nanocasting technique, Valdés-Solís et al. (2007b) obtained $MnFe_2O_4$ nanoparticles as heterogeneous catalysts for the Fenton-like reaction. These solid nanocatalysts were active over a wide range of pH values (6–13) and H_2O_2 concentrations (0.005–3 M).

2.4. Iron oxide-coated allophane nanocatalysts in Fenton-like reactions

Allophane is the main component of the clay fraction of soils derived from volcanic ash and weathered pumice (Andisols) which are widespread in southern Chile. Iron oxides of short-range order, notably ferrihydrite, are also widespread in Andisols although their concentration rarely exceeds 10% (Galindo, 1974). These constituents often occur as coatings of clay mineral particles.

Allophane may be defined as "a group of clay-size minerals with short-range order which contain silica, alumina, and water in chemical combination" (Parfitt, 1990). Allophanes occur as hollow spherules with an external diameter between 3.5 and 5.5 nm and a wall thickness of 0.7–1.0 nm. Defects in the wall structure give rise to perforations of about 0.3 nm in diameter permitting water molecules to enter the inner-spherule void (Henmi and Wada, 1976; Wada and Wada, 1977; Hall et al., 1985; Brigatti et al., 2006). Parfitt (1990) has distinguished three types of allophane with different structural features: (a) Al-rich type, also referred to as 'proto-imogolite' or 'imogolite-like' allophane, with an Al/Si ratio of ~2, (b) Si-rich type, sometimes referred to as 'halloysite-like' allophane, with an Al/Si ratio of ~1, and (c) stream-deposit allophane with Al/Si ratios ranging from 0.9 to 1.8. As the name suggests, type (c) allophane does not occur in soil. The specific surface area of allophane, determined by adsorption of polar liquids (ethylene glycol, ethylene glycol monoethyl ether), ranges from 300 to 600 m^2 g^{-1}, and from 145 to 170 m^2 g^{-1} when measured by adsorption of nitrogen gas and applying the BET equation (Diaz et al., 1990).

Montarges-Pelletier et al. (2005) have synthesized allophanes with a wide range of Al/Si ratios (0.19–1.96) in order to assess the effect of composition on texture. Transmission electron microscopy (TEM) shows differences in aggregate size and density. Aggregates of allophanes with a relatively low Al/Si ratio are less dense than those with high Al/Si ratios, probably because the former samples have a low isoelectric point and surface charge. The shape of the nitrogen adsorption-desorption isotherms also varies with Al/Si ratio. Samples with an Al/Si ratio < 0.5 have high adsorption volumes at P/P_o ~1, suggesting the presence of relatively large mesopores and a wide pore-size distribution. Samples with an Al/Si ratio of 0.5–0.8 show marked hysteresis between the adsorption and desorption branches, indicative of a narrow pore-size distribution.

Samples with an Al/Si ratio of 0.8–1.3 show high microporosity, low adsorbed nitrogen volume, and limited mesoporosity. Samples with an Al/Si ratio > 1.3 have a low nitrogen adsorption capacity.

Diaz et al. (1990) were able to synthesize allophane-like aluminosilicates by both coprecipitation of sodium silicate and aluminium chloride and hydrolysis of tetraethylortosilicate and terbutoxyde of aluminium. Besides being faster, the coprecipitation method gave materials with similar surface charge charateristics to those shown by natural allophanes. Mora et al. (1994) and Jara et al. (2005) also used the coprecipitation approach to prepare synthetic allophane-like materials which they then coated with iron oxides, using a wet impregnating technique. They proposed that the iron oxide (coat) was attached to the allophane surface through Si-O-Fe and Al-O-Fe bonds.

The ^{57}Fe Mössbauer spectrum at 300 K of iron-oxide coated synthetic allophane, is shown in Fig. 2.1. The presence of a broad paramagnetic doublet with a quadrupole splitting (Δ) of 0.86 mm s^{-1}, a line width (γ) of 0.51 mm s^{-1}, and an isomer shift (δ) of 0.36 mm s^{-1} is typical of high-spin ferric iron in octahedral coordination (to O and OH ligands), corresponding to a ferrihydrite-like material (Childs and Johnston, 1980; Mora et al., 1994; Jara et al., 2005). Fig.2.2 shows transmission electron micrographs of the same iron-oxide coated synthetic allophane. Individual hollow allophane spherules with an outer diameter of about 5 nm can seen to form 30-50 nm aggregates that, in turn, coalesce into globular clusters, similar to what Hall et al. (1985) have found with naturally occurring (soil) allophanes. The point of zero charge (PZC) of the samples was determined using the method described by Parks (1967), while the isoelectric point (IEP) was assessed by electrophoretic mobility measurements. The measured values of ~4.2 for the

PZC and ~8.5 for the IEP, were consistent with the presence of an iron oxide coating over allophane-like particles, causing an overall increase in surface acidity.

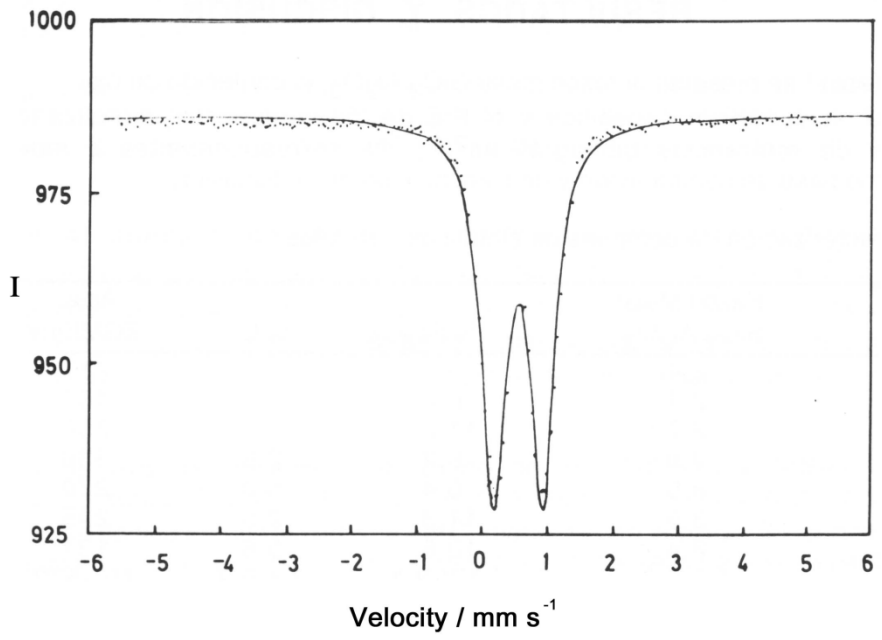

Figure 2.1. ^{57}Fe Mössbauer spectrum (at 300 K) of synthetic allophane coated with iron oxide (adapted from Mora et al., 1994)

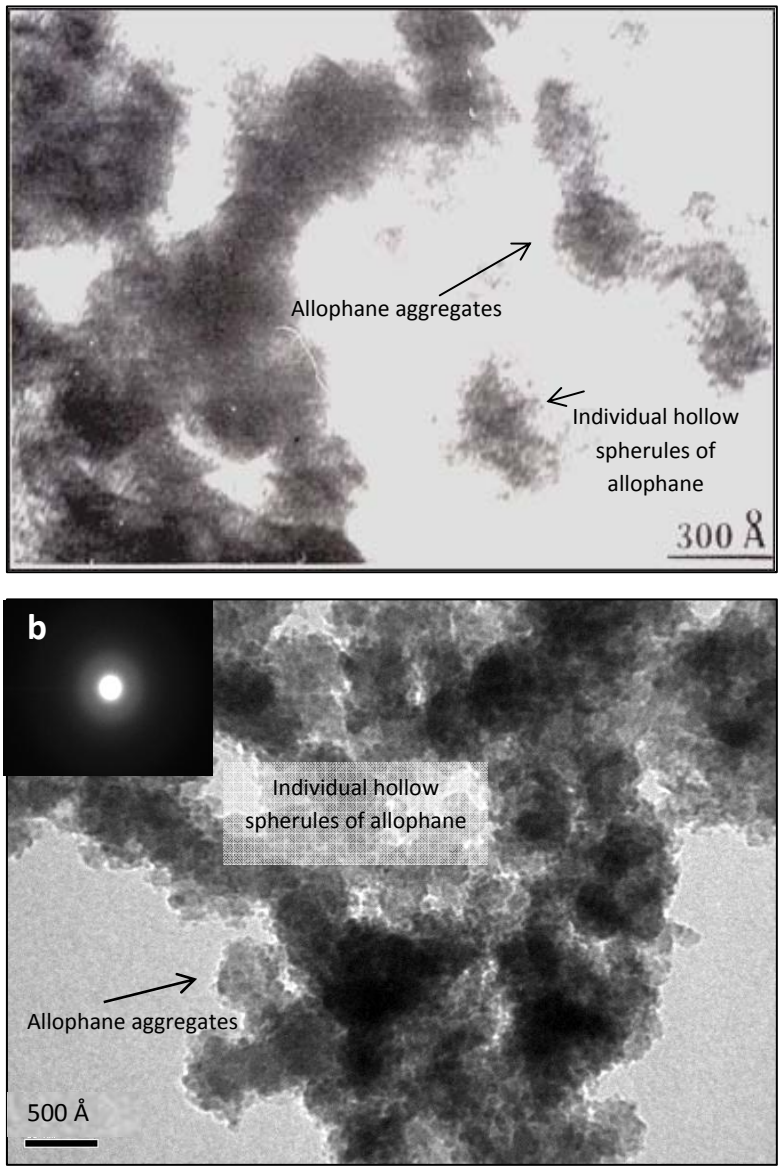

Figure 2. 2. Transmission electron micrographs of synthetic allophane

Top: adapted from Mora et al. (1994); Bottom: unpublished data

The nanosize clay fraction separated from an Andisol (Piedras Negras series) in southern Chile, has an Al/Si ratio of 0.24 and a BET nitrogen surface area of 124 m^2 g^{-1} (unpublished results). The shape of the nitrogen adsorption-desorption curves of this natural nanoclay was very similar to that reported by Montarges-Pelletier et al. (2005) for a synthetic allophane-like material with

an Al/Si ratio < 0.5, indicating a high volume of mesopores, and a wide distribution of pore sizes. The nanoclay has a PZC of 3.8 and an IEP of 7.0. These values are similar to those shown by an iron oxide-coated allophane-like material reported by Mora and co-workers (Mora, 1992; Mora et al., 1994; Jara et al., 2005).

The potential use of allophane nanoparticles and allophanic soils for pollution control has been described by several investigators (Diez et al., 1999, 2005; Vidal et al., 2001; Navia et al., 200*3,* 2005; Yuan and Wu, 2007). Allophane is also potentially useful as a catalyst carrier, deodorizer, humidity-controlling agent, membrane for separating CO_2, and support for enzyme immobilization (Suzuki et al., 2000; Ohashi et al., 2002; Abidin et al., 2007a, 2007b; Calabi Floody et al., 2009). Little information, however, is available about the ability of iron oxide-coated allophane nanoparticles to catalyze the decomposition of organic compounds through Fenton-like reactions.

Ureta-Zañartu et al. (2002) studied the electro-oxidation of chlorophenols using electrodes of glassy carbon (GC) covered with synthetic iron oxide-coated aluminosilicates (AlSiFe-GC) with three different Si/Al ratios and isoelectric points of 3.2, 7.2 and 8.2. The catalytic activity of all three AlSiFe-GC electrodes was similar, indicating that the basicity of AlSiFe did not affect the electrooxidation process. Subsequently, Pizarro et al. (2005) evaluated the catalytic potential of iron oxides, separated from volcanic soils, using the gas- shift reaction of iron in water. More recently, Cea (2006) investigated the decomposition of pentachlorophenol (PCP), 2,4,6-trichlorophenol (2,4,6-TCF) and 2,4-dichlorophenol (2,4-DCF) catalyzed by the clay fraction of an Andisol under ultraviolet radiation. The reaction followed first-order kinetics, the rate of photolysis being dependent on the degree of chlorine substitution, and decreasing in the order: PCP > 2,4,6-TCF > 2,4-DCF.

The stability of iron-oxide coated allophane as heterogeneous catalyst in Fenton-like reactions has not been previously investigated. Our research group has looked into the dissolution of synthetic allophane and its iron-oxide coated counterpart between pH 4 and pH 7. The preliminary data (unpublished) for synthetic allophane showed that 8.6 mg Al and 16 mg Si per gram allophane were dissolved at pH 4.5. The corresponding values for iron-oxide coated allophane were 1.2 mg Al/g and 3.3 mg Si/g. Dissolution decreased dramatically (< 1 mg/g) at near neutral pH, and became negligible at pH > 7. Similary, the stability of iron-rich minerals (as heterogeneous catalyst) is strongly dependent on solution pH. As already mentioned, the solubility of such minerals increases at low pH. On other hand, the iron species incorporated into pillared interlayered clays (PILCs) is relatively resistant to (acid) leaching, and appears to be more stable than its counterpart in zeolites or oxide minerals. This observation may be ascribed strong binding (coordination) of the iron species to the interlayer surface of the clay mineral (De Leon et al., 2008). By the same token, octahedrally coordinated iron within the layer structure of clay minerals is more stable against leaching than exchangeable iron in the interlayer space (Cheng et al., 2007).

2.5. Conclusions

Clays and iron oxide minerals possess structural and surface charge characteristics that are conducive to their use as supports of catalytically active (Fe, Cu) phases, or as solid heterogeneous catalysts for the Fenton-like reaction. These minerals can operate over a wide range of pH and temperature, are easy to separate, and retain activity during successive treatments. The catalytic efficiency of solid catalysts in decomposing organic pollutants through the heterogeneous Fenton-like reaction is influenced by the following factors: concentration and

type of catalyst, surface area of catalyst, hydrogen peroxide concentration, medium temperature, medium pH, and pollutant structure.

The use of nanocatalysts is a promising alternative to conventional catalysis. Because of their large surface area and low diffusional resistance, nanoparticles are more efficient than conventional heterogeneous catalysts. The ability of nanocatalysts to operate in the absence of ultraviolet radiation is an added advantage. Iron oxide-coated allophane nanoparticles can catalyze the degradation of persistent organic pollutants through the Fenton-like reaction, and are useful for treating industrial effluents. The Fenton-like reaction may also be used for *in situ* remediation of contaminated soil, sediment, and groundwater because nanosize clays and iron oxides are ubiquitous in the natural environment.

2.6. References

Abidin, Z., Matsue, N., Henmi, T., 2007a. Differential formation of allophane and imogolite: experimental and molecular orbital study. J. Computer-Aided Mater. Design 14, 15–18.

Abidin, Z., Matsue, N., Henmi, T., 2007b. Nanometer-scale chemical modification of nano-ball allophane. Clays Clay Miner. 55, 443–449.

Andrade, L.S., Ruotolo, L.A.M., Rocha-Filho, R.C., Bocchi, N., Biaggio, S.R., Iniesta, J., García-Garcia, V., Montiel, V., 2007. On the performance of Fe and Fe, F doped Ti-Pt/PbO_2 electrodes in the electrooxidation of the Blue Reactive 19 dye in simulated textile wastewater. Chemosphere 66, 2035–2043.

Andreozzi, R., Caprio, V., Marotta, R., 2002a. Oxidation of 3,4-dihydroxybenzoic acid by means of hydrogen peroxide in aqueous goethite slurry. Water Res. 36, 2761–2768.

Andreozzi, R., D'Apuzzo, A., Marotta, R. 2002b. Oxidation of aromatic substrates in water/goethite slurry by means of hydrogen peroxide. Water Res. 36, 4691–4698.

Araña, J., Pulido, M.P., Rodríguez, L.V.M., Peña, A.A., Doña, R. J.M., González, D.O., Pérez, P.J. 2007. Photocatalytyc degradation of phenol and phenolic compounds Part I. Adsorption and FTIR study. J. Hazard. Mater. 146, 520–528.

Aravindhan R., Fathima N.N., Rao, J.R.; Nair, B.U., 2006. Wet oxidation of acid brown dye by hydrogen peroxide using heterogeneous catalyst Mn-salen-Y zeolite: A potential catalyst. J. Hazard. Mater. 138, 152–159.

Arnold, S.M., Hickey, W.J., Harris, R.F., 1995. Degradation of atrazine by Fenton`s reagent: condition optimization and product quantification. Environ. Sci. Technol. 29, 2083–2089.

Bach, A., Zelmanov, G., Semiat, R., 2008. Cold catalytic recovery of loaded activated carbon using iron oxide-based nanoparticles. Water Res. 42, 163–168.

Baldrian, P., Merhautová, V., Gabriel, J., Nerud, F., Stopka, P., Hrubý,M., Benes, M.J., 2006. Decolorization of synthetic dyes by hydrogen peroxide with heterogeneous catalysis by mixed iron oxides. Appl. Catal. B: Environ. 66, 258–264.

Balmer, M.E., Sulzberger, B. 1999. Atrazine degradation in irradiated iron/oxalate systems: Effects of pH and oxalate. Environ. Sci. Technol. 33, 2418–2424.

Barrault, J., Abdellaoui, M., Bouchoule, C., Majesté, A., Tatibouët, J.M., Louloudi, A., Papayannakos, N., Gangas, N.H., 2000a. Catalytic wet peroxide oxidation over mixed (Al-Fe) pillared clays. Appl. Catal. B: Environ. 27, L225–L230.

Barrault, J., Bouchoule, C., Echachoui, K., Frini-Srasra, N., Trabelsi, M., Bergaya, F., 1998. Catalytic wet peroxide oxidation (CWPO) of phenol over mixed (AlCu)-pillared clays. Appl. Catal. B: Environ. 15, 269–274.

Barrault, J., Tatibouët, J.M., Papayannakos, N., 2000b. Catalytic wet peroxide oxidation of phenol over pillared clays containing iron or copper species. C.R. Acad. Sci. Paris, Sér. IIC, Chemistry 3, 777–783.

Barreiro, J.C., Capelato, M.D., Martin-Neto, L., Hansen, H.C.B., 2007. Oxidative decomposition of atrazine by a Fenton-like reaction in a H_2O_2/ferrihydrite system. Water Res. 41, 55–62.

Barros, A.L., Pizzolato, T.M., Carissimi, E., Schneider, I.A.H., 2006. Decolorizing dye wastewater from the agate industry with Fenton oxidation process. Miner. Eng. 19, 87–90.

Bell, A.T. 2003. The impact of nanoscience on heterogeneous catalysis. Science 299, 1688–1691.

Bergaya, F., Aouad, A., Mandalia, T., 2006. Pillared clays and clay minerals. In: Bergaya, F., Theng, B.K.G., Lagaly, G. (Eds), Handbook of Clay Science. Elsevier, Amsterdam, pp. 393–421.

Bobu, M., Yediler, A., Siminiceanu, I., Schulte-Hostede, S., 2008. Degradation studies of ciprofloxacin on a pillared iron catalyst. Appl. Catal. B: Environ. 83, 15–23.

Bokare, A.D., Chikate, R.C., Rode, V., Paknikar, M., 2008. Iron-nickel bimetallic nanoparticles for reductive degradation of azo dye Orange G in aqueous solution. Appl. Catal. B: Environ. 79, 270–278.

Brigatti, M.F., Galan, F., Theng, B.K.G., 2006. Structures and mineralogy of clay minerals. In: Bergaya, F., Theng, B.K.G., Lagaly, G., (Eds), Handbook of Clay Science. Elsevier, Amsterdam, pp. 19–86.

Calabi Floody, M., Theng, B.K.G., Reyes, P., Mora, M.L., 2009. Natural nanoclays: applications and future trends – a Chilean perspective. Clay Miner. 44, 161–176.

Carriazo, J., Guélou, E., Barrault, J., Tatibouët, J.M., Molina, R., Moreno, S., 2005a. Synthesis of pillared clays containing Al, Al-Fe or Al-Ce-Fe from a bentonite: Characterization and catalytic activity. Catal. Today 107–108, 126–132.

Carriazo, J., Guélou, E., Barrault, J., Tatibouët, J.M., Molina, R., Moreno, S., 2005b. Catalytic wet peroxide oxidation of phenol by pillared clays containing Al–Ce–Fe. Water Res. 39, 3891–3899.

Carriazo, J.G., Guelou, E., Barrault, J., Tatibouët, J.M., Moreno, S., 2003. Catalytic wet peroxide oxidation of phenol over Al-Cu or Al-Fe modified clays. Appl. Clay Sci. 22, 303–308.

Catrinescu, C., Teodosiu, M., Macoveanu, M., Miehe-Brendlé, J., Le Dred, R., 2003. Catalytic wet peroxide oxidation of phenol over Fe-exchanged pillared beidellite. Water Res. 37, 1154–1160.

Caudo, S., Centi, G., Genovese, C., Perathoner, S., 2007. Copper- and iron-pillared clay catalysts for the WHPCO of model and real wastewater streams from olive oil milling production. Appl. Catal. B: Environ. 70, 437–446.

Caudo, S., Centi, G., Genovese, C., Perathoner, S., 2008. Copper-pillared clays (Cu-PILC) for agro-food wastewater purification with H_2O_2. Micropor. Mesopor. Mater. 107, 46–57.

Cea, M., 2006. Mecanismos fisicoquímicos involucrados en la retención de compuestos organoclorados en un suelo alofánico. Doctor en Ciencias de Recursos Naturales, Universidad de La Frontera, Chile.

Centi, G., Perathoner, S., Torre, T., Verduna, M.G., 2000. Catalytic wet oxidation with H_2O_2 of carboxylic acids on homogeneous and heterogeneous Fenton-type catalysts. Catal. Today 55, 61–69.

Chan, K.H., Chu, W., 2005. Model applications and mechanism study on the degradation of atrazine by Fenton's system. J. Hazard. Mater. 118, 227–237.

Chen, A., Ma, X., Sun, H., 2008. Decolorization of KN-R catalyzed by Fe-containing Y and ZSM-5 zeolites. J. Hazard. Mater. 156, 568–575.

Chen, J., Zhu, L., 2006. Catalytic degradation of Orange II by UV-Fenton with hydroxyl-Fe-pillared bentonite in water. Chemosphere 65, 1249–1255.

Chen, J., Zhu, L., 2007. Heterogeneous UV-Fenton catalytic degradation of dyestuff in water with hydroxyl-Fe pillared bentonite. Catal. Today 146, 463–470.

Cheng, M., Ma, W., Li, J., Huang, Y., Zhao, J., Wen, Y., Xu, Y., 2004. Visible-light-assisted degradation of dye pollutants over Fe(III)-loaded resin in the presence of H_2O_2 at neutral pH values. Environ. Sci. Technol. 38, 1569–1575.

Cheng, M., Song, W., Ma, W., Chen, C., Zhao, J., Lin, J., Zhu, H., 2008. Catalytic activity of iron species in layered clays for photodegradation of organic dyes under visible irradiation. Appl. Catal. B: Environ. 77, 355–363.

Childs, C.W., Johnston, J.H., 1980. Mössbauer spectra of proto-ferrihydrite at 77 K and 295 K, and a reappraisal of the possible presence of akaganéite in New Zealand soils. Aust. J. Soil Res. 18, 245–250.

Chirchi, L., Ghorbel, A., 2002. Use of various Fe-modified montmorillonite samples for 4-nitrophenol degradation by H_2O_2. Appl. Clay Sci. 21, 271–276.

Chou, S., Huang, C., 1999. Application of a supported iron oxyhydroxide catalyst in oxidation of benzoic acid by hydrogen peroxide. Chemosphere 38, 2719–2731.

De León, M.A., Castiglioni, J., Bussi, J., Sergio, M., 2008. Catalytic activity of an iron-pillared montmorillonitic clay mineral in heterogeneous photo-Fenton process. Catal. Today 133–135, 600–605.

Deng, Y., 2007. Physical and oxidative removal of organics during Fenton treatment of mature municipal landfill leachate. J. Hazard. Mater. 146, 334–340.

Deng, Y., Englehardt, J.D., 2006. Treatment of landfill leachate by the Fenton process. Water Res. 40, 3683–3694.

Dhakshinamoorthy, A., Pitchumani, K., 2008. Clay entrapped nickel nanoparticles as efficient and recyclable catalysts for hydrogenation of olefins. Tetrahedron Lett. 49, 1818–1823.

Díaz, P., Galindo, G., Escudey, M., 1990. Sintesis de aluminosilicatos semejantes a los existentes en suelos volcanicos. Bol. Soc. Chil. Quim. 35, 385–389.

Diez, M.C., Mora, M.L., Videla, S., 1999. Adsorption of phenolic compounds and color from bleached kraft mill effluent using allophanic compounds. Water Res. 33, 125–130.

Diez, M.C., Quiroz, A., Ureta-Zañartu, S., Vidal, G., Mora, M.L., Gallardo, F., Navia, R., 2005. Soil retention capacity of phenols from biologically pre-treated kraft mill wastewater. Water, Air, Soil Pollut.163, 325–339.

Doocey, D.J., Sharratt, P.N., Cundy, C.S., Plaisted, R.J., 2004. Zeolite-mediated advanced oxidation of model chlorinated phenolic aqueous waste Part 2: Solid phase catalysis. Process Safety Environ. Prot. 82, 359–364.

Du, Z., Feng, C., Li, Q., Zhao, Y., Tai, X., 2008. Photodegradation of NPE-10 surfactant by Au-doped nano-TiO_2. Colloids Surfaces A: Physicochem. Eng. Aspects 315, 254–258.

El-Hamshary, H., El-Sigeny, S., Abou Taleb, M.F., El-Kelesh, N.A., 2007. Removal of phenolic compounds using (2-hydroxyethyl methacrylate/acrylamidopyridine) hydrogel prepared by gamma radiation. Sep. Purif. Technol. 57, 329–337.

Farjerwerg, K., Castan, T., Foussard, J-N., Perrard, A., Debellefontaine, H., 2000. Dependency on some operating parameters during wet oxidation of phenol by hydrogen peroxide with Fe-ZSM-5 zeolite. Environ. Technol. 21, 337–344.

Farjerwerg, K., Debellefontaine, H., 1996. Wet oxidation of phenol by hydrogen peroxide using heterogeneous catalysis Fe-ZSM-5: a promising catalyst. Appl. Catal. B: Environ. 10, L229–L235.

Farjerwerg, K., Foussard, J-N., Perrard, A., Debellefontaine, H., 1997. Wet oxidation of phenol by hydrogen peroxide: The key role of pH on the catalytic behaviour of Fe-ZSM-5. Water Sci. Technol. 35, 103–110.

Farré, M.J., Doménech, X., Peral, J., 2007. Combined photo-Fenton and biological treatment for Diuron and Linuron removal from water containing humic acid. J. Hazard. Mater. 147, 167–174.

Feng, J., Hu, X., Yue, P.L., Zhu, H.Y., Lu, G.Q., 2003a. Degradation of azo-dye Orange II by a photoassisted Fenton reaction using a novel composite of iron oxide and silicate nanoparticles as a catalyst. Ind. Eng. Chem. Res. 42, 2058–2066.

Feng, J., Hu, X., Yue, P.L., Zhu, H.Y., Lu, G.Q., 2003b. A novel clay-based Fe- nanocomposite and its photo-catalytic activity in photo-assisted degradation of Orange II. Chem. Eng. Sci. 58, 679–685.

Feng, J., Hu, X., Yue, P.L., 2004b. Novel bentonite clay-based Fe-nanocomposite as a heterogeneous catalyst for photo-Fenton discoloration and mineralization of Orange II. Environ. Sci. Technol. 38, 269–275.

Feng, J., Hu, X., Yue, P.L., 2004c. Discoloration and mineralization of Orange II using different heterogeneous catalysts containing Fe: A comparative study. Environ. Sci. Technol. 38, 5773–5778.

Feng, J., Hu, X., Yue, P.L., 2006. Effect of initial solution pH on the degradation of Orange II using clay-based Fe nanocomposites as heterogeneous photo-Fenton catalyst. Water Res. 40, 641–646.

Feng, J., Hu, X., Yue, P.L., Qiao, S., 2009. Photo-Fenton degradation of high concentration Orange II (2 mM) using catalysts containing Fe: A comparative study. Sep. Purif. Technol. 67, 213–217.

Feng, J., Wong, R.S.K., Hu, X., Yue, P.L., 2004a. Discoloration and mineralization of Orange II by using Fe^{3+}-doped TiO_2 and bentonite clay-based Fe nanocatalysts. Catal. Today 98, 441–446.

Fenton, H.J.H., 1894. Oxidation of tartaric acid in the presence of iron. Chem. Soc. J. Lond. 65, 899–910.

Fernandez, J., Bandara, J., Lopez, A., Albers, P., Kiwi, J. 1998. Efficient photo-assisted Fenton catalysis mediated by Fe ions on Nafion membranes active in the abatement of non-biodegradable azo-dye. Chem. Commun., 1493–1494.

Fernandez, J., Bandara, J., Lopez, A., Buffet, Ph, Kiwi, J. 1999. Photoassisted Fenton degradation of nonbiodegradable azo dye (Orange II) in Fe-free solution mediated by cation transfer membranes. Langmuir, 15, 185–192.

Ferrarese, E., Andreottola, G., Oprea, I.A., 2008. Remediation of PAH-contaminated sediments by chemical oxidation. J. Hazard. Mater. 152, 128–139.

Flores, Y., Flores, R., Gallegos, A.A., 2008. Heterogeneous catalysis in the Fenton-type system reactive black 5/H_2O_2. J. Mol. Catal. A. 281, 184–191.

Galindo, G., 1974. Electric charges, sorption of phosphate and cation exchange equilibria in Chilean Dystrandepts. Ph.D Thesis**,** University of California Riverside.

Gallard, H., De Laat, J., 2000. Kinetic modelling of Fe(III)/H_2O_2 oxidation reactions in dilute aqueous solution using atrazine as a model organic compound. Water Res. 34, 3107–3116.

Georgi, A., Kopinke, F.-D., 2005. Interaction of adsorption and catalytic reactions in water decontamination processes Part I. Oxidation of organic contaminants with hydrogen peroxide catalyzed by activated carbon. Appl. Catal. B: Environ. 58, 9–18.

Giordano, G., Perathoner, S., Centi, G., De Rosa, S., Granato, T., Katovic, A., Siciliano, A., Tagarelli, A., Tripicchio, F., 2007. Wet hydrogen peroxide catalytic oxidation of olive oil mill wastewaters using Cu-zeolite and Cu-pillared clay catalysts. Catal. Today 124. 240–246.

Guélou, E., Barrault, J., Fournier, J., Tatibouët, J-M., 2003. Active iron species in the catalytic wet peroxide oxidation of phenol over pillared clays containing iron. Appl. Catal. B: Environ. 44, 1–8.

Gumy, D., Fernández-Ibáñez, P., Malato, S., Pulgarin, C., Enea, O., Kiwi, J. 2005. Supported Fe/C and Fe/Nafion/C catalysts for the photo-Fenton degradation of Orange II under solar irradiation. Catal. Today 101, 375–382.

Halász, J., Hegedüs, M., Kun, É., Méhn, D., Kiricsi, I., 1999. Destruction of chlorobenzenes by catalytic oxidation over transition metal containing ZSM-5 and Y (FAU) zeolites. Stud. Surf. Sci. Catal. 125, 793–800.

Hall, P.L., Churchman, G.J., Theng, B.K.G., 1985. Size distribution of allophone unit particles in aqueous suspensions. Clays Clay Miner. 33, 345–349.

Hanna, K., Kone, T., Medjahdi, G., 2008. Synthesis of the mixed oxides of iron and quartz and their catalytic activities for the Fenton-like oxidation. Catal. Commun. 9, 955–959.

Henmi, T., Wada, K., 1976. Morphology and composition of allophane. Am. Mineral. 61, 379–390.

Huang, H-H., Lu, M-C., Chen, J-N. 2001. Catalytic decomposition of hydrogen peroxide and 2-chlorophenol with iron oxides. Water Res. 35, 2291–2299.

Huu Phu, N., Kim Hoa, T.T., Van Tan, N., Vinh Thang, H., Le Ha, P., 2001. Characterization and activity of Fe-ZSM-5 catalysts for the total oxidation of phenol in aqueous solutions. Appl. Catal. B: Environ. 4, 267–275.

Iurascu, B., Siminiceanu, I., Vione, D., Vicente, M. A., Gil, A., 2009. Phenol degradation in water through a heterogeneous photo-Fenton process catalyzed by Fe-treated laponite. Water Res. 43, 1313–1322.

Jara, A.A., Goldberg, S., Mora, M.L., 2005. Studies of the surface charge of amorphous aluminosilicates using surface complexation models. J. Colloid Interface Sci. 292, 160–170.

Joo, S.H., Zhao, D., 2008. Destruction of lindane and atrazine using stabilized iron nanoparticles under aerobic and anaerobic conditions: Effects of catalyst and stabilizer. Chemosphere 70, 418–425.

Kanel, S.R., Neppolian, B., Jung, H., Choi, H., 2004. Comparative removal of polycyclic aromatic hydrocarbons using iron oxide and hydrogen peroxide in soil slurries. Environ. Eng. Sci. 21, 741–751.

Kasiri, M.B., Aleboyeh, H., Aleboyeh, A., 2008. Degradation of Acid Blue 74 using Fe-ZSM5 zeolite as a heterogeneous photo-Fenton catalyst. Appl. Catal. B: Environ. 84, 9–15.

Kitis, M., Kaplan, S.S., 2007. Advanced oxidation of natural organic matter using hydrogen peroxide and iron-coated pumice particles. Chemosphere 68, 1846–1853.

Kloprogge, J.T., 1998. Synthesis of smectites and porous pillared clay catalysts: A review. J. Porous Mater. 5, 5–41.

Kong, S-H., Watts, R.J., Choi, J-H., 1998. Treatment of petroleum-contaminated soils using iron mineral catalyzed hydrogen peroxide. Chemosphere 37, 1473–1482.

Kurt, U., Apaydin, O., Gonullu, M.T., 2007. Reduction of COD in wastewater from an organized tannery industrial region by electro-Fenton process. J. Hazard. Mater. 143, 33–40.

Kušić, H., Koprivanac, N., Selanec, I., 2006. Fe-exchanged zeolite as the effective heterogeneous Fenton-type catalyst for the organic pollutant minimization: UV irradiation assistance. Chemosphere 65, 65–73.

Kuznestsova, E.V.P., Vanina, M.P., Preis, S., 2008. The activation of heterogeneous Fenton-type catalyst Fe-MFI. Catal. Commun. 9, 381–385.

Kwan, W.P., Voelker, B.M., 2002. Decomposition of hydrogen peroxide and organic compounds in the presence of dissolved iron and ferrihydrite. Environ. Sci. Technol. 36, 1467–1476.

Kwan, W.P., Voelker, B.M., 2003. Rates of hydroxyl radical generation and organic compound oxidation in mineral-catalyzed Fenton-like systems. Environ. Sci. Technol. 37, 1150–1158.

Kwan, W.P., Voelker, B.M., 2004. Influence of electrostatics on the oxidation rates of organic compounds in heterogeneous Fenton systems. Environ. Sci. Technol. 38, 3425–3431.

Kwon, S.C., Fan, M., Wheelock, T.D., Saha, B., 2007. Nano- and micro-iron oxide catalysts for controlling the emission of carbon monoxide and methane. Sep. Purif. Technol. 58, 40–48.

Larachi, F., Lévesque, S., Sayari, A., 1998. Wet oxidation of acetic acid by H_2O_2 catalyzed by transition metal-exchanged NaY zeolites. J. Chem. Technol. Biotechnol. 73, 127–130.

Lee, B.D., Iso, M., Hosomo, M., 2001. Prediction of Fenton oxidation positions in polycyclic aromatic hydrocarbons by Frontier electron density. Chemosphere 42, 431–435.

Li, Y., Lu, Y., Zhu, X., 2006. Photo-Fenton discoloration of the azo dye X-3B over pillared bentonites containing iron. J. Hazard. Mater. 132, 196–201.

Lee, C., Yoon, J., 2004. Temperature dependence of hydroxyl radical formation in the *hv*/Fe^{3+}/H_2O_2 and Fe^{3+}/H_2O_2 systems. Chemosphere 56, 923–924.

Li, Y.C., Bachas, L.G., Bhattacharyya, D., 2007. Selected chloro-organic detoxifications by polychelate (poly(acrylic acid)) and citrate-based Fenton reaction at neutral pH environment. Ind. Eng. Chem. Res. 46, 7984–7992.

Lin, S.-S., Gurol, M.D., 1998. Catalytic decomposition of hydrogen peroxide on iron oxide: kinetics, mechanism, and implications. Environ. Sci. Technol. 32, 1417–1423.

Lines, M.G., 2008. Nanomaterials for practical functional uses. J. Alloys Compd. 449, 242–245.

Liou, M-J., Lu, M-C., 2008. Catalytic degradation of explosives with goethite and hydrogen peroxide. J. Hazard. Mater. 151, 540–546.

Liou, R-M., Chen, S-H., Hung, M-Y., Hsu, C-S., Lai, J-Y., 2005. Fe (III) supported on resin as effective catalyst for the heterogeneous oxidation of phenol in aqueous solution. Chemosphere 59, 117–125.

Liu, W-T., 2006. Nanoparticles and their biological and environmental applications. J. Biosci. Bioeng. 102, 1–7.

Lu, F., Liu, J., Xu, J., 2008. Synthesis of chain-like Ru nanoparticle arrays and its catalytic activity for hydrogenation of phenol in aqueous media. Mater. Chem. Phys. 108, 369–374.

Lu, M-C., Chen, J-N., Huang, H-H., 2002. Role of goethite dissolution in the oxidation of 2-chlorophenol with hydrogen peroxide. Chemosphere. 46, 131–136.

Mahmoodi, N.M., Arami, M., Limaee, N.Y., Gharanjig, K., Nourmohammadian, F., 2007. Nanophotocatalysis using immobilized titanium dioxide nanoparticle: Degradation and mineralization of water containing organic pollutant: Case study of Butachlor. Mater. Res. Bull. 42, 797–806.

Makhotkina, O.A., Kuznetsova, E.V., Preis, S.V., 2006. Catalytic detoxification of 1,1-dimethylhydrazine aqueous solutions in heterogeneous Fenton system. Appl. Catal. B: Environ. 68, 85–91.

Malato, S., Blanco, J., Maldonado, M.I., Oller, I., Gernjak, W., Pérez-Estrada, L., 2007. Coupling solar photo-Fenton and biotreatment at industrial scale: Main results of a demonstration plant. J. Hazard. Mater. 146, 440–446.

Mamalis, A.G., 2007. Recent advances in nanotechnology. J. Mater. Process. Technol. 181, 52–58.
Martínez, F., Calleja, G., Melero, J.A., Molina, R., 2007. Iron species incorporated over different silica supports for the heterogeneous photo-Fenton oxidation of phenol. Appl. Catal. B: Environ. 70, 452–460.

Matta, R., Hanna, K., Chiron, S., 2007. Fenton-like oxidation of 2,4,6-trinitrotoluene using different iron minerals. Sci. Total Environ. 385, 242–251.

Mecozzi, R., Di Palma, L., De Filippis, P., 2008. Effect of modified Fenton treatment on the thermal behavior of contaminated harbor sediments. Chemosphere 71, 843–852.

Mishra, T., Parida, K.M., Rao, S.B., 1996. Transition metal oxide pillared clay: 1. A comparative study of textural and acidic properties of Fe(III) pillared montmorillonite and pillared acid activated montmorillonite. J. Colloid Interface Sci. 183, 176–183.

Mishra, T., Mohapatra, P., Parida, K.M., 2008. Synthesis, characterisation and catalytic evaluation of iron-manganese mixed oxide pillared clay for VOC decomposition reaction. Appl. Catal. B: Environ. 79, 279–285.

Miyazaki, K., Islam, N., 2007. Nanotechnology systems of innovation – An analysis of industry and academia research activities. Technovation 27, 661–675.

Montarges-Pelletier, E., Bogenez, S., Pelletier, M., Razafitianamaharavo, A., Ghanbaja, J., Lartiges, B., Michot, L., 2005. Synthetic allophane-like particles: textural properties. Colloids and Surfaces A: Physicochem. Eng. Aspects 255, 1–10.

Mora, M.L., Escudey, M., Galindo, G., 1994. Sintesis y caracterización de suelos alofanicos. Bol. Soc. Chil.Quim. 39, 237–243.

Mora, M.L., 1992. Sintesis, caracterización y reactividad de un suelo alofanico modelo. Departamento de Química, Universidad de Santiago de Chile.

Muthuvel, I., Swaminathan, M., 2008. Highly solar active Fe(III) immobilised alumina for the degradation of Acid Violet 7. Sol. Energy Mater. Sol. Cells 92, 857–863.

Navia, R., Fuentes, B., Lorber, K.E., Mora, M.L, Diez, M.C., 2005. In-series columns adsorption performance of Kraft mill wastewater pollutants onto volcanic soil. Chemosphere 60, 870–878.

Navia, R., Levet, L., Mora, M.L., Vidal, G., Diez, M.C., 2003. Allophanic soil adsorption system as a bleached kraft mill aerobic effluent post-treatment. Water, Air Soil Pollut. 148, 323–333.

Neamtu, M., Catrinescu, C., Kettrup, A., 2004a. Effect of dealumination of iron(III)-exchanged Y zeolites on oxidation of Reactive Yellow 84 azo dye in the presence of hydrogen peroxide. Appl. Catal. B: Environ. 51, 149–157.

Neamtu, M., Zaharia, C., Catrinescu, C., Yediler, A., Macoveanu, M., Kettrup, A., 2004b. Fe-exchanged Y zeolite as catalyst for wet peroxide oxidation of reactive azo dye Procion Marine H-EXL. Appl. Catal. B: Environ. 48, 287–294.

Nogueira, R,F.P., Trovó, A.G., da Silva, M.R.A., Villa, R.D., de Oliveira, M.C., 2007. Fundamentos e aplicações ambientais dos processos Fenton e foto-Fenton. Quim. Nova. 30, 400–408.

Noorjahan, M., Kumari, V.D., Subrahmanyam, M., Panda, L., 2005. Immobilized Fe(III)-HY: an efficient and stable photo-Fenton catalyst. Appl. Catal. B: Environ. 57, 291–298.

Núñez, L., García-Hortal, J.A., Torrades, F., 2007. Study of kinetic parameters related to the decolourization and mineralization of reactive dyes from textile dyeing using Fenton and photo-Fenton processes. Dyes Pigm. 75, 647–652.

Nurmi, J., Tratnyek, P.G., Sarathy, V., Baer, D.R., Amonette, J.E., Pecher, K., Wang, C., Linehan, J.C., Matson, D.W., Penn, R.L., Driessen, M.D., 2005. Characterization and properties of metallic iron nanoparticle: Spectroscopy, electrochemistry, and kinetics. Environ. Sci. Technol. 39, 1221–1230.

Nutt, M.O., Heck, K.N., Alvarez, P., Wong, M.S., 2006. Improved Pd-on-Au bimetallic nanoparticle catalysts for aqueous-phase trichloroethene hydrodechlorination. Appl. Catal. B: Environ. 69, 115–125.
Ohashi, F., Wada, S.-I., Suzuki, M., Maeda, M., Tomura, S., 2004. Synthetic allophane from high-concentration solutions: nanoengineering of the porous solid. Clay Miner. 37, 451–456.

Oller, L., Malato, S., Sánchez-Pérez, J.A., Gernjak, W., Maldonado, M.L., Pérez-Estrada, L.A., Pulgarín, C., 2007a. A combined solar photocatalytic-biological field system for the mineralization of an industrial pollutant at pilot scale. Catal. Today 122, 150–159.

Oller, I., Malato, S., Sánchez-Pérez, J.A., Maldonado, M.L., Gassó, R., 2007b. Detoxification of wastewater containing five common pesticides by solar AOPs–biological coupled system. Catal. Today 129, 69–78.

Ortiz de la Plata, G.B., Alfano, O.M., Cassano, A.E., 2008. Optical properties of goethite catalyst for heterogeneous photo-Fenton reactions. Comparison with a titanium dioxide catalyst. Chem. Eng. J. 137, 396–410

Ovejero, G., Sotelo, J.L., Martínez, F., Gordo, L., 2001a. Novel heterogeneous catalysts in the wet peroxide oxidation of phenol. Water Sci. Technol. 44, 153–160.

Ovejero, G., Sotelo, J.L., Martínez, F., Melero, J.A., Gordo, L., 2001b. Wet peroxide oxidation of phenolic solutions over different iron-containing zeolitic materials. Ind. Eng. Chem. Res. 40, 3921–3928.

Pan, J., Wang, C., Guo, S., Li, J., Yang, Z., 2008. Cu supported over Al-pillared interlayer clays catalysts for direct hydroxylation of benzene to phenol. Catal. Commun. 9, 176–181.

Parfitt, R.L., 1990. Allophane in New Zealand – A review. Aust. J. Soil Res. 28, 343–360.

Parks, G.A., 1967. Aqueous surface chemistry of oxides and complex oxide minerals. Isoelectric point and zero point of charge. Adv. Chem. Ser. 67, 121–160.

Pérez-Estrada, L.A., Malato, S., Agüera, A., Fernández-Alba, A.R., 2007. Degradation of dipyrone and its main intermediates by solar AOPs Identification of intermediate products and toxicity assessment. Catal. Today 129, 207–214.

Perez, J.M., 2007. Iron oxide nanoparticles hidden talent. Nature Nanotech. 2, 535–536.

Pignatello, J.J., 1992. Dark and photoassisted Fe^{3+}-catalyzed degradation of chlorophenoxy herbicides by hydrogen peroxide. Environ. Sci. Technol. 26, 944–951.

Pizarro, C., Escudey, M., Moya, S.A., Fabris, J.D., 2005. Iron oxides from volcanic soils as potential catalysts in the water gas shift reaction. J. AIP Conf. Proceedings 756, 56–59.

Popiel, S., Witkiewicz, Z., Chrzanowski, M., 2008. Sulfur mustard destruction using ozone, UV, hydrogen peroxide and their combination. J. Hazard. Mater. 153, 37–43.

Primo, O., Rivero, M.J., Ortiz, I., 2008a. Photo-Fenton process as an efficient alternative to the treatment of landfill leachates. J. Hazard. Mater. 153, 834–842.

Primo, O., Rueda, A., Rivero, M.J., Ortiz, I., 2008b. An integrated process, Fenton reaction ultrafiltration, for the treatment of landfill leachate: Pilot plant operation and analysis. Ind. Eng. Chem. Res. 47, 946–952.

Pulgarin, C., Peringer, P., Albers, P., Kiwi, J., 1995. Effect of Fe-ZSM-5 zeolite on the photochemical and biochemical degradation of 4-nitrophenol. J. Mol. Catal. A: Chem. 95, 61–74.

Ramírez, J.H., Costa, C.A., Madeira, L.M., Mata, G., Vicente, M.A., Rojas-Cervantes, M.L., López-Peinado, A.J., Martín-Aranda, R.M., 2007a. Fenton-like oxidation of Orange II solutions using heterogeneous catalysts based on saponite clay. Appl. Catal. B: Environ. 71, 44–56.

Ramírez, J.H., Maldonado-Hódar, F.J., Pérez-Cadenas, A.F., Moreno-Castilla, C., Costa, C.A., Madeira, L.M., 2007b. Azo-dye Orange II degradation by heterogeneous Fenton-like reaction using carbon-Fe catalysts. Appl. Catal. B: Environ. 75, 312–323.

Rincón, A-G., Pulgarin, C., 2007. Fe^{3+} and TiO_2 solar-light-assisted inactivation of E. coli at field scale. Implications in solar disinfection at low temperature of large quantities of water. Catal. Today 122, 128–136.

Rios-Enriquez, M., Shahin, N., Durán-de-Bazúa, C., Lang, J., Oliveros, E., Bossmann, S.H., Braun, A.M., 2004. Optimization of the heterogeneous Fenton-oxidation of the model pollutant 2,4-xylidine using the optimal experimental design methodology. Sol. Energy 77, 491–501.

Saltmiras, D.A., Lemley, A.T., 2002. Atrazine degradation by anodic Fenton treatment. Water Res. 36, 5113–5119.

Sanabria, N., Álvarez, A., Molina, R., Moreno, S., 2008. Synthesis of pillared bentonite starting from the Al–Fe polymeric precursor in solid state, and its catalytic evaluation in the phenol oxidation reaction. Catal. Today 133–135, 530–533.

Schwingel de Oliveira, I., Viana, L., Verona, C., Vargas, F. V.L., Nunes, A.C.M., Pires, M., 2007. Alkydic resin wastewaters treatment by Fenton and photo-Fenton processes. J. Hazard. Mater. 146, 564–568.

Shah, S., Dzikovski, B., Shah, V., 2007. Development of a new approach for microbial decontamination of water using modified Fenton's reaction. Environ. Pollut. 148, 674–678.

Siedlecka, E.M., Wieckowska, A., Stepnowski, P., 2007. Influence of inorganic ions on MTBE degradation by Fenton's reagent. J. Hazard. Mater. 147, 497–502.

Sirés, I., Centellas, F., Garrido, J.A., Rodríguez, R.M., Arias, C., Cabot, P-L., Brillas, E., 2007. Mineralization of clofibric acid by electrochemical advanced oxidation processes using a boron-doped diamond anode and Fe^{2+} and UVA light as catalysts. Appl. Catal. B: Environ. 72, 373–381.

Sum, O.S.N., Feng, J., Hu, X., Yue, P.L., 2005. Photo-assisted Fenton mineralization of an azo-dye black 1 using a modified laponite clay-based Fe nanocomposite as a heterogeneous catalyst. Top. Catal. 33, 233–242.

Suzuki, M., Ohashi, F., Inukai, K., Maeda, M., Tomura, S., Mizota, T., 2000. Hydration enthalpies of inorganic porous materials with different structures. Mineral. J. 22, 1–10.

Tekbas, M., Yatmaz, H.C., Bektas, N., 2008. Heterogeneous photo-Fenton oxidation of reactive azo dye solutions using iron exchanged zeolite as a catalyst. Micropor. Mesopor. Mater. 115, 594–602.

Theng, B.K.G., Yuan, G., 2008. Nanopaticles in the soil environment. Elements 4, 395–399.

Ting, W-P., Huang, Y-H., Lu, M-C., 2007. Catalytic treatment of petrochemical wastewater by electroassisted Fenton technologies. React. Kinet. Catal. Lett. 92, 41–48.

Ureta-Zañartu, M.S., Mora, M.L., Diez, M.C., Berríos, C., Ojeda, J., Gutiérrez, C., 2002. Chlorophenol electrooxidation on iron oxide-covered aluminosilicates deposited on glassy carbon. J. Appl. Electrochem. 32, 1211–1218.

Valdés-Solís, T.P., Valle-Vigón, P., Sevilla, M., Fuertes, A.B., 2007a. Encapsulation of nanosized catalysts in the hollow core of a mesoporous carbon capsule. J. Catal. 251, 239–243.

Valdés-Solís, T.P., Valle-Vigón, P., Álvarez, S., Marbán, G., Fuertes, A.B., 2007b. Manganese ferrite nanoparticles synthesized through a nanocasting route as a highly active Fenton catalyst. Catal. Commun. 8, 2037–2042.

Valkaj, K.M., Katović, A., Zrnčević,, S., 2007. Investigation of the catalytic wet peroxide oxidation of phenol over different types of Cu/ZSM-5 catalyst. J. Hazard. Mater. 144, 663–667.

Ventura, A., Jacquet, G., Bermond, A., Camel, V., 2002. Electrochemical generation of the Fenton's reagent: application to atrazine degradation. Water Res. 36, 3517–3522.

Vidal, G., Navia, R., Levet, L., Mora, M.L., Diez, M.C., 2001. Kraft mill anaerobic color enhancement by a fixed-bed adsorption system. Biotechnol. Lett. 23, 861–865.

Wada, S-I., Wada, K., 1977. Density and structure of allophane. Clay Miner. 12, 289–298.

Watts, R.J., Dilly, S.E., 1996. Evaluation of iron catalysts for the Fenton-like remediation of diesel-contaminated soils. J. Hazard. Mater. 51, 209–224.

Watts, R.J., Kong, S., Dippre, M., Barnes, W.T., 1994. Oxidation of sorbed hexachlorobenzene in soils using catalyzed hydrogen peroxide. J. Hazard. Mater. 39, 33–47.

Watts, R.J., Stanton, P.C., Howsawkeng, J., Teel, A.L., 2002. Mineralization of a sorbed polycyclic aromatic hydrocarbon in two soils using catalyzed hydrogen peroxide. Water Res. 36, 4283–4292.

Wu, J.J., Muruganandham, M., Yang, J.S., Lin, S.S., 2006. Oxidation of DMSO on goethite catalyst in the presence of H_2O_2 at neutral pH. Catal. Commun. 7, 901–906.

Yang, L.B., Shen, Y.H., Xie, A.J., Liang, J.J., Zhang, B.C., 2008. Synthesis of Se nanoparticles by using TSA ion and its photocatalytic application for decolorization of cango red under UV irradiation. Mater. Res. Bull. 43, 572–585.

Yeh, C. K-J., Hsu, C-Y., Chiu, C-H., Huang, K-L., 2008. Reaction efficiencies and rate constants for the goethite-catalyzed Fenton-like reaction of NAPL-form aromatic hydrocarbons and chloroethylenes. J. Hazard. Mater. 151, 562–569.

Yuan, G., Wu, L., 2007. Allophane nanoclay for the removal of phosphorus in water and wastewater. Sci. Technol. Adv. Mater. 8, 60–62.

Zelmanov, G., Semiat, R., 2008. Iron(3) oxide-based nanoparticles as catalysts in advanced organic aqueous oxidation. Water Res. 42, 492–498.

Zeep, R.G., Faust, B.C., Hoigne, J., 1992. Hydroxyl radical formation in aqueous reactions (pH 3-8) of iron(II) with hydrogen peroxide: the photo-Fenton reaction Environ. Sci. Technol. 26, 313–319.

Zrnčević, S., Gomzi, Z., 2005. CWPO: An environmental solution for pollutant removal from wastewater. Ind. Eng. Chem. Res. 44, 6110–6114.

3

Catalytic oxidation of phenol by the Fenton-like reaction over iron or copper oxide-supported allophane clay materials: influence of catalyst SiO_2/Al_2O_3 ratio

Catalytic oxidation of phenol by the Fenton-like reaction over iron or copper oxide-supported allophane clay materials: influence of catalyst SiO_2/Al_2O_3 ratio

Elizabeth G. Garrido-Ramirez[a], M.V. Sivaiah[b], Joël Barrault[b], Sabine Valange[b], Benny.K.G. Theng[c], Maria Soledad Ureta-Zañartu[d] and María de la Luz Mora[a]

[a]Scientific and Technological Bioresource Nucleus (BIOREN),Universidad de La Frontera, Av. Francisco Salazar 01145, Temuco, Chile

[b]Laboratoire de Catalyse en Chimie Organique, CNRS UMR6503, ENSIP, 1 Rue Marcel Dore, 86022 Poitiers Cedex, France

[c]Landcare Research, Private Bag 11052, Palmerston North 4442, New Zealand

[d]Facultad de Química y Biología, Departamento de Ciencias del Ambiente, Universidad de Santiago de Chile, Av. Libertador Bernardo O´Higgins 3363, Santiago, Chile

3.1. Abstract

Allophane clay materials with SiO_2/Al_2O_3 ratios of 1.0 (AlSi1) and 2.2 (AlSi2) were synthesized by a co-precipitation route and further impregnated with iron or copper species. The structure of the parent AlSi1 sample is similar to that of a typical Al-rich soil allophane, while the parent AlSi2 material resembles the structure of a hydrous feldspathoid with a large interspherule surface, thereby exhibiting a high surface area. The ability of the various iron or copper-based allophane samples to behave as efficient and stable catalysts in phenol oxidation by Fenton-like reaction was investigated in ambient conditions for the first time. Their structural and textural properties were determined by X-ray diffractometry, N_2 adsorption-desorption at 77 K, electrophoretic mobility measurements, infrared spectroscopy, transmission and scanning electron microscopy, as well as by thermo-gravimetric analysis. The catalytic activity of the iron

or copper oxide-supported allophanes was markedly influenced by their SiO_2/Al_2O_3 ratio and by their respective structure. The iron-based AlSi2 catalysts with tail-like structure and high surface area proved to be far more active than their corresponding AlSi1 counterparts. The highest catalytic efficiency in terms of total organic carbon abatement was obtained at 40°C for the calcined iron oxide-supported AlSi2 allophane sample, for which very low leaching level of iron species was noticed (0.37 mg L^{-1}). By contrast, large differences in terms of catalytic efficiency (conversion rates) and stability were observed for the copper-based counterparts, thereby indicating that the iron oxide-supported allophanes with a hydrous feldspathoid structure are highly active and stable in the phenol oxidation by Fenton-like reaction.

Keywords

Allophane, iron or copper oxide-supported allophane, Fenton-like reaction, phenol oxidation

3.2. Introduction

In being able to generate strongly oxidizing hydroxyl radical species, advanced oxidation processes (AOP) are effective in decomposing a wide range of organic pollutants [1-3]. Typical AOP include ozonation, wet air oxidation, wet peroxide oxidation, Fenton reaction as well as photocatalytic processes. The Fenton reaction involves reacting Fe^{2+} species with H_2O_2 under acidic conditions (pH ~ 3.0) to produce reactive hydroxyl radicals in mild reaction conditions, thereby limiting investment costs. The redox properties of other transition metal ions, such as copper, cerium and manganese can similarly be used to generate hydroxyl radicals from hydrogen peroxide under atmospheric pressure and temperature closed to the ambient [4-6]. However, in this homogeneous Fenton process, many problems typical of homogeneous catalysis

are encountered, such as catalyst separation and regeneration, as well as the application of a strict control of pH to prevent precipitation of iron hydroxide. These drawbacks may be overcome by using Fenton-like heterogeneous catalysts (i.e. solids containing transition metal cations, mostly iron or copper ions) that can operate over a wide range of pH, are easily recovered after use and remain active during successive cycles of reaction [7].

A variety of solid catalysts have been prepared and described on the basis of their activity and stability in the oxidation of various organic pollutants by Fenton-like reaction [2]. Such Fenton-type heterogeneous catalysts include transition metal-exchanged zeolites [7,8], pillared interlayered clays containing iron or copper species [4,9, 10,11-13], activated carbon impregnated with iron or copper oxide [14,15], iron-supported mesostructured silica supports [16,17], iron-based perovskite or spinel oxides [18,19], and iron-oxide minerals [20]. The efficiency and stability of solid catalysts are strongly related to the nature and dispersion of the active phase and the interaction between the active centers and the support. In this respect, catalytic supports exhibiting high surface area, as well as large and uniform pores are preferred because they can facilitate the dispersion of active sites and enhance diffusion of reactants/products in liquid phase reactions [21].

Because of their low cost, abundance and environmentally friendly nature, naturally available iron oxide and iron-based clay minerals can suitably act as catalysts in heterogeneous Fenton reactions [6,22]. Allophane is a clay-size mineral of widespread occurrence in volcanic ash soils. The unit particle of allophane is a hollow spherule with an external diameter between 3.5 and 5.5 nm and a wall thickness of 0.7–1.0 nm. Defects in the wall structure give rise to openings of

about 0.3 nm in diameter [23-26]. Three types of naturally occurring allophane minerals are known to exist: (1) Al-rich soil allophane with an imogolite-like structure and a SiO_2/Al_2O_3 ratio of ~ 1.0; (2) Si-rich soil allophane with a SiO_2/Al_2O_3 ratio of ~ 2.0; and (3), stream-deposit allophane with a hydrous feldspathoid-like structure exhibiting a SiO_2/Al_2O_3 ratio of 1.1.–2.2 [27,28]. Some synthetic aluminosilicates with a SiO_2/Al_2O_3 molar ratio > 2.2 have also been included in the stream-deposit allophane category [29].

Allophane nanoparticles in Chilean Andisols are commonly associated with iron oxide of short range order, among them ferrihydrite, which is a hydrated ferric iron oxide compound [30,31]. This finding has stimulated research on the synthesis of allophane materials and its interaction with iron oxide [31-36]. Besides being a good adsorbent of organic pollutants [37,38], iron oxide-supported allophane can also act as support for enzyme immobilization [39]. In addition, when deposited on a glassy carbon electrode, the iron-based material is able to electro-oxidize phenol [40]. The use of iron oxide-supported allophane clays materials as catalysts in the degradation of organic pollutants by a Fenton-like reaction has been recently reviewed by [41].

The main objective of the present study is to elaborate environmentally friendly catalysts based on allophane-type structure, fulfilling important requirements in the Fenton-like reaction, such as activity in ambient conditions (atmospheric pressure and temperature close to the ambient), stability and low cost. For that purpose, two allophane clay materials with varying SiO_2/Al_2O_3 ratios are synthesized by a co-precipitation route and further act as support for iron or copper oxide. Various characterization techniques, such as X-ray diffraction, nitrogen sorption isotherms, thermal analysis, infrared spectroscopy, electron microscopy coupled to EDX

analyses, as well as electrophoretic mobility measurements are used to evaluate the final structural and textural properties of the parent allophane materials and their corresponding iron or copper oxide-supported counterparts. Their catalytic performances are determined for the first time in total phenol oxidation using hydrogen peroxide as oxidant, with the aim of investigating the influence of the allophane SiO_2/Al_2O_3 ratio on the phenol elimination activity and total organic carbon (TOC) decay. The stability of both iron and copper active species during the catalytic reaction is also evaluated. Phenol is used as a model molecule, because of the high toxicity exhibited by phenolic wastes, which are one of the most prevalent forms of pollutants in waste water stemming from industry.

3.3. Experimental

3.3.1. Supports preparation

Allophane clay materials were synthesized by co-precipitation of potassium silicate and aluminum chloride following the procedures described by Mora *et al.* [31] and Diaz *et al*. [32]. Briefly, 0.47 L of potassium silicate solution (2 mol L^{-1}) was prepared by dissolving 50 g of silica in concentrated KOH (5.3 mol L^{-1}) solution. In parallel, an aluminum chloride solution (2 mol L^{-1}) was prepared by dissolving 14 g of aluminum in 500 mL of HCl (1:1). A given amount of aluminum chloride acting as Al_2O_3 source (45 mmol) was placed in a Teflon beaker to which 330 mL of deionised water was added. A quantity of potassium silicate as silica source (135 mmol) was then added dropwise under continuous stirring. The pH of the suspension was adjusted to pH 5.0 (by addition of HCl or KOH solutions) at a constant temperature (25ºC). After stirring for 45 additional minutes, the suspension was centrifuged and repeatedly washed (by centrifugation) until the supernatant solution was free of chloride. The resulting as-synthesized allophane sample

has a SiO_2/Al_2O_3 ratio of 2.2 (determined by energy dispersive X-ray spectroscopy) and was labelled as AlSi2. Allophane with a SiO_2/Al_2O_3 ratio of ~1.0, designated as AlSi1, was obtained by mixing an aqueous solution of aluminium chloride (2.15 mol L^{-1}) with a solution of potassium silicate (1 mol L^{-1}) as described above.

3.3.2. Iron or copper oxide-supported allophane

AlSi2 sample was impregnate with iron or copper oxide by a wet impregnation method [31], using $Fe(NO_3)_3.9H_2O$ and $Cu(NO_3)_2.3H_2O$ as iron and copper source, respectively. The pH of iron nitrate and copper nitrate stock solutions was fixed to 3.0 and 5.0, respectively. Briefly, appropriate amounts of iron (corresponding to 2 or 6 wt% Fe) or copper nitrate solutions (corresponding to 6 wt% Cu) were added to 2 g of AlSi2 allophane suspension and made up to 60 mL with deionised water. Each solution was then concentrated in a rotary evaporator at 25ºC. The resulting product was separated by centrifugation, homogenized by washing three times with 1 mol L^{-1}KCl solution, before being repeatedly washed with deionised water until no chloride ion was detected in the supernatant solution. The samples, labelled as AlSi2Fe2 (2 wt% of iron), AlSi2Fe6 (6 wt% of iron) and AlSi2Cu6 (6 wt% of copper) were air-dried, ground and oven-dried at 105ºC for 24 h. Portions of the AlSi2Fe6 and AlSi2Cu6 samples were calcined in air at 300ºC for 1 h. The corresponding thermally treated samples were referred to as $AlSi2Fe6_{(T300)}$ and $AlSi2Cu6_{(T300)}$, respectively. The same methodology was used to impregnate the AlSi1 sample with 6 wt% of iron (AlSi1Fe6).

3.3.3. Characterization of the catalysts

The textural properties of the parent allophane materials and of their corresponding synthesized and calcined iron or copper oxide-supported counterparts were evaluated by N_2 adsorption-desorption at 77 K on a Micromeritics ASAP 2010 instrument. Prior to N_2 adsorption, the samples were degassed under vacuum at 250°C for at least 6 hours. The specific surface area was determined from the linear part of the BET plot. The isoelectric point (IEP) values were obtained with a Malvern Zetasizer 2000 instrument, by determining zeta potentials over the pH range 3-10, derived from electrophoretic mobility measurements using 0.5 mg samples in 200 mL of 0.001 mol L^{-1}KCl. The pH was carefully adjusted with 0.01 mol L^{-1} HCl or KOH solutions. Thermogravimetric analysis (TGA) and differential thermogravimetric analysis (DTA) measurements were recorded with a microbalance (Q600 DTA) from 25 to 1000 ºC at a heating rate of 10 ºC min^{-1} in flowing air (100 mL min^{-1}) with 20 mg of sample. Fourier transform infrared spectra (FTIR) were recorded on a Tensor 27 Brucker spectrometer over a wavenumber range of 400−4000 cm^{-1}. Samples were pressed into KBr discs (0.5 mg in 100 mg KBr). Powder X-ray diffraction (XRD) patterns were obtained on a Bruker AXS D5005 equipment using CuKα radiation at 40 KV, 40 mA and in the 2θ values range 10-70°. The surface and morphology of the allophane samples were examined by transmission electron microscopy (TEM) using a Jeol-1200 EXII instrument operating at 120 kV, as well as by scanning electron microscopy (SEM) using a Jeol JSM–S410 apparatus. For SEM analysis, the samples were suspended in analytical grade methanol, sonicated for 5 min before being coated with gold-palladium. Images were obtained at 20 KeV and a magnification of 5000X. Energy dispersive X-ray spectroscopy (EDX) was also

used for Si, Al, Fe and Cu spot detection over the sample surface. The EDX analyses were performed at 20 KeV, an angle of 28.8º and a magnification of 500X.

3.3.4. Catalytic oxidation of phenol

Catalytic tests were performed in ambient conditions (at atmospheric pressure and at 25 or 40°C) in a thermostated semi-batch glass reactor (250 mL) equipped with a stirrer and a pH electrode to continuously monitor the pH value of the reaction solution. For each test, the reactor was loaded with 100 mL of an aqueous phenol solution ($5x10^{-4}$ mol L^{-1}) and 0.1 g of catalyst. Hydrogen peroxide solution (0.1 mol L^{-1}) was added continuously to the phenol solution containing the catalyst at a constant flow rate of 2 mL h^{-1} through a dosimeter over a period of 4 hours for iron-based allophane and 6 hours for copper-based counterparts. The pH was continuously adjusted at 3.7 (case of Fe-loaded catalysts) or at 5.0 (case of copper-based catalysts) and the reaction was performed under air flow (100 mL min^{-1}) bubbling directly through the reaction solution. The extent of phenol oxidation was monitored by gas chromatography (GC) using a GC Varian apparatus, equipped with a flame ionization detector [42]. The total organic carbon (TOC) content was measured with an Omni TOC 4.05 meter equipment. The stability of the iron and copper oxide-supported allophane samples (iron and copper leaching) was systematically evaluated by inductively coupled plasma atomic emission spectrometry (ICP) at the end of the catalytic reaction.

3.4. Results and Discussion

3.4.1. Characterization

3.4.1.1. Allophane clay materials

The chemical composition, textural properties and isoelectric point values of the parent allophanes materials and of their corresponding iron or copper oxide-supported counterparts before or after thermal treatment, are summarized in Table 3.1. For the sake of clarity, the characterization of the structural, textural, morphological, thermal and spectroscopic properties of the parent AlSi1 and AlSi2 allophane samples will be discussed first and those of the analogous impregnated allophane materials will be presented in section 3.4.1.2.

Table 3.1. Chemical composition, textural properties and isoelectric point value of the parent synthesized allophanes and of their corresponding iron or copper oxide-supported counterparts, before or after thermal treatment.

Sample	SiO_2/Al_2O_3 ratio[1]	Chemical composition[1] (wt %)				Textural/charge properties		
		SiO_2	Al_2O_3	Fe_2O_3	CuO	BET surface area (m^2g^{-1})	Total pore volume[2] ($cm^3\ g^{-1}$)	IEP[3]
AlSi1	0.99	49.7	50.3	-	-	< 1	n.d.	7.8
AlSi2	2.2	69.0	31.0	-	-	191	0.477	5.2
AlSi1Fe6	0.98	49.0	50.1	0.9	-	N.D.	N.D.	-
AlSi2Fe2	2.4	66.7	28.5	4.8	-	252	0.492	6.2
AlSi2Fe6	2.6	66.0	25.5	8.5	-	287	0.361	7.0
$AlSi2Fe6_{(T300)}$	2.5	64.6	25.6	9.8	-	199	0.434	-
AlSi2Cu6	2.2	64.9	30.2	-	4.9	183	0.437	7.3
$AlSi2Cu6_{(T300)}$	2.2	63.7	28.6	-	7.7	165	0.431	-

[1] Determined by energy dispersive X-ray spectroscopy

[2] Total pore volume at $P/P_0 = 0.95$

[3] Isoelectric Point derived from eletrophoretic mobility experiments

N. D.. = not determined

Large difference in specific surface area values are observed for the parent AlSi1 and AlSi2 allophane samples, depending on their SiO_2/Al_2O_3 ratio and their respective structure (unit particle). The AlSi2 allophane clay exhibits a BET surface area value of 191 $m^2\ g^{-1}$, while that of

the corresponding AlSi1 sample is less than 1 m^2 g^{-1}. Such a low surface area was already mentioned for a synthetic allophane with a SiO_2/Al_2O_3 ratio of ~ 1.0 [43]. The high surface area of the AlSi2 allophane material is however lower than those reported by Ohashi *et al.* [44], Arai *et al.* [45] and Kaufhold *et al*. [46] for analogous natural and synthetic allophanes (265–542 m^2 g^{-1}). Grinding and heating of the sample may account for a reduction in specific surface areas, as already reported by Kitagawa [23] and Kaufhold *et al.* [46]. The higher BET area of the AlSi2 sample than that of the corresponding AlSi1 counterpart is obviously due to its unit particle structure. Following Khan *et al.* [47], it is suggested that portions of the outer polymerized tetrahedral Si sheet in the AlSi2 allophane material (Fig. 3.1a) project outward from the spherule surface and connect with similar "tails" from adjacent spherules after heating (Fig. 3.2a). As a result, a large interspherule surface is available for adsorption of nitrogen molecules. On the other hand, the AlSi1 sample with a lower SiO_2/Al_2O_3 ratio does not form tail-like structures, because here the outer spherule wall (framework) consists of Al octahedral sheets (Fig. 3.1b). When heated, the unit particles (spherules) of AlSi1 coalesce to form a compact aggregate (Fig. 3.2b), making much of the interspherule surface inaccessible to nitrogen molecules. The proposed mechanism is consistent with the measured BET surface area values of AlSi1 and AlSi2 allophane samples (Table 3.1). Representative SEM micrographs of the parent AlSi1 and AlSi2 allophane materials are shown in Fig. 3.3. The AlSi1 sample exhibits indeed a compact morphology due to the presence of large blocks (Fig 3.3a), while the AlSi2 allophane, constituted by aggregated particles, is relatively porous, in agreement with its high specific surface area (Fig 3.3b). The corresponding TEM micrographs show that the morphology of both allophanes varies according to their SiO_2/Al_2O_3 ratio. TEM image of the AlSi1 sample (Fig. 3.4a) indicates globular compact aggregates of variable size and shape presumably because this aluminium-rich

sample has a gel-like consistency when wet [48]. By contrast, the micrograph of the AlSi2 allophane (Fig. 3.4b) reveals the presence of highly "porous" aggregated particles comprising hollow spherules with an outer diameter of 3−4 nm, as already observed for hydrous feldspathoid allophane materials.

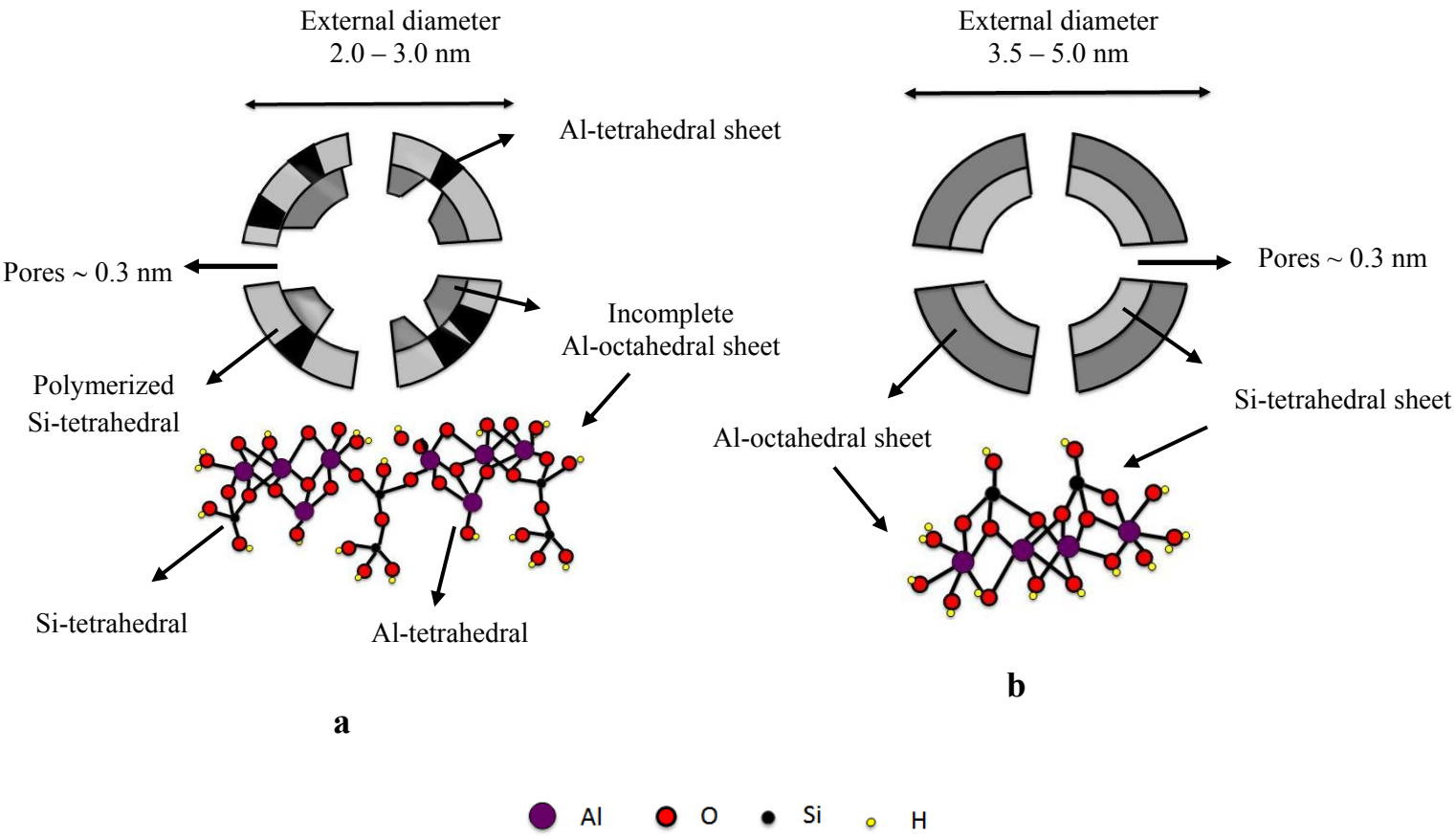

Fig. 3.1. Structure of hydrous feldspathoid-like AlSi2 allophane (a) and Al-rich imogolite-like SiAl1 allophane (b).

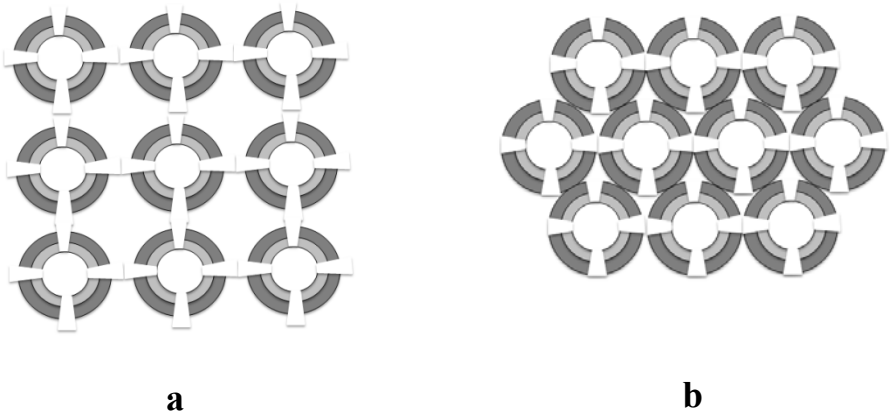

Fig. 3.2. Proposed aggregation state for AlSi2 (a) and AlSi1 (b) allophane materials, induced by heating.

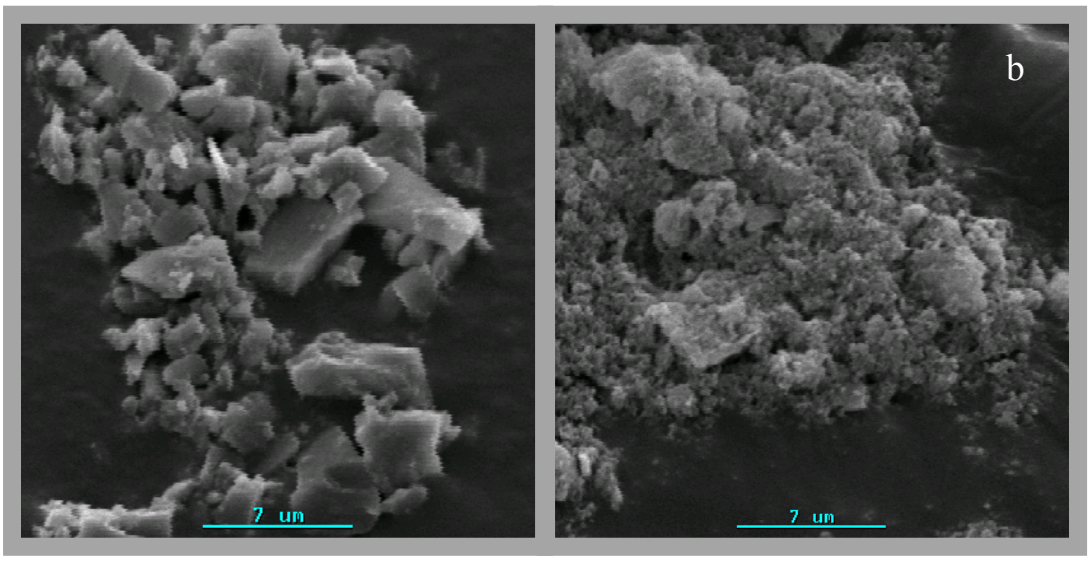

Fig. 3.3. Scanning electron micrographs of the parent AlSi1 (a) and AlSi2 (b) allophane materials.

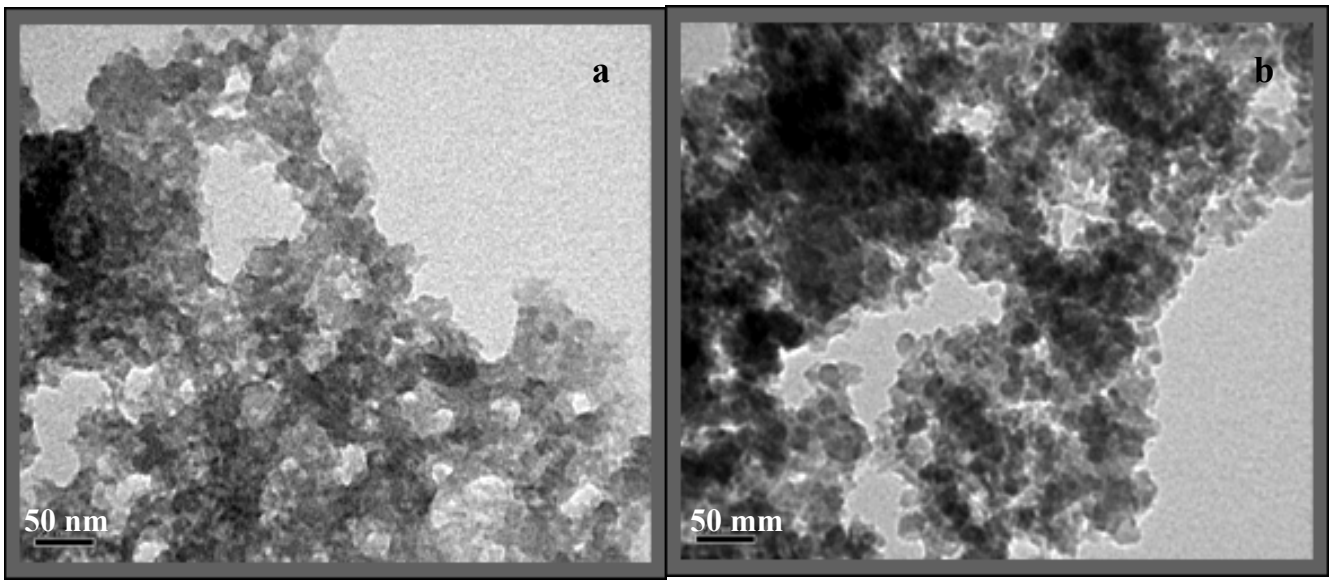

Fig. 3.4. Transmission electron micrographs of the synthesized parent AlSi1 (a) and AlSi2 (b) allophane materials.

X-ray diffraction patterns of the parent AlSi1 and AlSi2 allophanes materials are presented in Fig. 3.5. The X-ray diffractogram of the AlSi1 sample shows broad lines at 3.41, 2.25 and 1.41 Å, characteristic of imogolite-like allophane, whereas the pattern of the AlSi2 material exhibits broad lines centered at 3.32 and 2.25 Å, typical of hydrous feldspathoid allophane [27,28,46,50-52].

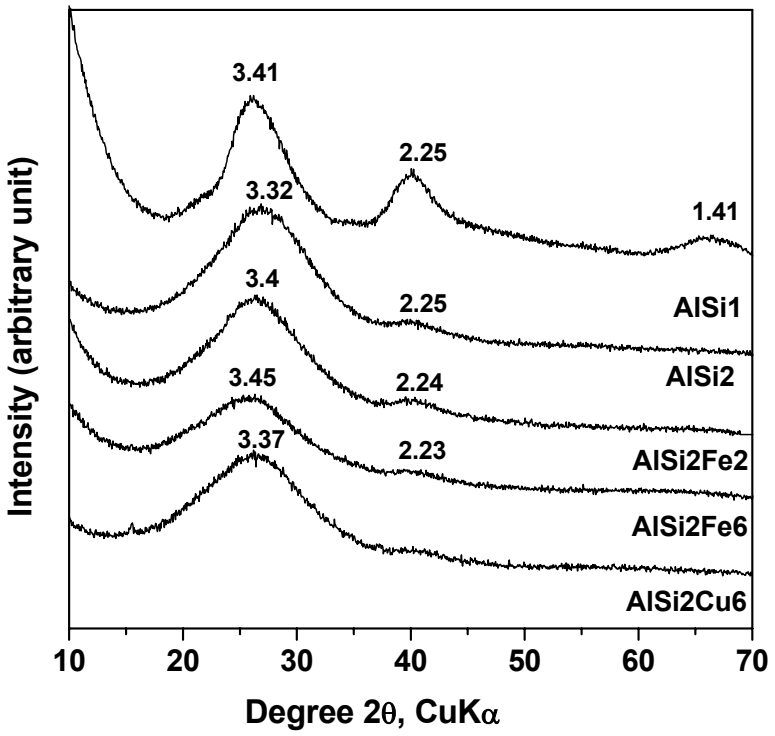

Fig. 3.5. X-ray diffraction patterns of the parent AlSi1 and AlSi2 allophanes and of the corresponding AlSi2 samples impregnated with iron or copper oxide.

Fig. 3.6 shows the TGA (Fig. 3.6a) and DTA curves (Fig. 3.6b) for both allophane materials. The steep weight loss between 25 and 100 ºC is due to dehydration, while the gradual decrease in weight from 100 to 1000 ºC is ascribed to structural dehydroxylation [53]. For all samples, the DTA curves show an endothermic peak in the range of 63−83 ºC coupled to an exothermic peak, whose maximum is ranging from 200 to 300 ºC. These observations are typical of allophane clay materials with SiO_2/Al_2O_3 ratios ranging from 1.0 to 2.0 [51,53-56]. The structural formula of AlSi1 and AlSi2 allophanes, deduced from chemical and thermogravimetric analyses, are shown in Table 3.2.

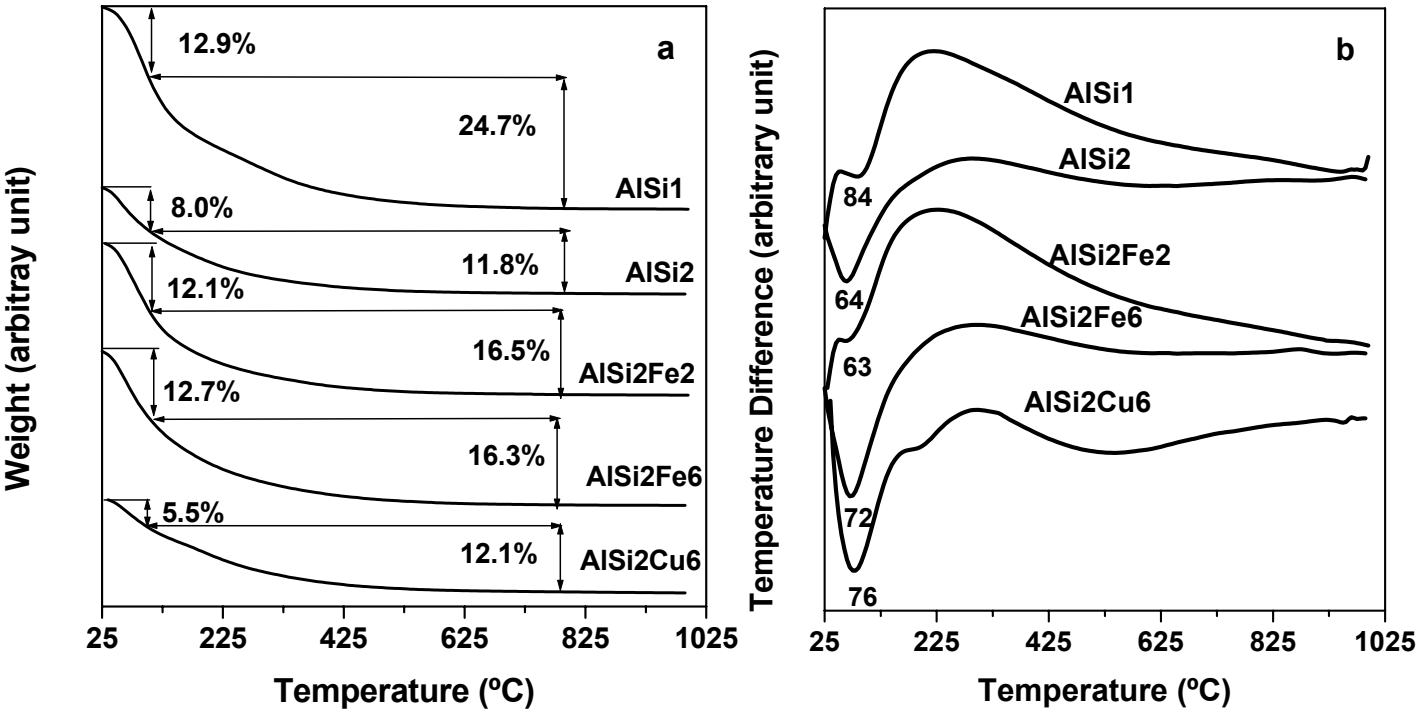

Fig. 3.6. (a) Thermogravimetry curves (a) and differential thermal analysis curves (b) for AlSi1 and AlSi2 allophane samples before and after impregnated with iron or copper oxide.

Table 3.2. Structural formula of the synthesized parent allophanes (AlSi1 and AlSi2) determined from chemical composition and thermogravimetric analysis

Sample	Structural formula
AlSi1	$(Si_{0.99}Al_{2.01}O_{0.02}(OH)_{6.96})\bullet 1.85(H_2O)$
AlSi2	$(Si_{1.38}Al_{1.24}O_{2.5}(OH)_{2.38})\bullet 0.81(H_2O)$

Fig.3.7 shows the IR spectra of the AlSi1 and AlSi2 allophane samples. The broad bands centered at 3490 and 3440 cm^{-1} are assigned to OH stretching vibration of structural hydroxyl groups and adsorbed water. The band near 1640 cm^{-1} is due to OH bending vibration of adsorbed water. The IR spectrum of the parent AlSi1 allophane shows a broad band centered at 968 cm^{-1} and assigned to Si-O or Al-O stretching vibration [31,44]. The band in the 800 to 400 cm^{-1} region may be attributed to the vibration of Al–O and Al–OH groups in the outer Al gibbsitic sheet [43,57] as observed for natural (soil) and synthetic Al-rich imogolite-like allophane materials [27-29,54]. The spectrum of the corresponding parent AlSi2 sample is typical of hydrous feldspathoid allophane, where the outer polymerized Si tetrahedral sheet forms the framework. Partial substitution of Al for Si in tetrahedral sites occurs, while the inner Al octahedral sheet is incomplete (fragmented) as indicated in Fig. 1b [27-29,50,58]. The bands at 1030, 700 and 450 cm^{-1} arise from the tetrahedral aluminosilicate framework, while the band at 590 cm^{-1} is due to octahedral aluminum and the shoulder at 870 cm^{-1} is attributed to Si-OH groups.

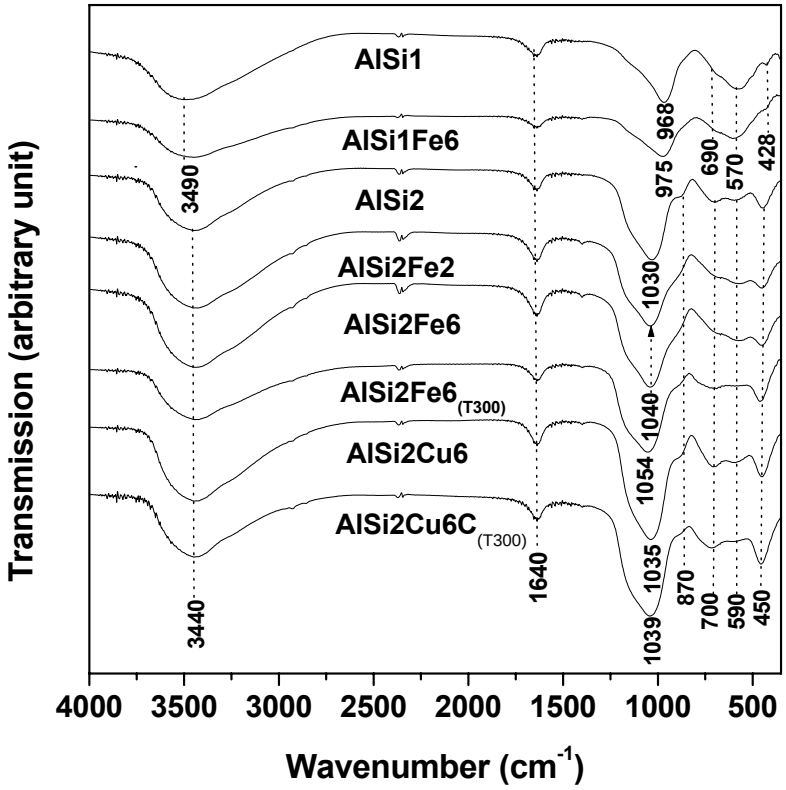

Fig. 3.7. Fourier-transform infrared (FTIR) spectra for the synthesized parent AlSi1 and AlSi2 allophane samples and for their corresponding iron/copper oxide-supported and calcined (at 300°C) counterparts.

3.4.1.2. Iron or copper oxide-supported allophanes

In accordance with previous literature data [31,35], the textural and surface (IEP) properties of the synthetic allophanes are modified when their particles are impregnated with iron species (Table 3.1). These authors have indeed reported that the isoelectric point value of synthetic allophane samples with SiO_2/Al_2O_3 ratio ≈ 2.4 changed from 4.47 for the parent clay material to

8.6 for the iron-supported sample, which suggests a complete coverage of the allophane surface by iron species.

In our study, the amount of iron supported on the surface of the AlSi1 allophane sample is far below the expected value (6 wt%), as shown in Table 3.1. Such a behavior is related to both the structure (unit cell particle) and the corresponding isoelectric point value of the AlSi1 clay sample. Since the IEP value of the parent AlSi1 allophane is much higher (7.8) than that of the analogous parent AlSi2 sample (5.2), there would be less repulsion of $Fe(OH)_2^+$, $FeOH^{2+}$ and Fe^{3+} species in solution at pH 3 by the AlSi2 allophane than with the AlSi1 sample, thereby leading to a higher amount of supported iron species over AlSi2. Data of Table 3.1 indicate that the iron-supported AlSi2 samples (AlSi2Fe2 and AlSi2Fe6) exhibit a resulting IEP value intermediate between that of the untreated parent allophane and that of the coating species (≈ 8.6 for ferrhydrite-like materials) [35,59]. Such result confirms that the external surface of AlSi2Fe2 (IEP 6.2) and AlSi2Fe6 (IEP 7.0) samples is enriched with iron species, while being not completely covered. Mora *et al.* [31] indeed measured an IEP value of 8.6 for synthetic iron-based allophane clay materials that exhibited a complete surface coverage. Following Gil-Llambías and Escudey Castro [60], an apparent surface coverage (ASC) of 27 and 49% was calculated for the AlSi2Fe2 and AlSi2Fe6 samples, respectively. The analogous copper-supported AlSi2 allophane sample (AlSi2Cu6) exhibits an IEP value of 7.3, which results in an ASC of 31%. The observed increase in surface acidity of the allophane nanoparticles, after being impregnated with iron or copper species, may be ascribed to the formation of Si-O-Fe or Si-O-Cu bonds [31,35].

Table 3.1 also shows that the iron-based allophane AlSi2Fe2 and AlSi2Fe6 samples exhibit an increased BET surface area compared with that of the parent AlSi2 clay material, whereas that of the corresponding AlSi2Cu6 sample is similar to the one of the unsupported AlSi2. Komadel and Madejová [61] reported that an acid treatment resulted in an increase of the specific surface area of clay minerals. By contrast, the decrease in surface area of the iron or copper oxide-supported allophanes thermally treated at 300 ^{o}C ($(AlSi2Fe6)_{T300}$ and $(AlSi2Cu6)_{T300}$samples) may be ascribed to the heat-induced reduction in (micro)porosity due to interspherule aggregation, as already shown by Heller-Kallai [62].

Similarly, infrared spectroscopy indicates that the impregnation of iron or copper species on the allophane particles used as support modified their surface properties. Fig. 3.7 shows that the band at 968 cm^{-1} in the spectrum of the parent AlSi1 allophane (attributable to Si-O or Al-O stretching vibration) shifted to 975 cm^{-1} in the spectrum of the iron oxide-supported counterpart (AlSi1Fe6 sample). In the case of the AlSi2sample, the band associated with tetrahedral aluminum (700 and 450 cm^{-1}) was shown to weaken when the allophane material was impregnated with 2 or 6 wt% of iron, while the band due to octahedral aluminum (590 cm^{-1}) intensified. The shoulder at 870 cm^{-1} assigned to Si-OH bond vibration also weakened for the sample with the highest iron content (AlSi2Fe6). These observations may be explained in terms of covalent bond formation between surface $Si\text{-}O^-$ groups and Fe^{3+}, $Fe(OH)_2^+$ as well as $Fe(OH)^{2+}$species in solution, due to the generation of electrostatic attractions, as suggested by Mora *et al.* [31] and Jara *et al.* [35]. Similarly, the changes in the IR spectrum of the copper-based AlSi2 allophane sample may be due to covalent bonding, as a result of electrostatic attractions between the allophane $Si\text{-}O^-$groups and the positively charged Cu^{2+} and $Cu(OH)^+$ species [63].

Wide-angle XRD patterns of the AlSi1 and AlSi2 samples impregnated with iron or copper species exhibit similar characteristics than those of the corresponding parent allophanes (Fig. 3.5). No iron oxide or copper oxide reflections are discernable on the diffractograms, suggesting the exclusive presence of very small dispersed amorphous Fe^{3+} or Cu^{2+} species that cause the classical line broadening on the XRD patterns. Likewise, the XRD patterns of the thermally treated Fe or Cu-based allophones are similar to those obtained for the parent uncalcined samples (not shown).

3.4.2. Catalytic activity

3.4.2.1. Phenol oxidation over iron-supported allophanes

The catalytic activity of the iron-based allophanes (with different SiO_2/Al_2O_3 ratios) was assessed by measuring phenol oxidation in dilute aqueous solution at pH 3.7 by Fenton-like reaction in combination with total organic carbon (TOC) decay. The corresponding results are shown in Fig. 3.8 and Table 3.3. The catalytic activity is first evaluated with the AlSi1 allophane support, giving rise to a minimum phenol removal (16%) and TOC abatement (3%) after 4 h of reaction. Likewise, phenol or TOC decays are not observed in the absence of either catalyst or oxidant (data not shown). With AlSi2 allophane as catalyst, the concentration of phenol and TOC is decayed by 38% and 13% after 4 h of reaction, respectively. The higher efficiency of AlSi2 allophane in phenol decomposition than that of the corresponding AlSi1 sample may be explained in terms of structural and textural differences between both supports. Compared with AlSi1, the AlSi2 allophane exhibits a large surface area coupled to a high pore volume, thereby

favoring the adsorption of more phenol molecules, presumably through hydrogen bonding to superficial silanol groups [64].

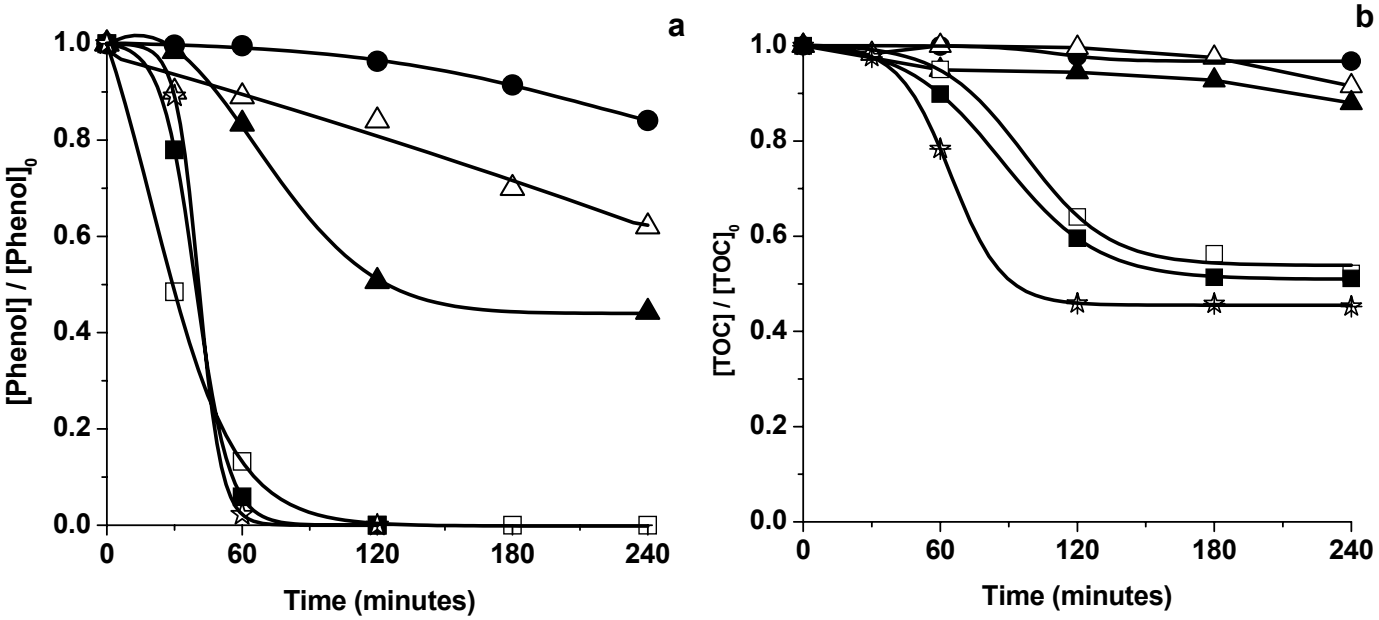

Fig. 3.8. Phenol oxidation (a) and total organic carbon (TOC) decay (b) over 4 h of reaction catalysed by AlSi1 and AlSi2 allophane samples before and after impregnated with iron oxide: AlSi1 (●); AlSi2 (Δ); AlSi1Fe6 (▲); AlSi2Fe2 (□); AlSi2Fe6 (■); and $AlSi2Fe6_{(T300)}$ (✯).

Table 3.3. Phenol conversion, total organic carbon (TOC) decay, mineralization efficiency and Fe leaching for the synthesized parent and iron oxide-supported AlSi2 allophane samples, as well as for their corresponding calcined counterparts.

Sample	Temperature (ºC)	Phenol conversion (%)	TOC decay[1] (%)	Mineralization efficiency (TOC/Phenol)	Dissolved iron in solution (mg L^{-1})	Fe leached (wt%)
AlSi1	25	16 (4h)	3.2	0.20	-	-
AlSi2	25	38 (4h)	13	0.34	-	-
AlSi1Fe6	25	56 (4h)	12	0.21	0.08	1.33
AlSi2Fe2	25	87 (1h)	48	0.48	0.41	1.2
AlSi2Fe6	25	94 (1h)	49	0.49	1.1	1.8
$AlSi2Fe6_{(T300)}$	25	98 (1h)	55	0.55	1.0	1.7
$AlSi2Fe6_{(T300)}$	40	94 (1h)	63	0.63	0.37	0.51

[1] After 4 h of reaction

Except for the iron oxide-supported AlSi1 catalyst (AlSi1Fe6), for which only 56% of phenol is converted at the end of the experiment (Table 3.3), for all iron-based AlSi2 allophane samples, complete phenol oxidation is achieved in less than 2 h of reaction (Fig. 3.8a). Large differences in phenol conversion rates are however noticed, since an induction period is observed for the iron oxide-coated allophane samples, as shown in Fig. 3.8a. The first step in the Fenton-like reaction is the generation of reactive $^{\bullet}OH$ radicals in mild reaction conditions thanks to the Fe^{3+}/Fe^{2+} redox pairs, acting as active sites, on the catalyst surface [21]. In the (heterogeneous) Fenton

process, the reactive hydroxyl $^{\bullet}OH$ radicals are formed from the reaction between $Fe^{2+}$and hydrogen peroxide (Eq. 3.1), whereas they derived from Fe^{3+} in the Fenton-like process. The apparent rate constant of this later reaction is slower than the one of the reaction departing from Fe^{2+}, which may account for the occurrence of an induction period. According to previous work [31,35], the supported iron species on the allophane surface are similar to ferrihydrite-like materials, which are indeed composed of a hydrous ferric oxyhydroxide.

$$Fe^{2+} + H_2O_2 \leftrightarrow Fe^{3+} + {}^{\bullet}OH + OH^- \qquad \text{(Eq. 3.1)}$$

$$C_6H_5OH + {}^{\bullet}OH \rightarrow C_6H_5(OH)_2 \xrightarrow{Fe^{3+} \rightarrow Fe^{2+}} C_6H_4(OH)_2 + H^+ \qquad \text{(Eq. 3.2)}$$

However, as soon as the reactive hydroxyl radicals are generated following Eq. 3.1, the coupling of both processes (Eq. 3.1 and Eq. 3.2) is shown to increase the reaction rate. As expected, an increase in the phenol conversion rate is observed when increasing the AlSi2 allophane iron content. 51% of phenol conversion is reached after 30 min of reaction for the catalyst exhibiting the highest iron content, namely the AlSi2Fe6 sample. Similarly, the rate of TOC decay follows the same trend and increases from the AlSi1Fe6 sample (with an Al-rich soil allophane structure) to the $AlSi2Fe6_{(T300)}$ sample exhibiting a hydrous feldspathoid structure (Fig. 3.8b). The thermally treated iron oxide-supported AlSi2 allophane catalyst indeed exhibits the highest TOC abatement value at 25°C (55%). Taking the ratio of TOC/phenol decay rate as an index of organic compound "mineralization" [65], the mineralization efficiency is shown to decrease in the order: $AlSi2Fe6_{(T300)}$ (0.55) > AlSi2Fe6 (0.49) > AlSi2Fe2 > (0.48) > AlSi2 > (0.34) > AlSi1Fe6 (0.21) > AlSi1 (0.2) (Fig. 3.9 and Table 3.3). Equation (3.2) indicates that phenol is

first converted into hydroquinone and catechol (both represented by $C_6H_4(OH)_2$), that are subsequently oxidized to *o*- and *p*-benzoquinone. As a result, the color of the suspension changed from clear to brownish due to the formation of *p*-benzoquinone as an intermediate product [66]. The principal products of phenol oxidation by Fenton reaction are catechol, hydroquinone, muconic acid, maleic acid, oxalic acid and acetic acid [4,67]. The low conversion rate of these acids [9,68] would account for the observed TOC decay value not exceeding 55% after 4 h reaction at 25ºC.

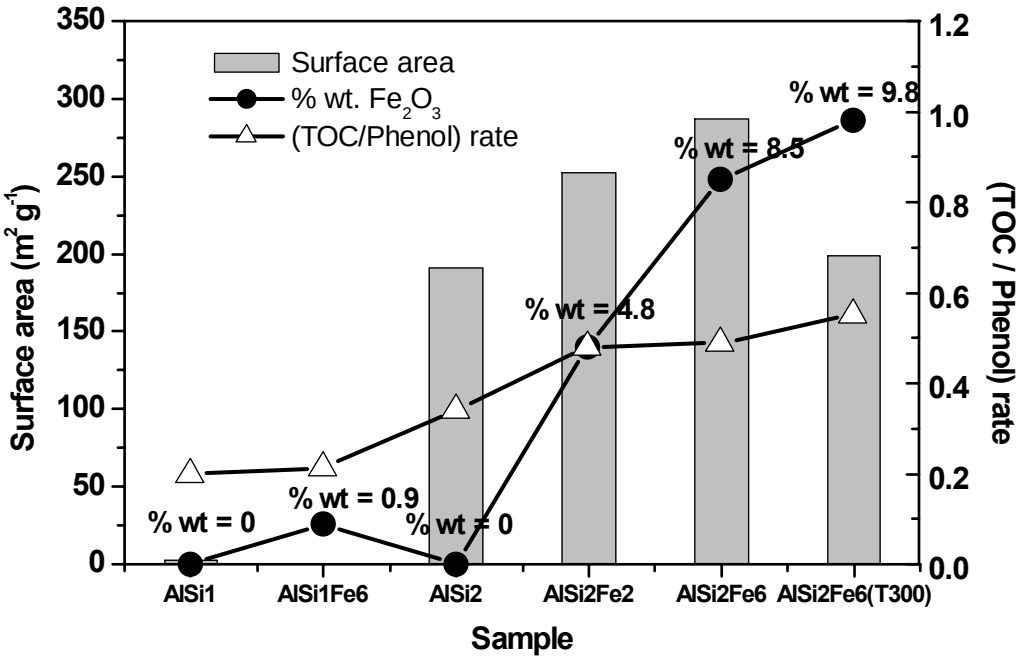

Fig. 3.9. Surface area, mineralization efficiency (TOC/Phenol) and iron oxide content (% wt. Fe_2O_3) for parental AlSi1 and AlSi2 allophanes, iron-based allophane, and iron-based allophane after heating.

The influence of the reaction temperature on the catalytic behavior was then studied with a fresh calcined iron-based allophane, namely the $AlSi2Fe6_{(T300)}$ material, by varying the temperature from 25 to 40°C. The results are presented in Fig. 3.10 and Table 3.3. As expected for an activated oxidation reaction, when the reaction temperature increased, an enhancement of the phenol conversion and TOC abatement rates are observed. Whatever the reaction temperature, the organic pollutant is totally converted after 1 h of reaction, thereby confirming that the $AlSi2Fe6_{(T300)}$ allophane catalyst is very active in total phenol oxidation. The TOC decay (and the mineralization efficiency) is increased up to 63% at 40°C compared to 55% at 25°C after 4 h of reaction. Moreover, very low leaching level of iron species is observed (0.37 mg L^{-1}, corresponding to 0.52% of the initial Fe content), which indicates that the active phase is stable in the reaction medium at 40°C. With the purpose to quantify the effect of dissolved iron species in the reaction medium (homogeneous catalysis), the catalytic activity was evaluated in a solution containing 0.4 mg L^{-1} of Fe^{3+}, giving rise to a minimum TOC conversion (10%) after 4 h of reaction. No additional experiments were conducted at higher temperature, because the catalyst efficiency would decline when the reaction temperature exceeds 70ºC, due to hydrogen peroxide decomposition into O_2 and H_2O.

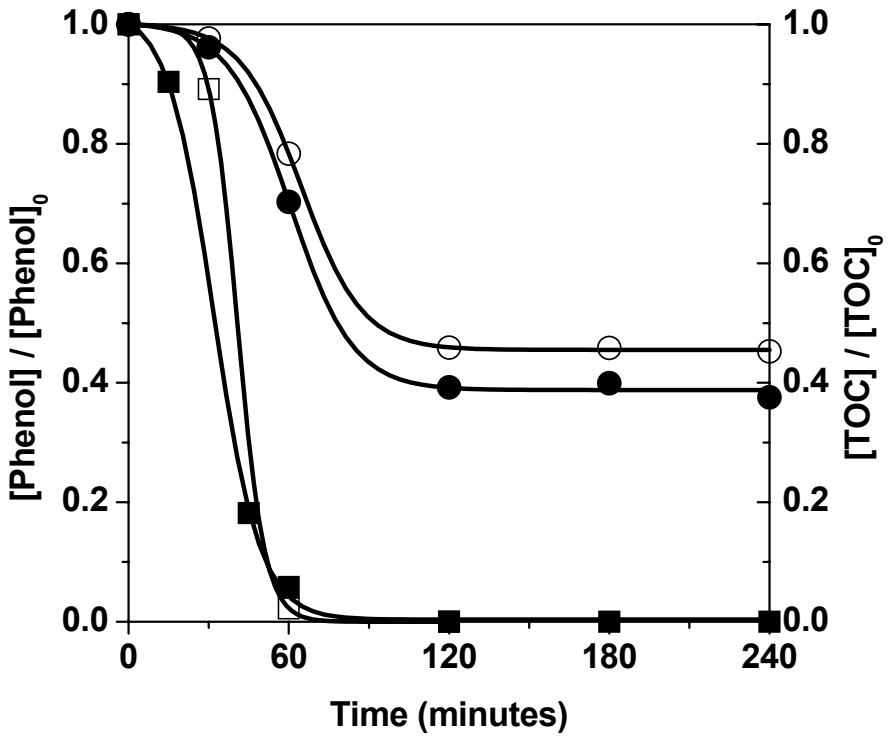

Fig. 3.10. Influence of the reaction temperature on the phenol oxidation and TOC decay rates for $AlSi2Fe6_{(T300)}$ allophane catalyst at pH = 3.7: Phenol/25 ºC (□); TOC/25 ºC (○); Phenol/40 ºC (■); TOC/40 ºC (●).

3.4.2.2. Phenol oxidation over copper-supported allophanes

The results of the catalytic activity of the copper-based allophane samples, before and after thermal treatmentat 300 ^{o}C (AlSi2Cu6 and $AlSi2Cu6_{(T300)}$), are shown in Fig. 3.11 and Table 3.4. The copper-based hydrous feldspathoid allophane samples proved to be less effective in oxidizing phenol than their iron oxide-supported counterparts. The reaction time required for total

phenol oxidation increased from 4 to 8 h, while the induction time lengthened to 2 h, in accordance with the results obtained by Barrault *et al.* [4] and Carriazo *et al.* [69] with pillared clays containing copper species.

The catalytic phenol oxidation over copper oxide-coated allophane materials involves a reaction between the hydrogen peroxide and the catalyst's copper species, giving rise to $^{\bullet}OH$ and $HO_2^{\bullet}$radical species according to equations (3.3) and (3.4):

$$Cu^{2+} + H_2O_2 \rightarrow Cu^{+} + HO_2^{\bullet} + H^{+} \qquad \text{(Eq. 3.3)}$$

$$Cu^{+} + H_2O_2 \rightarrow Cu^{2+} + {}^{\bullet}OH + OH^{-} \qquad \text{(Eq. 3.4)}$$

The generated $^{\bullet}OH$ radicals then react with phenol, yielding hydroquinone or catechol which are further oxidized to benzoquinone as shown by equation (3.5) [70]:

$$C_5H_5OH + {}^{\bullet}OH \rightarrow C_6H_5(OH)_2 \xrightarrow{Cu^{2+} \rightarrow Cu^{+}} C_6H_4O_2 + H_2O \qquad \text{(Eq. 3.5)}$$

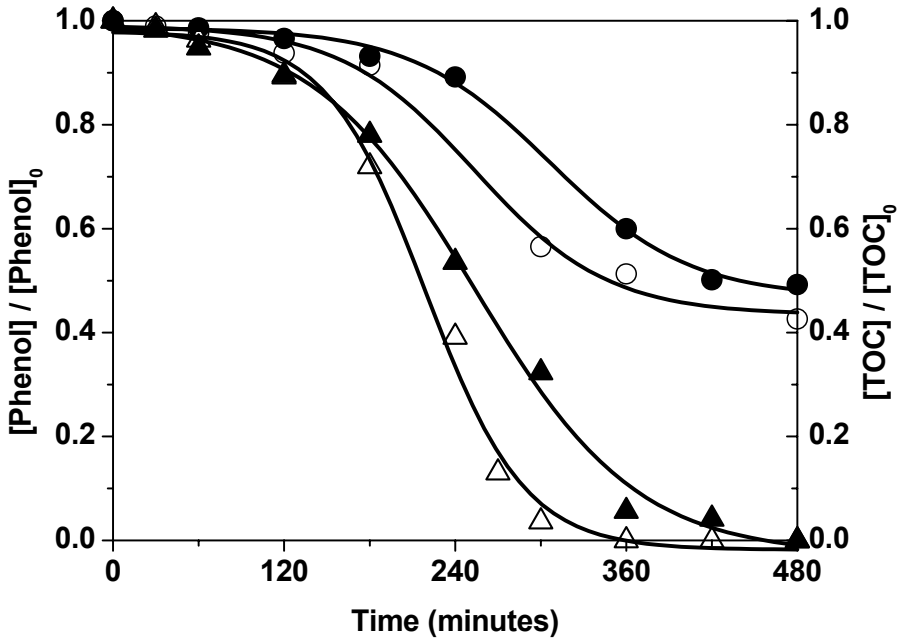

Fig. 3.11. Phenol and TOC decay after 8 h of reaction over copper oxide-supported AlSi2 allophane catalyst before and after calcination at 300 ^{o}C: Phenol, AlSi2Cu6 (Δ); TOC, AlSi2Cu6 (○); Phenol, AlSi2Cu6$_{(T300)}$ (▲); TOC, AlSi2Cu6$_{(T300)}$ (●).

Table 3.4. Phenol conversion, total organic carbon (TOC) decay, mineralization efficiency and Cu leaching for the synthesized parent AlSi2 allophane sample impregnated with copper oxide and their corresponding calcined counterparts.

Catalyst	Temperature (ºC)	Phenol conversion (%)	TOC decay[1] (%)	Mineralization efficiency (TOC/Phenol)[1]	Dissolved copper in solution (mg L^{-1})	Cu leached (wt%)
AlSi2Cu6	25	96 (5h)	57	0.57	2.9	5.2
$AlSi2Cu6_{(T300)}$	25	100 (8h)	51	0.51	1.9	3.1
AlSi2Cu6	40	100 (5h)	68	0.68	4.1	7.5

[1] 8 h of reaction

The TOC decay values obtained after 4 h of reaction at 25°C for the copper-based allophanes before and after calcination are shown to be far below those determined for the corresponding iron oxide-coated allophane catalysts. The AlSi2Cu6 and $AlSi2Cu6_{(T300)}$ samples exhibit a TOC conversion of 24 and 11 % after 4 h, respectively, while TOC decay values in the range 49-55% are obtained for the analogous AlSi2Fe6 and $AlSi2Fe6_{(T300)}$ catalysts. As shown in Table 3.4, experiments of 8 h are required to reach similar TOC abatement values with the parent and calcined Cu-based allophanes (57 and 51%, respectively), thereby confirming that the mineralization efficiency (TOC/phenol ratio) exhibited by the copper oxide-supported allophane samples is lower than that of the corresponding Fe-based phases. Moreover, leaching of copper species is also observed in both cases (Table 3.4). The presence of soluble copper species into the reaction medium accounts for a significant homogeneous catalytic contribution. The catalytic activity evaluated in a solution containing 2 and 5 mg L^{-1} indeed gives rise to TOC decay values

of 12and 20% at 25ºC after 4 h of reaction. This behavior could stem from an insufficient stabilization of the impregnated copper oxide on the surface of the AlSi2 allophane support or could be caused by the presence, in acidic conditions, of intermediate reaction products leading to the complexation of Cu^{2+} ions, thus forming soluble moieties.

Fig. 3.12 shows that increasing the reaction temperature from 25 to 40 ºC results in a similar increase in the rate of TOC decay and in a reduction of the induction period as well. A TOC decay of 68% is observed after 8 h reaction (57% after 4 h) and complete phenol oxidation is attained in less than 3 h. However, the level of Cu leached in solution is shown to increase up to 4.1 mg L^{-1}, which corresponds to 7.5 wt% of the initial Cu content, thereby confirming that the copper oxide-supported allophane catalysts are far less stable in the oxidation of phenol than their iron-based counterparts.

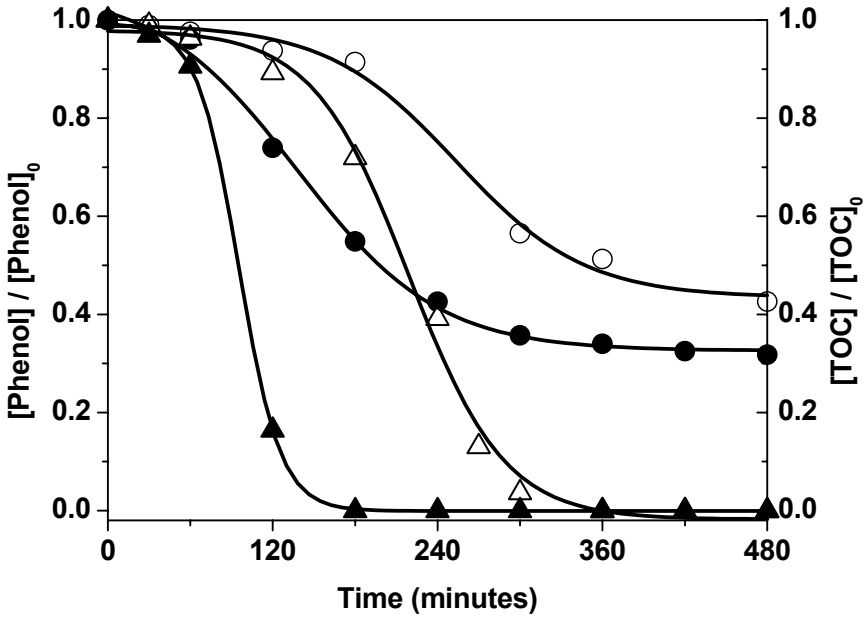

Fig. 3.12. Influence of the reaction temperature on the phenol oxidation and TOC decay rates for AlSi2Cu6 allophane catalyst at pH = 5.0: Phenol/25 ºC (Δ); TOC/25 ºC (○); Phenol/40 ºC (▲); TOC/40 ºC (●)

3.5. Conclusions

A series of iron and copper-based allophane clay materials, with variable SiO_2-Al_2O_3 ratio and exhibiting different structures, was prepared and their catalytic properties was further evaluated for the first time in total phenol oxidation in aqueous medium using hydrogen peroxide as oxidant in ambient conditions. The catalytic efficiency of the iron or copper oxide-supported allophanes was shown to greatly depend on the structural, textural and surface properties of both AlSi1 and AlSi2 allophane supports. The SiO_2/Al_2O_3 ratio of the synthetic parent allophanes is indeed the primary factor affecting the catalytic activity. The structure of allophane with a SiO_2/Al_2O_3 ratio of 2.2 (AlSi2) is similar to that of hydrous feldspathoids, where the Si

tetrahedral sheet constitutes the framework. The iron-impregnated samples based on the AlSi2 allophane support and exhibitinga large interspherule surface, behaved as efficient catalysts for phenol oxidation by Fenton-like reaction at atmospheric pressure and temperature close to the ambient (40°C). The thermally treated Fe-allophane ($AlSi2Fe6_{T300}$) was the most active catalyst, which in addition, proved to be stable in solution, since the concentration of Fe leached was as low as 0.37 mg L^{-1} (0.52% of the initial content). By contrast, the copper-based allophane catalysts were far less efficient in oxidizing phenol than their iron-supported counterparts, as indicated by strong differences in terms of phenol conversion rates (induction period), TOC abatement values and stability of the active phase.

3.6. Acknowledgments

This work was supported by a CONICYT Doctoral Scholarship as well as by a Scholarship for Implementation of Doctoral Theses 2010 (AT-24100139). MECESUP (Project FRO0601) and FONDECYT (Projects 11070241 and 1100746) are gratefully acknowledged for their financial support.

3.7. References

[1] K. Ayoub, E. van Hullebusch, M. Cassir, A. Bermond, A. J. Hazard. Mater. 178 (2010) 10–28.

[2] S. Navalon, M. Alvaro, H. Garcia. Appl. Catal. B: Environ. 99 (2010) 1–26.

[3] I. Oller, S. Malato, J.A. Sánchez-Pérez. Sci. Total Environ. 409 (2010) 4141−4166.

[4] J. Barrault, J.M. Tatibouët, N. Papayannakos. C.R. Acad. Sci. Paris, Sér. II C, Chem. 3 (2000) 777–783.

[5] J. Carriazo, E. Guélou, J. Barrault, J.M. Tatibouët, R. Molina, S. Moreno. Catal. Today. 107–108 (2005) 126–132.

[6] J. Carriazo, E. Guélou, J. Barrault, J.M. Tatibouët, R. Molina, S. Moreno. Water Res. 39 (2005) 3891–3899.

[7] G. Giordano, S. Perathoner, G. Centi, S. De Rosa, T. Granato, A. Katovic, A. Siciliano, A. Tagarelli, F. Tripicchio. Catal. Today 124 (2007) 240–246.

[8] M.B. Kasiri, H. Aleboyeh, A. Aleboyeh. Appl. Catal. B: Environ. 84 (2008) 9–15.

[9] J. Barrault, C. Bouchoule, K. Echachoui, N. Frini-Srasra, M. Trabelsi, F. Bergaya. 1998. Appl. Catal. B: Environ. 15 (1998) 269−274.

[10] J. Barrault, M. Abdellaoui, C. Bouchoule, A. Majesté, J.M. Tatibouët, A. Louloudi, N. Papayannakos, N.H. Gangas. Appl. Catal. B: Environ. 27 (2000) 225−230.

[11] J.M. Tatibouët, E. Guélou, J. Fournier. Top. Catal. 33 (2005) 1−4.

[12] C. Catrinescu, C. Teodosiu, M. Macoveanu, J. Miehe-Brendlé, R. Le Dred, Water Res. 37 (2003) 1154–1160.

[13] F. Martínez, M.I. Pariente, J.A. Melero, J.A. Botas, J. Adv. Oxid. Tech. (2008) 11, 65-74.

[14] A. Georgi, F.D. Kopinke. 2005. Appl. Catal. B: Environ. 58 (2005) 9–18.

[15] C. Castro, M. Guerreiro, M. Goncalves, L. Oliveira, A.S. Anastácio. J. Hazard. Mater. 164 (2009) 609−614.

[16] R. Molina, F. Martínez, J.A. Melero, D.H. Bremner, A.Chakinala, Appl. Catal. B. 66 (2006) 198-207.

[17] L. Xiang, S. Royer, H. Zhang, J.-M. Tatibouët, J. Barrault, S. Valange, J. Hazard. Mater. 172 (2009), 1175-1184.

[18] A. Xu, M. Yang, R. Qiao, H. Du, C. Sun, J. Hazard. Mater. 147 (2007) 449-456.

[19] J. Faye, E. Guélou, J. Barrault, J.-M- Tatibouët, S. Valange, Top. Catal. 52 (2009) 1211–1219.

[20] K. Hanna, T. Kone, G. Medjahdi. Catal. Commun. 9 (2008) 955–959.

[21] J.S. Choi, S.S. Yoon, S.H. Jang, W.S. Ahn. Catal. Today. 111 (2006) 280−287.

[22] R.J. Watts, S.Kong, M. Dippre, W.T. Barnes, J. Hazard. Mater. 39 (1994) 33–47.

[23] Y. Kitagawa. Am. Mineral. 56 (1971) 465-474.

[24] S.I. Wada, K. Wada. Clay Miner. 12 (1977) 289–298.

[25] M. Calabi-Floody, B.K.G. Theng, P. Reyes, M.L. Mora. Clay Miner. 44 (2009) 161–176.

[26] M. Calabi-Floody, J.S. Bendall, A. A. Jara, M.E. Welland, B.K.G. Theng, C. Rumpel, M.L. Mora. Geoderma 16 (2011) 159–167.

[27] M.F., Brigatti, E. Galan, B.K.G. Theng. Structures and mineralogy of clay minerals. In: Bergaya, F., Theng, B.K.G., Lagaly, G. (Eds.), Handbook of Clay Science. Elsevier, Amsterdam (2006), pp. 19–86.

[28] R.L. Parffit. Clay Miner. 44 (2009) 135–155.

[29] V.C. Farmer, G.S.R. Krishnamurti, P. M. Huang. Clays Clay Miner. 39 (1991) 561−570.

[30] M. Escudey, G. Galindo. J. Colloid Interface Sci. 93 (1983) 78−83.

[31] M.L. Mora, M. Escudey, G. Galindo. Bol. Soc. Chil.Quim. 39 (1994) 237–243.

[32] P. Díaz, G. Galindo, M. Escudey. Bol. Soc. Chil. Quim. 35 (1990) 385–389.

[33] M.L. Mora, J. Canales. Commun. Soil. Sci. Plant. Anal. 26 (1995) 2805−2817.

[34] A. Violante, M.A. Rao, A. De Chiara, L. Gianfreda. Eur. J. Soil Sci. 47 (1996) 241–247.

[35] A.A. Jara, S. Goldberg, M.L. Mora. J. Colloid Interface Sci. 292 (2005) 160–170.

[36] A.A. Jara, A. Violante, M. Pigna, M.L. Mora. Soil Sci. Soc. Am. J. 70 (2006) 337–346.

[37] M.C. Diez, M.L. Mora, S. Videla. 1999. Water Res. 33 (1999) 125–130.

[38] J. Espinoza, E. Fuentes, M. Baéz, M. 2009. Environ. Pollut. 157 (2009) 3387−3395.

[39] D. Menezes-Blackburn, M. Jorquera, L. Gianfreda, M. Rao, R. Greiner, E. Garrido, M.L. Mora. Bioresource Technol. 102 (2011) 9360−9367.

[40] M.S. Ureta-Zañartu, M.L. Mora, M.C. Diez, C. Berríos, J. Ojeda, C. Gutiérrez. 2002. Chlorophenol. J. Appl. Electrochem. 32 (2002) 1211–1218.

[41] E.G. Garrido-Ramírez, B.K.G. Theng, M.L. Mora. Appl. Clay Sci. 47 (2010) 182−192.

[42] M.A. Hossain, S.M. Salehuddin. As. J. Energy Env. 10 (2009) 91−98.

[43] E. Montarges-Pelletier, S. Bogenez, M. Pelletier, A. Razafitianamaharavo, J. Ghanbaja, B. Lartiges, L. Michot. Colloids Surfaces A: Physicochem. Eng. Aspects 255 (2005) 1–10.

[44] F. Ohashi, S.I. Wada, M. Suzuki, M. Maeda, S. Tomura. Clay Miner. 37 (2002) 451–456.

[45] Y. Arai, D.L. Spark, J. Adavi. Environ. Sci. Technol. 39 (2005) 2537−2544.

[46] S. Kaufhold, R. Dohrmann, Z. Abidin, T. Henmi, T. Matsue, L. Eichinger, A. Kaufhold, R. Jahn. Appl. Clay Sci. 50 (2010) 25–33.

[47] H. Khan, R. Khan, N. Matsue, T. Henmi. J. Environ. Sci. Technol. 2 (2009) 22−30.

[48] N. Wells, B.K.G. Theng. 1985. J. Colloid Interface Sci. 104 (1985) 398–408.

[49] N. Wells, C.W. Childs, C.J. Downes. Geochim. Cosmochim. Acta. 41 (1977) 1497−1506.

[50] M.J. Avena, C.P. De Pauli. Colloids Surfaces A: Physochem. Eng. Aspects 118 (1996) 75−87.

[51] K. Okada, K. Nishimuta, Y. Kameshima, A. Nakajima, K.J.D. Mackenzie. Clays Clay Miner. 53 (2005) 372−379.

[52] B. Creton, D. Bougeard, J.S. Smirnov, J. Guilment, O. Poncelet. J. Phys. Chem. C. 112 (2008) 358−364.

[53] Y. Kitagawa. 1974. Am. Mineral. 59 (1974) 1094−1098.

[54] R.L. Parffit, T. Henmi. Clays Clay Miner. 28 (1980) 285−294.

[55] G.G. Lindner, H. Nakazawa, S. Hayashi. Micropor. Mesopor. Mat. 21 (1998) 381−386.

[56] Z.Abidin, N. Matsue, T. Henmi, Clays Clay Miner. 55 (2007) 443−449.

[57] E. Opiso, T. Sato, T. Yoneda. J. Hazard. Mater. 170 (2009) 79–86.

[58] C.W. Childs, R.L. Parfitt, R.H. Newman. Clay Miner. 25 (1990) 329–341.

[59] G.A. Parks. Adv. Chem. Ser. 67 (1967) 121–160.

[60] F.J. Gil Llambías, A.M. Escudey Castro. Chem.Com.(1982) 478−479.

[61] P. Komadel, J. Madejova. 2006. Acid activation of clay minerals, In: Bergaya, F., Theng, B.K.G., Lagaly, G. (Eds.), Handbook of Clay Science. Elsevier, Amsterdam, pp. 393−422.

[62] L. Heller-Kallai. 2006. Thermally modified clay minerals. In: Bergaya, F., Theng, B.K.G., Lagaly, G. (Eds.), Handbook of Clay Science. Elsevier, Amsterdam, pp. 289−308.

[63] A. Ghoneim, N. Matsue, T. Henmi, T. Intl. J. Soil Sci. 1 (2006) 243−250.

[64] S. Arellano-Cárdenas, T. Gallardo-Velázquez, G. Osorio-Revilla, M. López-Cortéz, B. Gómez Perea. J. Mex. Chem. Soc. 49 (2005) 287−297.

[65] I.U. Castro, D.C. Sherrington, A. Fortuny, A. Fabregat, F. Stüber, J. Font, C. Bengoa. Catal. Today. 157(2010) 66-70.

[66] S. Zrnčević, Z. Gomzi. Ind. Eng. Chem. Res. 44 (2005) 6110−6114.

[67] A. Quintanilla, J.A. Casas, A.F. Mohedano, J.J. Rodríguez. Appl. Catal. B: Environ. 67 (2006) 206−216.

[68] Calleja, G., Melero, J.A., Martínez, F., Molina, R. Water Res. 39 (2005) 1741−1750.

[69] J. Carriazo, E. Guelou, J. Barrault, J. M. Tatibouët, S. Moreno. 2003. Appl. Clay Sci. 22 (2003), 303–308.

[70] L. Wang, A. Kong, B. Chen, H. Ding, Y. Shan, M. He. J. Mol. Catal. A: Chem. 230 (2005) 143−150.

4

Oxidation of a high Concentration of Atrazine by Fenton-like reaction and heterogeneous electro-Fenton process using an iron oxide-supported allophane

Oxidation of a high Concentration of Atrazine by Fenton-like reaction and heterogeneous electro-Fenton process using an iron oxide-supported allophane

E.G. Garrido-Ramírez[1], M.L. Mora[1], J.F. Marco[2] and M.S. Ureta-Zañartu[3]

[1]Scientific and Technological Bioresource Nucleus (BIOREN),
Universidad de La Frontera, Av. Francisco Salazar 01145, Temuco, Chile
[2]Instituto de Química Física "Rocasolano", CSIC, Spain
[3] Facultad de Química y Biología, Departamento de Ciencias del Ambiente, Universidad de Santiago de Chile

4.1. Abstract

We have studied the atrazine (ATZ) oxidation in a high concentration (46 – 92 μM) by Fenton-like reaction and heterogeneous electro-Fenton process, using a synthetic iron oxide-supported allophane (AlSi2Fe6). The effects of the initial pH, hydrogen peroxide concentration, as well, the amount of AlSi2Fe6 deposited on glassy carbon electrodes were studied. Both processes were efficient for atrazine degradation under acidic conditions (pH ~ 3). However, at more neutral pH (~ 6) it was also possible to carry out the reaction, achieving 68% atrazine oxidation in the Fenton-like reaction and 76% in the heterogeneous electro-Fenton process. Heterogeneous electro-Fenton process was more efficient than Fenton-like reaction; due mainly to continuous electro-regeneration of iron species (Fe^{3+}/Fe^{2+}). ATZ degradation by heterogeneous electro-Fenton process occurs by dealkylation of ethylamino side chain for producing desethylatrazine (DEA) and desethyldeisopropyl atrazine (DEIA) as main degradation products. Iron oxide-supported allophane is an effective catalyst for atrazine oxidation at high concentrations via heterogeneous Fenton processes.

Keywords: Atrazine oxidation; Fenton-like reaction, heterogeneous electro-Fenton process, atrazine degradation products, iron oxide-supported allophane

4.2. Introduction

Atrazine (ATZ), 2-chloro-4-ethylamino-6-isopropylamine-1,3,5-triazine (Figure 4.1), is a selective herbicide used worldwide for control broadleaf and grassy weeds in corn and in both pre- and post emergencies in forestry plantations. ATZ is usually found as pollutant in groundwater sources and drinking water supplies (Lapworth and Gooddy 2006; Hilderbrandt et al., 2008; Tierney et al., 2008) and was classified by the USEPA (2000) as possible human endocrine disruptor. Due to its physicochemical properties (Table 1), ATZ remains in the environment for a long time and its degradation using conventional wastewater treatment methods, such as biological or chemical, is difficult (Jiang and Adams 2006). Therefore, it is essential to develop new technologies to achieve its degradation in an environment – friendly and affordable way.

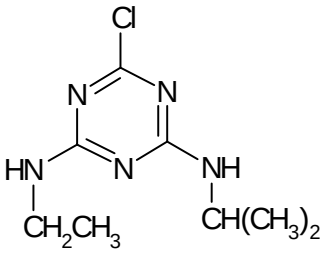

Figure 4.1. Chemical structure of atrazine

(2-chloro-4-ethylamino-6-isopropylamine-1,3,5-triazine)

Table 4.1. Atrazine physicochemical properties

Properties	Value
Molecular Weight	215.7[e]
Ionizability pK_a	1.7[a]; 1.68[d]
Aqueous solubility (mg/L)	33[a,b] (pH 7); 129[a] (pH 2)
Vapor pressure (mmHg)	2.9 x 10^{7}[a]
Henry's law constant (H)	2.96x10^{-9}[e] (20ºC)
Log K_{OW}	2.69[b] ; 2.48[d]
Soil retention (K_d; mL/g)	0.2 – 2.5[a]
Half life through hydrolysis	244 days [a]; > 25 week [d]
Half life in soils (days)	>41[c]
Half life in water (days)	>55[c]

[a] Weber et al. (2007) ; [b] Kima et al. (2008) ;[c] Hincapie-Pérez et al. (2006);[d] Konstantinou et al. (2000);[e] Joo and Zhao (2008)

Fenton reaction seems to be promising for degradation of a wide range of organic pollutants (Nogueira et al., 2007). The conventional Fenton process involves the reaction of Fe^{2+} species with H_2O_2, under acidic conditions (pH ~ 3), giving rise to hydroxyl radicals (Eq. 4.1), which are highly oxidative species. This catalytic reaction is propagated by the reduction of Fe^{3+} to Fe^{2+} (Eq. 4.2), with the generation of more radical species (Eq. 4.3-4.5) (Garrido-Ramírez et al., 2010).

$$Fe^{2+} + H_2O_2 \rightarrow Fe^{3+} + OH^- + OH^\bullet \qquad k_1 = 76\ M^{-1}\ s^{-1} \qquad [4.1]$$

$$Fe^{3+} + H_2O_2 \rightarrow Fe^{2+} + HO_2^\bullet + H^+ \qquad 0.001 \leq k_2 \leq 0.01\ M^{-1}\ s^{-1} \qquad [4.2]$$

$$Fe^{2+} + HO_2^{\bullet} \rightarrow Fe^{3+} + HO_2^{-} \qquad k_3=1.3x10^6\ M^{-1}\ s^{-1} \qquad [4.3]$$

$$Fe^{3+} + HO_2^{\bullet} \rightarrow Fe^{2+} + O_2 + H^{+} \qquad k_4=1.2x10^{-6}\ M^{-1}\ s^{-1} \qquad [4.4]$$

$$H_2O_2 + HO^{\bullet} \rightarrow HO_2^{\bullet} + H_2O \qquad k_5=2.7x10^7\ M^{-1}\ s^{-1} \qquad [4.5]$$

Atrazine degradation by Fenton reaction has been widely investigated, especially in aqueous diluted systems (ATZ ≤ 1 μM), using large iron or hydrogen peroxide concentrations (Arnolds et al., 1995; Gallard and De Laat 2000; Chan and Chu 2003; 2005). Under these conditions, values near 100% atrazine oxidation were achieved in a short time period. However, the acid medium necessary for avoiding the Fe^{3+} precipitation as oxyhydroxide that occurs at higher pH (Li et al., 2007; Bobu et al., 2008) and the apparent low rate constant (k_2) of the reduction of Fe^{3+} (Eq. 4.2) are some drawbacks of the conventional Fenton process. Besides, new processes that allow the atrazine degradation at higher concentrations are necessary. Some modifications have been proposed for the Fenton reaction in order to overcome these drawbacks, especially by coupling other processes, such as heterogeneous Fenton (Fenton-like reaction), electrochemical (Electro-Fenton, EF), photochemical (Photo-Fenton, PF) or both Electro-Photo-Fenton (EPF).

The heterogeneous Fenton reaction is based on the use of solid catalysts containing iron or copper species as Fenton reagent. In these cases, iron or copper oxides are "immobilized" within the structure and in the pore/layer space of the catalyst. As result, the catalyst is able to maintain the redox process and its ability to generate hydroxyl radicals from H_2O_2 over a wide pH range. Under these conditions the iron precipitation is avoided (Garrido-Ramírez et al., 2010). Supports, with large surface area and large, uniform pores, improve the organic pollutant degradation by

Fenton-like reaction, because they can facilitate dispersion of active sites, and enhance diffusion of reactants/products in liquid phase reactions (Choi et al., 2006).

Another promissory process based on the Fenton reaction is the electro-Fenton process, which consists of the continuous production of hydrogen peroxide on the cathode by the reduction of dissolved oxygen as shown in Equation (4.6). In this process small quantities of Fe^{2+} are required. The electro-generated H_2O_2 can then react with Fe^{2+} to produce •OH through a Fenton process (Eq.4.7). The regeneration of Fe^{2+} occurs either by a direct cathodic reaction (Eq. 4.8) or by the reaction with H_2O_2 (Eq.9).

$$O_2 + 2H^+ + 2e^- \rightleftarrows H_2O_2 \qquad [4.6]$$

$$H_2O_2 + Fe^{2+} \rightarrow Fe(OH)^{2+} + {}^{\bullet}OH \qquad [4.7]$$

$$Fe^{3+} + e^- \rightleftarrows Fe^{2+} \qquad [4.8]$$

$$Fe^{3+} + H_2O_2 \rightleftarrows (Fe - O_2H)^{2+} + H^+ \rightleftarrows Fe^{2+} + HO_2^{\bullet} \qquad [4.9]$$

An interesting improvement in the electro-Fenton process is the possibility of introducing the iron species as an active electrode material itself, transforming the homogeneous process into a heterogeneous one, which could prevent the oxyhydroxide precipitation with the increasing of pH. For example, an electrode as glassy carbon or graphite paste electrode can be modified with clays or iron minerals and used as Fenton reagent.

Some properties of the clays such as their exchange capacity, good catalytic support, large surface area, mechanical and chemical stability and low cost make them suitable as heterogeneous catalyst or electrode surface modifiers (Gomez et al., 2011). At this respect, clay minerals such as montmorillonites (Ghoneim and El-Desoky 2010), iron-enriched zeolites (Carvalho et al., 2006; Gligor et al., 2010), kaolinite (Gomez et al., 2011), allophanes (Garrido-Ramírez et al 2011 submitted) among others, have been used as solid catalysts in the Fenton-like reaction or for preparing modified electrodes.

In this context, allophane is a clay-size mineral found mainly in volcanic ash soils as hollow spherules in the nano-scale range (Calaby-Floody et al., 2009; 2011). In Chilean soils (Andisols), these nanoclays are in association with iron oxide of short range order, mainly ferrihydrite, which is often found as coatings of allophane particles (Escudey and Galindo 1983; Mora et al., 1994). It has been widely reported that the association of allophane with iron oxide produces an increase in the acidity of the surface active sites (Mora et al., 1994; Jara et al., 2005). Recently, we have shown (Garrido-Ramírez *et al.,* 2011 submitted) that synthetic iron or copper oxides-supported allophane with SiO_2/Al_2O_3 molar ratio ~ 2.2 and similar structure to hydrous feldsphatoid are active for phenol oxidation by Fenton-like reaction. The catalytic activity was dependent on physical and chemical properties, such as, amount of active sites, surface area and pore volume. Besides, synthetic iron oxide supported-allophanes were used in modified glassy carbon electrode for electro-oxidizing several chlorophenols under nitrogen atmosphere (Ureta-Zañartu et al., 2002). The results indicated that the Fe^{3+} acts as a redox promoter directly reacting with the phenol molecule by a chemical reaction, where the Fe^{2+} formed is quickly regenerated by electro-oxidation. The use of iron oxide supported-allophane, in which, the redox couple Fe^{3+}/Fe^{2+} can be

activated applying a potential difference in the electrochemical cell, is a promissory alternative for the electro-Fenton process, due to its low cost, natural abundance and environmental friendly characteristic.

The aim of this work is to study the atrazine oxidation in a high concentration by Fenton-like reaction and heterogeneous electro-Fenton process, using a synthetic iron oxide-supported allophane as solid catalyst.

4.3. Materials and Methods

4.3.1. Chemicals

Atrazine (Technical grade; 90%) was provided by Agricola Nacional SACEI (ANASAC). Desethyl-2-hydroxy-atrazina (DEHA), Deisopropyl-2-hydroxy-atrazine (DIHA, 99.7%), desethyl-atrazine (DEA, 99.4%), Deisopropyl-atrazine (DIA, 95.4%), Desethyl-deisopropyl-2-hydroxy-atrazine (97.5%), Desethyl-deisopropyl-atrazine (DEIA, 95%) and hydroxy-atrazine (ATZ-OH) were purchased from Sigma Aldrich (analytical grade). All reagents were used as received without further treatment, and the solutions were prepared in deionized twice distilled water. Acetonitrile used as organic solvent for the liquid chromatography was HPLC grade. Graphite powder, Riedel-de Haën, was washed in dilute nitric acid, filtered, eashed on the filter with twice-distilled water until neutral pH, and dried in an oven in an argon atmosphere at 120 ºC for 4h, cooled and stored under nitrogen.

4.3.2. Catalyst preparation

Iron oxide-supported allophanes (AlSi2Fe) were used as solid catalyst in the heterogeneous Fenton processes (Fenton-like reaction and electro-Fenton process). Allophane clays minerals were synthesized by co-precipitation of potassium silicate and aluminum chloride following the procedures described by Diaz *et al.* (1990) and Mora *et al*. (1994). Further, allophane samples were impregnated with 6% wt. iron oxide by a wet impregnation method (Mora et al. 1994), using $Fe(NO_3)_3.9H_2O$ as iron source. The physical and chemical properties of these compounds were recently reported (Garrido-Ramírez et al. 2011 submitted) and are shown in Table 4.2.

Table 4.2. Chemical composition and textural/charge properties of iron oxide-supported allophane (Garrido-Ramírez et al., 2011 submitted).

Parameters	Value
SiO_2/Al_2O_3 Ratio[1]	2.6
SiO_2 (wt %)	66.0
Al_2O_3 (wt %)	25.5
Fe_2O_3 (wt %)	8.5
BET Surface area (m^2g^{-1})	287
Total Pore Volume[2] (cm^3 g^{-1})	0.361
Isoelectric Point (IEP)[3]	7.0

[1] Determined by Energy dispersive X-ray spectroscopy; [2] Total pore volume at $P/P_0 = 0.95$
[3] IEP determined by Zeta-Sizer (Malvern Instrument)

4.3.3. X-ray photoelectron spectroscopy

AlSi2Fe6 was characterized by X-ray photoelectron spectroscopy (XPS). XPS data were recorded using a Leybold LHS-10 spectrometer with Mg Kα radiation, under a vacuum better than $5 \cdot 10^{-9}$ torr and a constant pass energy of 50 eV. The energy scale was calibrated using the C 1s binding energy of the adventitious carbon contamination layer, which was set at 284.6 eV. The background of the spectra was subtracted using the Shirley method and the data were fitted using mixed Gaussian-Lorentzian functions.

4.3.4. Electrodes preparation

Two types of electrodes were used. Modified carbon paste electrode with iron oxide-supported allophane (AlSi2Fe6-CPE) was prepared by a simple mixture of AlSi2Fe6 and graphite powder in a 1:9 (w/w) proportion. This mixture was homogenized with 11 drops of mineral oil (Aldrich). The resulting paste was packed into a hollow Teflon cylinder with 0.196 cm^2 of exposed area. The prepared electrode was sonicated for a better settlement and air bubbles elimination. The electrical contact was made using a steel rod. A similar paste without addition of AlSi2Fe6 (CPE) was used as control.

Modified glassy carbon electrodes (PINE, 0.5 cm^2 geometric area) were prepared painting the electrode surface with 1 mL of a suspension prepared as it was reported in a previous work (Ureta-Zañartu et al., 2002), and were labelled as AlSi2Fe6-GC. In brief, 50 mg of graphite plus, 1.5 mL of Nafion® perfluorinated ion-exchange resin (Aldrich) and 4 mL of an aqueous

suspension containing a given amount of AlSi2Fe6 were mixed and ultrasonically homogenized. In these cases the solvent was evaporated in a stove at controlled temperature (80ºC), in air, for 2 hours. As a blank, the electrode was painted with 1 mL of a suspension containing 50 mg of graphite power, 1.5 mL of Nafion® perfluorinated ion-exchange resin and 4 mL of distilled water.

4.3.5. Electrochemical characterization

The modified and unmodified carbon paste electrodes were characterized using cyclic voltammetry (CV), performed in a conventional three-compartment electrochemical cell at room temperature and under nitrogen gas. An electrochemical work station (CHI 660 C) was used for the measurements. The support electrolyte (Na_2SO_4 0.5 M) was adjusted at pH 3 with H_2SO_4 (0.02 M). An Ag/AgCl, KCl saturated electrode (Eº = V *vs*. NHE) was used as reference and platinum wire as counter electrode. All potentials are referred to the Ag/AgCl. Experiments were also run in the presence of atrazine (92 μM).

4.3.6. Fenton-like reaction and heterogeneous electro-Fenton process

Atrazine oxidation by Fenton-like reaction was determined using 1 mg/mL AlSi2Fe6 and 92 μM of atrazine. The reaction was performed at different initial pHs (2, 4 and 6) and hydrogen peroxide concentrations (0.2 and 0.3 M). All reactions were carried out in a recirculated temperature-controlled bath at 25±1 ºC. The pH was adjusted with drops of HCl (0.1 M) or NaOH (0.1 M). The samples were filtered using a 0.22 μm GV (Durapore) PVDF milipore filter. In blank experiments no H_2O_2 was added into the solution

Atrazine oxidation by heterogeneous electro-Fenton process was studied using AlSi2Fe6-GC as working electrode and a platinum wire as counter electrode. A single compartment electrochemical glass cell was employed using a typical three-electrode arrangement in order to hold both anode and cathode as close as possible. Oxygen was bubbled during 30 minutes before initiate the electrolysis and then was kept bubbling during all the process in order to maintain the solution saturated in oxygen. The solution was stirred mechanically with a magnetic bar to improve mass transfer and decrease the thickness of the Nernst diffusion layer. The initial ATZ concentration was 46 μM (30 mL), which was prepared in 90% 0.1 M Na_2SO_4 and 10 % methanol. Electrolysis were carried out at different initial pHs (3, 4 and 6) at atmospheric pressure and at room temperature. Aliquots of 1 mL were drawn every one-hour and immediately filtered (0.2 μm) and analyzed by HPLC. For the electrolysis experiments a fixed potential was applied and controlled with a Wenking POS73 Potentioscan.

4.3.7. Analytical methods

The decay in atrazine concentration and its reaction products were determined by HPLC provided with an array diode detector L-2455 (Elite Lachrom Hitachi) at 220 nm, using a reverse phase column RP18e (5 μm). Atrazine determination was performed using 40% acetonitrile and 60% ammonium acetate (0.1 mM) at 1 mL min^{-1} as mobile phase at 30 ºC. Atrazine degradation products were identified according to the method modified from Balci et al. (2009) using acetonitrile-ammonium acetate ($NH_4CH_3CO_2$, 5 mM, pH 4.6) in a gradient from 5 to 95% as mobile phase, at 1mL min^{-1} and 40 ºC. Calibration curves were performed with standard solution

of ATZ and their degradation products. In all cases, identification of intermediates was performed by comparison of retention times and UV spectra with those of pure standards.

Fe concentration was determined by atomic absorption spectrometry using an Unicam 969 AA Solar 594 Spectrometer.

4.4. Results and discussion

4.4.1. X-ray photoelectron spectroscopy

X-ray photoelectron spectrum of the iron oxide-supported-allophane (Figure 4.2) shows the presence of Si, Al, O and Fe. The photoelectron binding energies of the AlSi2Fe6 were similar to those reported for silica spring allophane or hydrous feldspathoid (Barr et al., 1996; 1997; Childs et al., 1997), which agrees with a previous report (Garrido-Ramírez et al 2011) that shows that AlSi2Fe6 has a similar structure of hydrous feldspathoid allophane.

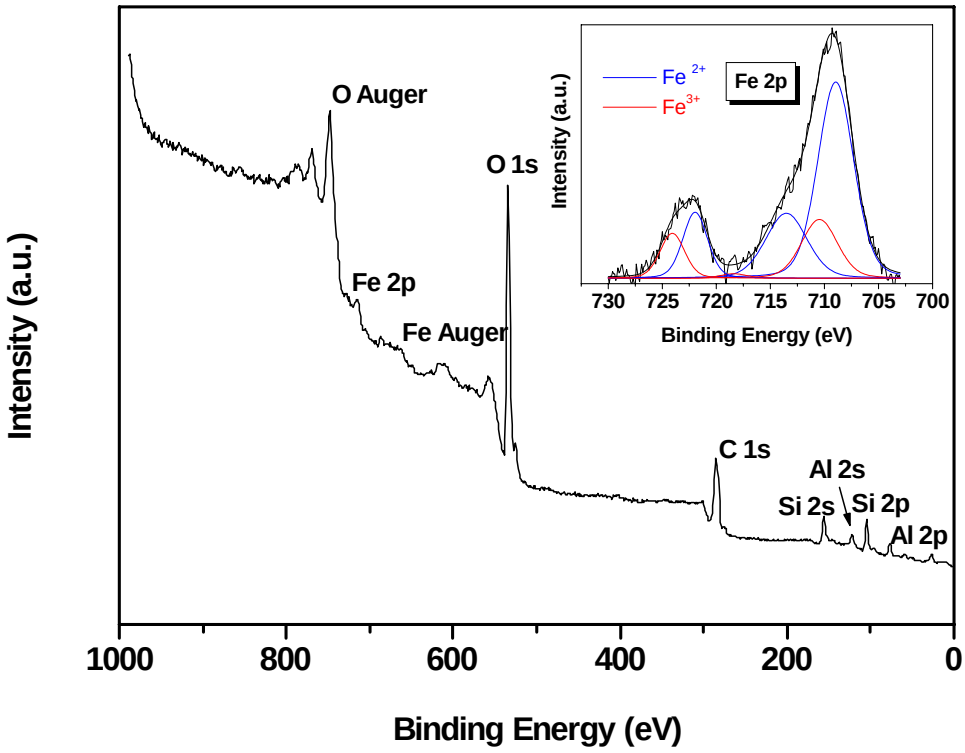

Figure 4.2. XP spectrum of iron oxide-supported allophane
Inset. XPS data obtained from the fit of the Fe 2p spectra

Inset of Figure 4.2 shows the Fe2p spectrum recorded from AlSi2Fe6. Apart from the characteristic $Fe2p_{3/2}$ and $Fe2p_{1/2}$ photoemission lines, the spectrum shows clear shake-up satellite structure at ca. 3.5-4.0 eV above the main Fe $2p_{3/2}$ peak. This satellite structure is unequivocally associated with the presence of Fe^{2+} (McIntyre and Zetaruk, 1977; Gracia et al., 2000). However, the presence of Fe^{3+} cannot be discarded either, because of the typical broadening of the lines of the Fe2p spectrum. Therefore, the spectrum was fitted considering two spin-orbit doublets (one with binding energies characteristic of Fe^{2+} and the other with binding energies characteristic of Fe^{3+}) plus two additional contributions: a major one to account for the Fe^{2+} shake-up satellite structure at about 713.5 eV and a minor one at 718.4 eV to account for the much weaker Fe^{3+} shake-up satellite structure, which is known to be present at around 718.4 eV. We used some restrictions to fit the spectrum in order to quantify the Fe^{3+}/Fe^{2+} ratio, because of the several concomitant processes, which contribute to the shape of the spectrum (i.e. pure photoemission processes, unresolved multiplet splitting and presence of shake-up structure (Gracia et al., 2000). These are: the same line width for the Fe $2p_{3/2}$ lines corresponding to both Fe^{2+} and Fe^{3+} chemical species, the same line width for the Fe $2p_{1/2}$ lines corresponding to both Fe^{2+} and Fe^{3+}, and the same Gaussian/Lorentzian ratio for all the peaks used in the fit, which was set to 80% Gaussian/20% Lorentzian. The results of the fit are collected in Table 4.3.

.

Table 4.3. XPS data obtained from the fit of the Fe 2p spectra of iron oxide-supported allophane

BE (eV)	FWHM (eV)	Area (%)	Assignment	Fe^{3+}/Fe^{2+} ratio
709.0 722.0	3.9 2.7	59	Fe^{2+} spin orbit doublet	
710.5 724.1	3.9 2.7	22	Fe^{3+} spin orbit doublet	0.3
713.5	4.5	18	Fe^{2+} satellite	
718.4	2.8	1	Fe^{3+} satellite	

As was previously discussed, the presence of Fe^{2+} is unequivocally identified here by XPS due to the strong satellite at 713.5 eV. This result agree with the XPS spectrum obtained by Ureta-Zañartu et al. (2002) for an aluminosilicate impregnated with iron oxide synthesized with the same experimental conditions used in this work. However, this result contrasts with previous Mössbauer results (Mora et al., 1994 and Jara et al., 2005), which only showed the presence of Fe^{3+} species on this type of sample. XPS is a surface technique which provides information from the topmost 3 nm, while the Mössbauer mode used in the mentioned paper is a bulk technique. Therefore, the discrepancy could be due to the different probe depths of both techniques. It might be possible too, that, because of the chemical nature of the Fe^{2+} species, its recoil free fraction could be very low and it would result undetected in a unique room temperature Mössbauer spectrum. This could be possible, for example, if the Fe^{2+} species were not a structural chemical species (i.e. it did not pertain to the structure of the aluminosilicate) and were, for example, a surface adsorbed species. It is known that the recoil free fraction of Fe^{2+} adsorbed or dispersed species in clays and catalysts may be nearly zero and its presence only becomes evident in

spectra recorded at cryogenic temperatures (Diamant et al., 1982; Chorkendorff and Niemantsverdriet, 2003).

4.4.2. Atrazine degradation by Fenton-like reaction

Atrazine degradation by Fenton-like reaction was studied at different initial pHs and hydrogen peroxide concentrations using an iron oxide-supported allophane (AlSi2Fe6) as heterogeneous catalyst. The corresponding results are shown in Figure 4.3 and Table 4.4. Atrazine decay follows pseudo-first order kinetics and, therefore, atrazine oxidation occurs by Eq. 4.10.

$$\mathrm{ATZ} + {}^{\bullet}\mathrm{OH} \rightarrow \mathrm{Products} \qquad [4.10]$$

Then, the rate of the reaction is given by

$$v_{10} = -\frac{d[\mathrm{ATZ}]}{dt} = k_{10}[\bullet\mathrm{OH}]\,[\mathrm{ATZ}] \qquad [4.11]$$

As ${}^{\bullet}$OH radical can be considered as constant during the process (the reaction 4.7 is faster than reaction 4.10, and $[H_2O_2] >> [ATZ]$, the equation 4.11 can be written as a pseudo first order reaction, which in its integrated form is:

$$\ln\frac{[ATZ]}{[ATZ]^{\circ}} = -k_{10}t \qquad [4.12]$$

The pseudo-first order rate constants (k_{10}) were determined by the slope of regression lines in the ln $[ATZ]/[ATZ]_0$ *vs*. time plot (Figure 4.3 and Table 4.5).

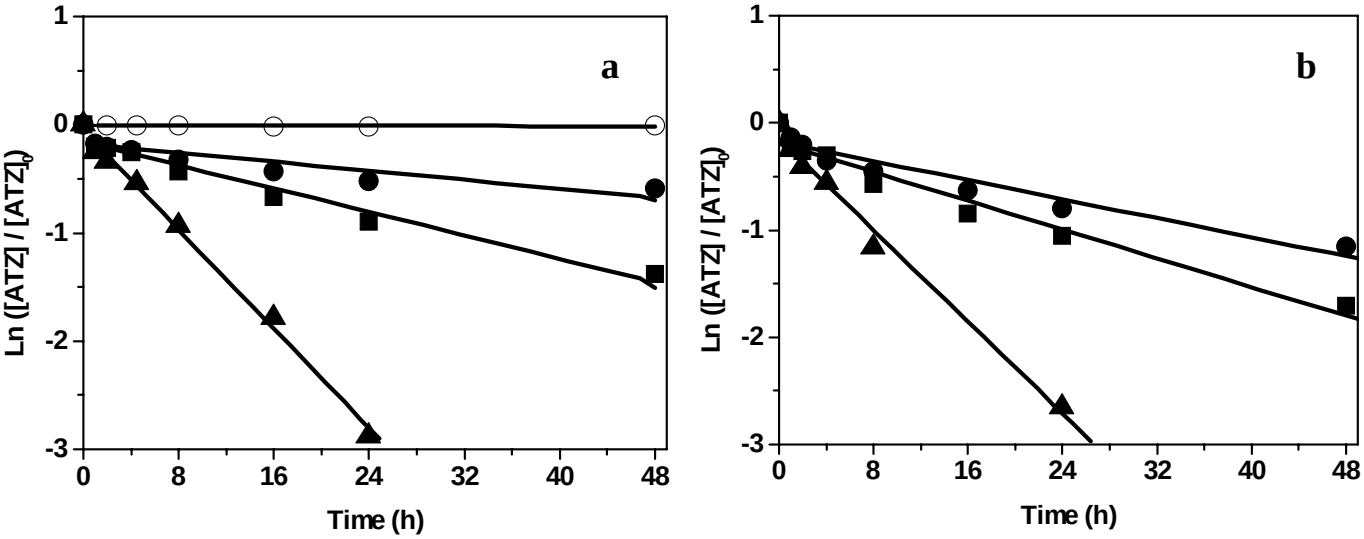

Figure 4.3. Rate of ATZ oxidation at different initial pHs and hydrogen peroxide concentrations by Fenton-like reaction: (a) $[H_2O_2]$ = 0.2 M; (b) $[H_2O_2]$ = 0.3 M. Symbols: adsorption at pH 3 (○); Fenton-like reaction at: pH = 3(▲); pH = 4 (■); pH = 6 (●). For all experiments $[ATZ]_0$ = 92 μM, 25ºC. Straight lines corresponding to a linear regression

Table 4.4. ATZ conversion and Fe leaching for iron oxide-supported allophane (AlSi2Fe6) at different hydrogen peroxide concentrations and pHs

[H_2O_2]	**Initial pH**	**ATZ conversion (%)**	**Dissolved iron in solution (mg L^{-1})**	**Fe leached (wt%)**
0	3.0	2 (48 h)	0.16	0.26
0.2	3.0	94 (24 h)	0.33	0.54
0.2	4.0	75 (48 h)	0.23	0.38
0.2	6.0	44 (48 h)	0.03	0.05
0.3	3.0	100 (24h)	0.55	0.90
0.3	4.0	82 (48 h)	0.22	0.36
0.3	6.0	68 (48 h)	0.01	0.02

Table 4.5. Apparent rate constant (k_{10}) and regression coefficient for ATZ oxidation by Fenton-like reaction at different hydrogen peroxide concentrations and pHs

H_2O_2 (M)	**pH**	**k_{10} min^{-1}**	**Regression coefficient (R^2)**
0.2	3.0	1.92×10^{-3}	0.99
0.2	4.0	4.5×10^{-4}	0.97
0.2	6.0	1.67×10^{-4}	0.77
0.3	3.0	2.28×10^{-3}	0.98
0.3	4.0	5.67×10^{-4}	0.96
0.3	6.0	3.67×10^{-4}	0.96

Atrazine oxidation was first evaluated in absence of either catalyst or hydrogen peroxide at pH 3.0. In absence of catalyst, using hydrogen peroxide 0.3 M, ATZ decay was below 10% after 48 h of reaction (data not shown). In absence of oxidant, when only the catalyst was present, a very low ATZ decay (2%) was obtained (curve ○). This result agrees with the experimental conditions used in this work (pH range over the pKa of ATZ and below IEP of AlSi2Fe6) for which a very small atrazine adsorption on AlSi2Fe6 catalyst is expected (Ahmad and Rahman 2009). In Figure 4.3, ATZ oxidation decreased as pH increased to more neutral values, while the use of a higher hydrogen peroxide concentration increases ATZ decay for all pH range. ATZ decay achieved a maximum at pH 3 in agreement with the optimum pH for the Fenton-based process (Gallard and De Laat 2000; Barreiro et al., 2007). However, in this work, it was possible to perform the reaction at initial pH 6 achieving a 68% ATZ decay in 48 h, using a hydrogen peroxide concentration of 0.3 M (Table 4.4). As was previously discussed, it is not possible to perform the homogeneous Fenton reaction at pH higher than 3, due to formation and precipitation of insoluble Fe^{3+} species. However, in the heterogeneous Fenton process (Fenton-like reaction) it is expected that the iron precipitation does not to occur, because iron is "immobilized" in the structure of the catalyst (Garrido-Ramírez et al., 2010). As was previously discussed in the section 4.4.1, XPS analysis shows the presence of Fe^{3+} and Fe^{2+} species. According to previous results (Mora et al., 1994; Jara et al., 2005), Fe^{3+} species are forming covalent bonds with the allophane surface, with species such as Si-O-Fe and Al-O-Fe, allowing perform the Fenton-like reaction at pH near to neutral, and avoiding the iron precipitation. While, it is possible that Fe^{2+} species may be adsorbed or occluded on the mesopores of allophane structure, due to this iron species were not detected by Mösbauer spectroscopy at room temperature (300 K).

The stability of the AlSi2Fe6 catalyst was determined by to study the iron dissolved at end of reactions (Table 4.4) at different pHs and hydrogen peroxide concentrations. In all experiments, very low leaching level of iron species was observed (< 0.55 mg L^{-1}, corresponding to 0.9 % of the initial Fe content), which indicate that the active phase is stable in a wide range of pH value. The higher iron dissolution was obtained at initial pH 3, which agree with previous works (Mora 1992; Garrido-Ramírez et al., 2010), that shown that the dissolution of iron oxide supported-allophane increase at acid pH (pH ~ 3) and decreases at neutral pH, becoming negligible at pH ~ 7. Beside, we hypothesize that the iron dissolved under acidic condition could be corresponding to Fe^{2+} species, which were not possible to detect by Mösbauer spectroscopy at room temperature. It is possible that these iron species could be adsorbed or occluded on the mesopores of the allophane structure, and therefore, could be solubilised under acidic conditions. As consequence the Fe leaching from AlSi2Fe6, could be explain the highest ATZ decay (~ 100%) at initial pH 3, where, the ATZ oxidation could be the results of both process (1) homogeneous Fenton reaction due to Fe^{2+} species leaching into the solution at pH 3 and (2) heterogeneous Fenton process due to Fe^{3+} "immobilized" in the structure of AlSi2Fe6.

4.4.3. Voltametric behaviour of carbon paste electrode modified with AlSi2Fe6

In order to determine the ability of carbon-based electrodes modified with AlSi2Fe6 in ATZ degradation by heterogeneous electro-Fenton process, as a first approach, their electrochemical properties were studied. As it was expected, the carbon paste and glassy carbon modified electrodes are very porous, which implies that the real area is higher than the geometric one. In

order to estimate the rugosity of the electrodes, voltammetry at different potential scan rates were used according to Trasatti and Petrii (1992). The rugosity factor R_F is defined as

$$R_F = \frac{{}_TC}{C^{\bullet}} \qquad [4.13]$$

Where ${}_TC$ is the total differential capacitance of the interface, and $C^{\bullet}$ is the reference capacitance, Total differential capacitance is evaluated by voltammetric curves obtained in a narrow potential range at different sweep rates. In a plot of current in the middle of the potential range against the potential scan rate, a straight line must be obtained, whose slope represents the total differential capacitance (${}_TC$). Considering that the electrodes prepared in this work are very porous, the reference $C^{\bullet}$ was determined by the capacitance value obtained with glassy carbon mirror polished, assuming roughness 1 for this electrode. Therefore, in this work the rugosity of the electrodes, R_F is referred to the glassy carbon. It is clear that this assumption only enables estimate the real area of the electrodes prepared, we think it is enough to make a comparison, throughout this work, between the different electrodes so prepared.

Figure 4.4 show cyclic voltammetry (CVs) at 0.1 V s^{-1} for CPE (solid line) and AlSi2Fe6-CPE (dashed line) in 0.5 M Na_2SO_4 at pH 3.0 under nitrogen saturated solution. The potential scan starts from open circuit potential (0.3 V) in the negative direction. At pH 3.0, CPE is stable between -0.4 and 1.2 V *vs*. Ag/AgCl with a double layer current near 0.42 μA (0.21 V), without maximum capacitance attributable to oxygenated carbon in the graphite. In the CV, a cathodic process at -0.4 V (2C) was observed, attributed to reduction of molecular oxygen that remained

trapped in the carbon paste (Bergé-Lefranc et al., 2008) electrode. The R_F parameter (calculated value ~ 30) did not change with the presence of AlSi2Fe, which indicated that the number of active carbon site remained constant, as it was expected, because the amount of carbon in the suspension is equal. CV curves for AlSi2Fe6-CPE under the same experimental conditions (dashed lines) shows the Fe^{3+}/Fe^{2+} couple as irreversible, with a cathodic peak at 0.00 V (1C) associated with Fe^{3+} reduction and the corresponding anodic peak (1A) at 0.71 V. In the negative potential region (2C), an increase in the cathodic current attributed to the presence of oxygen trapped in the CPE was also observed, evidencing that Fe^{2+} catalyze the oxygen reduction process.

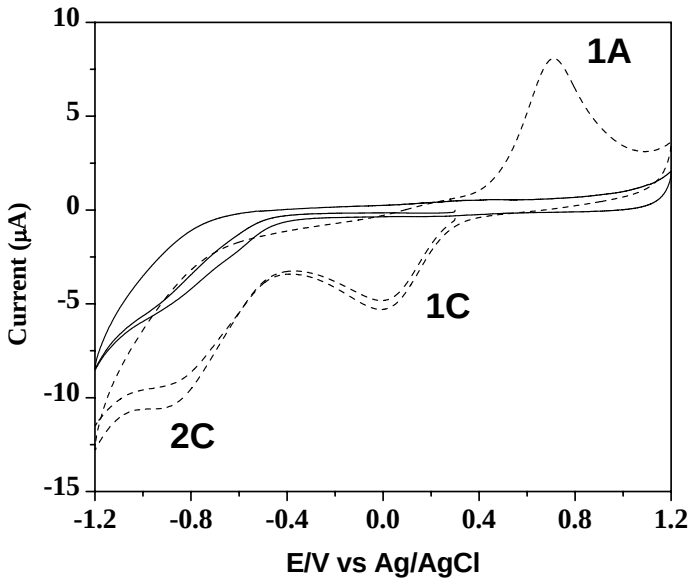

Figure 4.4. Cyclic voltammograms at 0.1 V s^{-1} of CPE (solid line) and AlSi2Fe6-CPE (dash line). Voltamogramms recorded in $[Na_2SO_4]$ = 0.5 M and initial pH ~3

In order to know about the reversibility of the Fe^{3+}/ Fe^{2+} couple CVs at different potential scan rate were obtained (Figure 4.5a). The plot of cathodic peak current (I_{1C}) *vs* the root of scan rate $v^{1/2}$ (Figure 4.5b) exhibits a linear correlation but is not directly proportional, evidencing that although it is a surface reaction, there is a diffusional control across the solid phase of the electrode. The diffusional control is in order to maintain the electro-neutrality in the film due to both charge and ionic transports across the solid phase of the electrode. The normalized current function (Ip /$v^{1/2}$) against scan rate plot of the 1C peak (Figure 4.5c) is practically constant, evidencing that no other processes are associated with the Fe^{3+}/Fe^{2+} process, so it can be assumed that irreversibility comes from problems through the ionic conductivity within the electrode. An Ep vs. log v plot (Figure 4.5d) for the cathodic peak (1C) gives a slope of -0.077 V/dec which, if the process is considered as irreversible and under diffusional control, the Tafel slope would be 0.154 V, in agreement with a mono-electron process, with a transfer coefficient (α) of 0.77 (Ardakani et al., 2006).

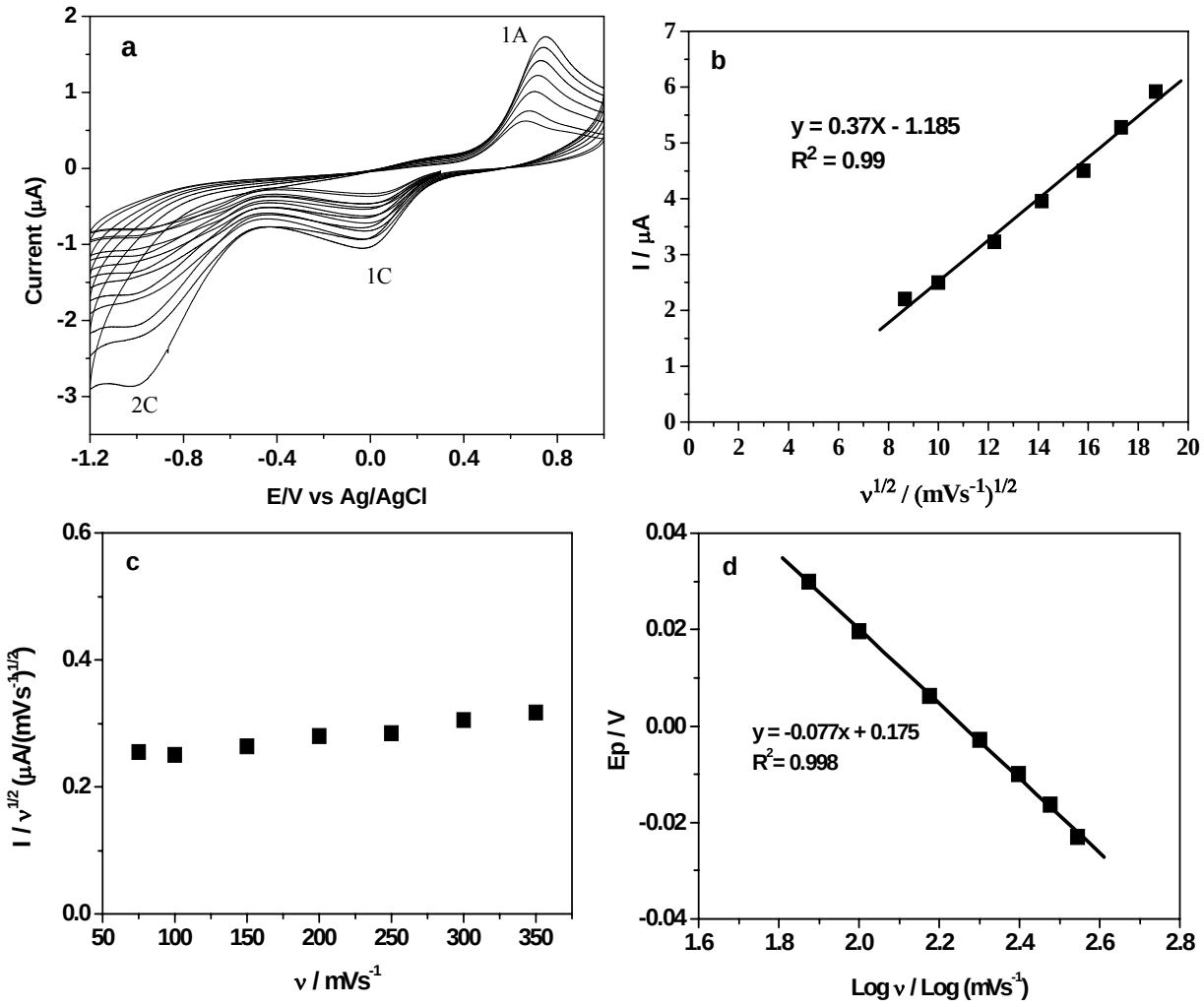

Figure 4.5. (a) Cyclic voltammograms of AlSi2Fe6-CPE at different scan rate (01-0.35 V s^{-1}). $[Na_2SO_4]$ = 0.5 M, pH 3.0; (b) I_{1c} *vs.* $\nu^{1/2}$ plot; (c) normalized current ($Ip/\nu^{1/2}$) *vs*. scan rate for peak 1C; (d) Dependence of peak potential Ep with potential scan rate(ν) for peak 1C.

Figure 4.6a shows CVs at 100 mV s^{-1} of AlSi2Fe6-CPE in presence and absence of 92 μM of ATZ using Na_2SO_4 (0.5M) as support electrolyte under N_2 saturated solution. ATZ was introduced in the cell under open circuit potential and the scan was started from 0.3 V in the

negative direction. A decrease in the anodic and cathodic peak current of Fe^{3+}/Fe^{2+} process was observed evidenced some interaction between both compounds. However, new charge transfer processes attributable to ATZ reactions were not observed, indicating the absence of direct electron transfer between the electrode surface and ATZ in solution. Similar results were obtained by Polcaro et al. (2005) and Malpass et al. (2006) for oxidation of ATZ using BDD electrode and DSA electrode, respectively.

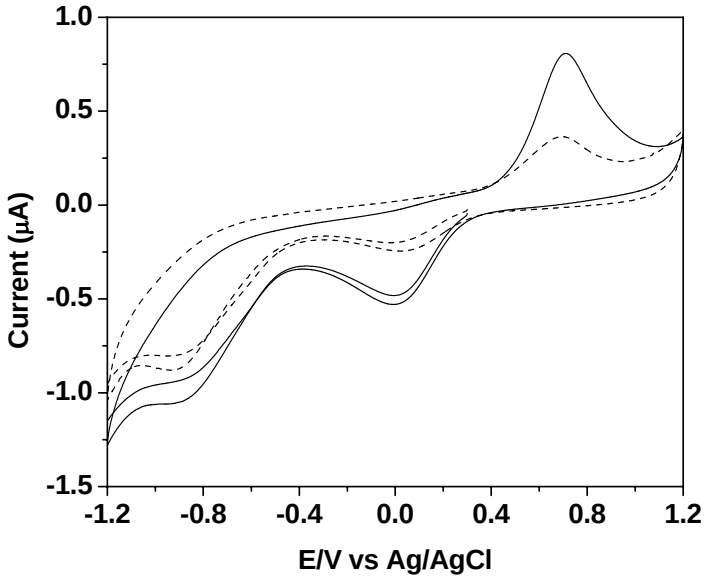

Figure 4.6. Cyclic voltamogramms at 0.1 V s^{-1} for AlSi2Fe6-CPE under N_2 saturated solution, using 0.5 M Na_2SO_4 as support electrolyte adjusted at pH 3.0. CV performed in presence (dashed line) and absence (solid line) of ATZ (96 μM)

Therefore, we postulate that it is possible to degrade ATZ by an indirect oxidation mechanism, saturating the electrolyte with oxygen. In order to generate $^{\bullet}OH$ radicals from the electro

generated H_2O_2 and Fe^{3+}/Fe^{2+} species present on the electrode. As was previously discussed, the increase in the cathodic current due to oxygen trapped in the CPE (Figure 4.4) evidencing that Fe^{2+} is able to catalyze the oxygen reduction process. In order to determine the oxygen potential reduction on the modified carbon-based electrode, cyclic voltammetry at 0.3 V s^{-1} for AlSi2Fe6-CPE were recorder in O_2 saturated solution using 0.5 M Na_2SO_4 adjusted at pH 3.0. The CVs were performed in presence and absence of ATZ (Figure 4.7). The potential scan begins at 0.3.V in the negative direction. It was observed that the oxygen reduction current is far higher than the Fe^{3+}/Fe^{2+} process, being the latter process difficult for detected, as can be seen in Figure 4.7 (solid line), where two consecutive scan were plotted. In the second scan, as be expected, a decrease in the reduction current was observed due to the decrease in O_2 concentration in the inter-phase. In presence of ATZ, a shift to more negative potential for the oxygen reduction process was observed, in agreement with a decrease in the availability of Fe^{2+} sites resulting from the interaction of these species with ATZ.

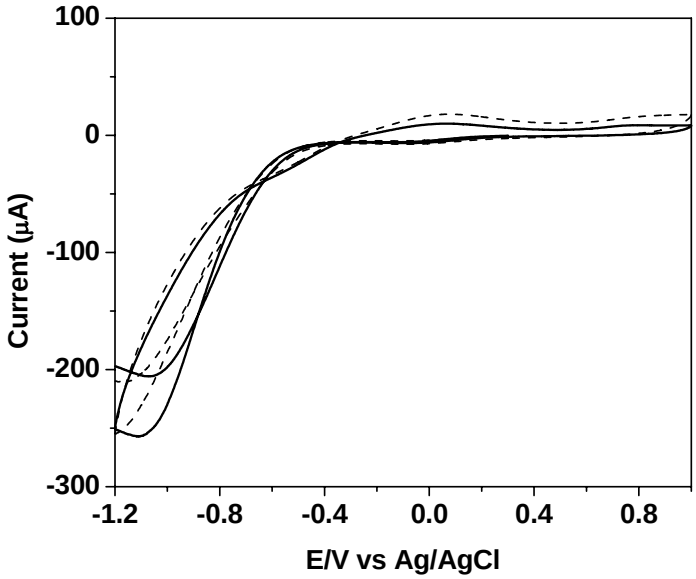

Figure 4.7. Cyclic voltammetry at 0.3 V s^{-1} for AlSi2Fe6-CPE in O_2 saturated 0.5 M Na_2SO_4 at pH 3.0, in the presence (dashed line) and the absence (solid line) of ATZ (96 μM).

4.4.4. ATZ oxidation by heterogeneous electro-Fenton reaction: bulk electrolysis

Atrazine oxidation by electro-Fenton process was studied using a glassy carbon electrode modified with different AlSi2Fe6/graphite ratios (Figure 4.8). The experiments were carried out in oxygen saturated solution at a fixed potential of -1.04 V (oxygen reduction potential determined previously by CV) and pH 3. ATZ oxidation in AlSi2Fe6-GC electrodes exhibits an exponential behaviour indicating pseudo first-order reaction kinetics. The apparent rate constants (k_{10}) were calculated from linear regression of pseudo first-order kinetic models after of induction time and are shown in Table 4.6.

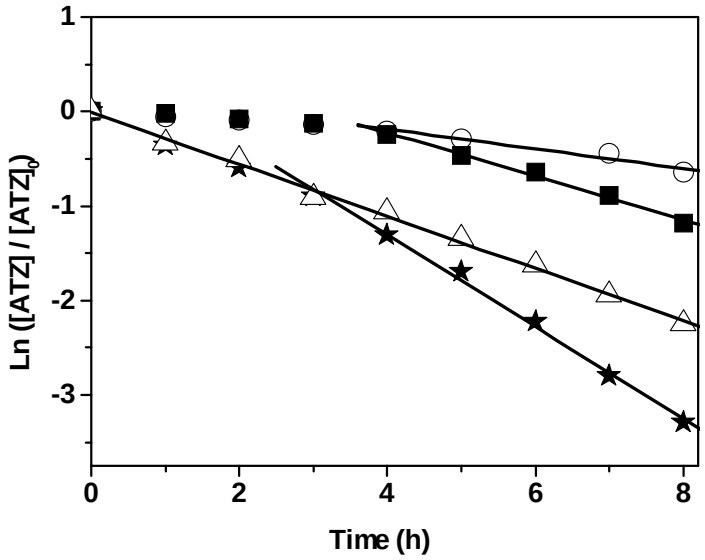

Figure. 4.8. Rate of ATZ oxidation by heterogeneous electro-Fenton process using different AlSi2Fe6 / graphite ratios deposited on GC electrode: blank GC (○); AlSi2Fe6 / graphite ratio= 0.2 (■);AlSi2F6 /graphite ratio= 0.6 (★);AlSi2Fe6 /graphite ratio =1.0 (Δ). $[ATZ]_0$ = 46 μM, room temperature, oxygen saturated solution, E= -1.04 V. Straight lines corresponding to a linear regression and were adjusted after the induction time

Table 4.6. Apparent rate constant (k) and regression coefficient for ATZ oxidation using different AlSi2Fe6/graphite ratio deposited on GC electrode by heterogeneous electro-Fenton process

AlSi2Fe6/graphite ratio	pH	ATZ conversion[1] (%)	k, min.$^{-1}$	Regression coefficient (R^2)
0	3.0	48	1.74 x 10^{-3}	0.960
0.4	3.0	69	3.82 x 10^{-3}	0.992
0.6	3.0	96	8.08 x 10^{-3}	0.996
1.0	3.0	89	4.58 x 10^{-3}	0.996
0.6	4.0	89	7.28 x 10^{-3}	0.996
0.6	6.0	76	5.00 x10^{-3}	0.996

[1] After 8 h of reaction

In absence of AlSi2Fe6 (curve ○), a 46% ATZ decay was obtained after 8 h of reaction. ATZ decay increase with the AlSi2Fe6/graphite ratio, achieving an optimum in ATZ decay (96 %), when AlSi2Fe6/graphite ratio of 0.6 was used as modifier electrode. For a higher AlSi2Fe6/graphite ratio, ATZ oxidation decreased, which could be the result of a decrease in the electrode conductivity due to higher AlSi2Fe6 content. In Figure 4.8, an induction period in ATZ decay was observed for the reactions performed in GC electrodes modified with AlSi2Fe6/graphite ratio ≤ 0.6. This induction period decrease as the AlSi2Fe6/graphite ratio increase. This induction period could be explained in terms of •OH radical generation from the reaction between Fe^{3+}/Fe^{2+} species present on the modified electrode and the hydrogen peroxide electrochemical generated by the oxygen reduction on the cathode. With the use of a higher

amount of iron species on the electrode, the generation of $^{\bullet}OH$ radicals could be higher and therefore, the induction time is reduced.

The effect of the different initial pHs in ATZ decay are shown in the Figure 4.9, while the pseudo first reaction constants, determined after of induction time, are listed in Table 4.5. ATZ oxidation was higher at pH 3.0, which agrees with the optimum pH reported by Fenton-based process (Gallard and De Laat 2000; Chan and Chu 2005). However, we were able to perform the electro-Fenton reaction at more neutral initial pHs (4 and 6), for which, an 89% and 76% ATZ decay were obtained for pH 4 and 6, respectively, after 4 h of reaction. These results suggest that AlSi2Fe6-GC electrodes are active over a wide range of initial pH and offer the potential to operate at near neutral pH without loss their catalytic activity.

The rates of ATZ oxidation by heterogeneous electro-Fenton process were higher than the Fenton-like reaction. As it is widely known, the rates of oxidation of organic compounds by Fenton process are dependent on iron and hydrogen peroxide concentration. In the iron oxide case, many studies have shown that the rate of oxidation of organic compounds is much slower by Fe^{3+}/H_2O_2 than by Fe^{2+}/H_2O_2 systems (see apparent rate constant (k_2) in the equation 4.1 and 4.2) (Gallard and De Laat 2000). In the heterogeneous electro-Fenton process due to negative potential applied in the electrolysis assay (-1.04 V), Fe^{3+} is quickly regenerated into Fe^{2+}, which could be explained by the high rate of ATZ oxidation compared with the Fenton-like process.

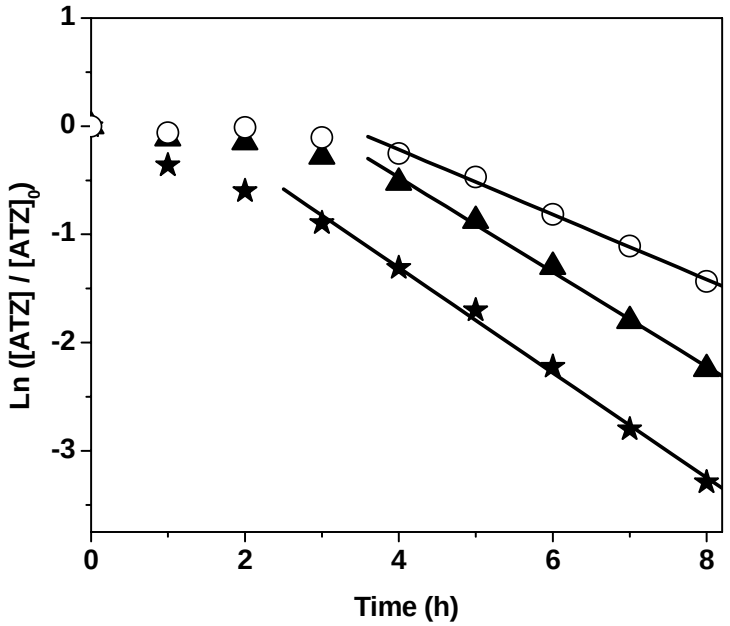

Figure 4.9. Rate ATZ oxidation by heterogeneous electro-Fenton process using 0.6 AlSi2Fe6 / graphite rate deposited on GC electrode, at different initial pH: pH ~ 6 (○); pH ~ 4 (▲); pH ~3 (★). For all experiments, [ATZ] = 46 µM; room temperature; oxygen solution saturated; -1.04 V. Straight lines corresponding to a linear regression, adjusted after induction time

4.4.5. Atrazine degradation products

Due to higher rate of ATZ oxidation by heterogeneous electro-Fenton reaction, this process was chosen for determine ATZ degradation products and propose the possible degradation mechanism. The reaction was performed at pH 3.0 and AlSi2Fe6 /graphite ratio of 0.6. Decrease in ATZ concentration was followed by the increase of two intermediates identified as desethyl-atrazine (DEA) and desethyl-deisopropyl-atrazine (DEIA). These results agree with the

degradation mechanism proposed by Balci et al. (2009) for ATZ oxidation by hydroxyl radicals generated through electrochemical assisted Fenton in the presence of molecular oxygen (Figure 4.10). According to Balci et al. (2009), ATZ oxidation can occurs in two parallel way (1) the reaction begin by an attack of $^{\bullet}OH$ through N-dealkylation of the side chains by hydrogen atom abstraction reactions, producing carbon centered radicals, which, in the presence of dissolved molecular oxygen gives rise to the formation of N-dealkylated derivates, such as deisopropyl-atrazine (DIA) and desethyl-atrazine (DEA), and (2) dechlorination due to attack of $^{\bullet}OH$ radicals at the C-Cl position, resulting in oxidation of the aromatic heterocyclic ring, with hydroxylation occurring simultaneously. Dechlorination leads the formation of hydroxy-atrazine (ATZ-OH) as primary intermediate. Secondary intermediates (desethyl-hydroxy-atrazine DEIA, deisopropyl-hydroxy-atrazine DIHA and desethyl-hydroxy-atrazine DEHA) are formed by dealkylation of the primary intermediates, while, desethy-isopropyl-hydroxy-atrazine (DEIHA, ameline) can be formed by dechlorination of DEIA. Finally, the oxidation of DEIHA could be lead to the formation of cyanuric acid (1,3,5-triazine-2,4,6-triol), which has a low reactivity with $^{\bullet}OH$ radicals and has been considered as a compound with a lower toxicity than atrazine and its degradation products (Hincapie-Perez et al., 2006). In similar way, Chan and Chu (2005) proposed that the ATZ degradation by homogeneous Fenton reaction in aqueous systems was initiated by alkylic-oxidation followed by dealkylation and dechlorination, while, ring-cleavage did not occur.

According to our results, ATZ degradation by heterogeneous electro-Fenton reaction occurs mainly by dealkylation of ethylamino side chain for produce DEA, which achieves a maximum at 6 h (Figure 4.11), decreasing for achieving constant after 9 h. Subsequent DEA decrease was

followed by an increment of DEIA due to dealkylation process. After 10 hours reaction a small peak of DEHIA was observed. However, it was not possible to quantify. This result suggests that ATZ dechlorination could be occur at higher reaction time. Similar results were obtained by Chan and Chu (2005) for ATZ oxidation by homogeneous Fenton reaction and by Ventura et al. (2002) in the ATZ degradation by en electro-chemical Fenton process. These works showed that the N-dealkylation of ATZ by Fenton-based process is the preferential pathway while competing with dechlorination of ATZ.

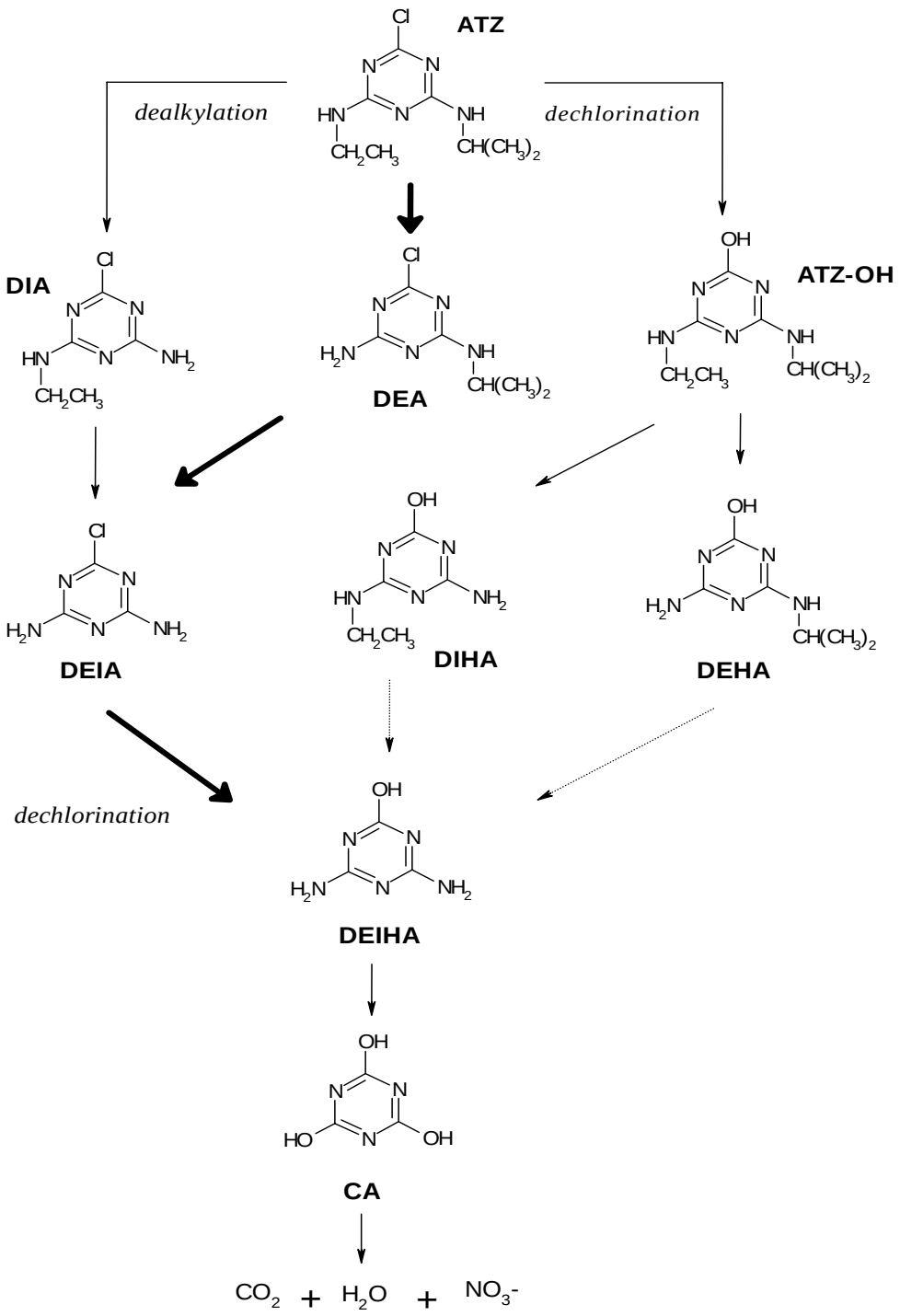

Figure 4.10. Mineralization pathway for ATZ degradation by •OH generated by electro-Fenton reaction (Modified from Balci et al., 2009), Black arrows indicate the ATZ degradation by heterogeneous electro-Fenton process using AlSi2Fe6-MGC electrodes

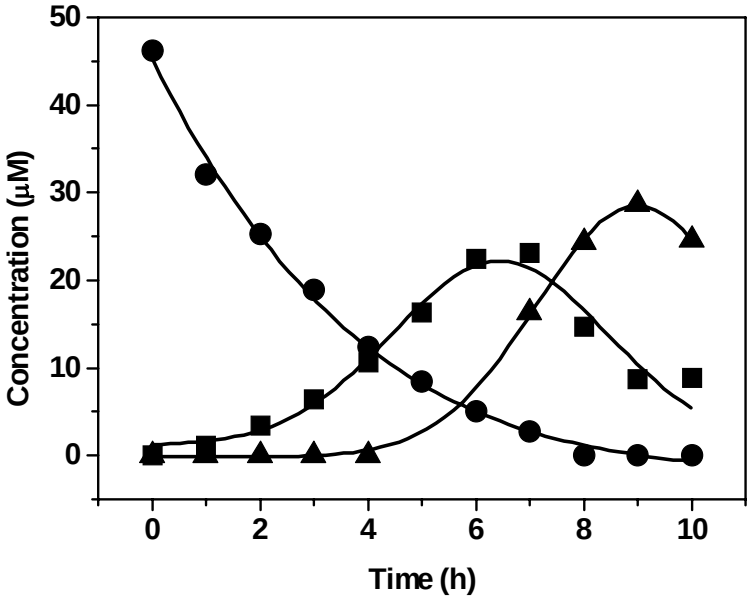

Figure 4.11. Concentration of atrazine and its aromatic intermediates detected during the heterogeneous electro-Fenton process: ATZ (•); DEA (■); DEIA (▲) ($[ATZ]_0$ = 46 μM; AlSi2Fe6-GC electrode with AlSi2Fe6/graphite rate of 0.3 at pH 3.0)

4.5. Conclusions

This study shows that iron oxide-supported allophane (AlSi2Fe6) can effectively degrade atrazine in high concentrations by both: as solid catalyst in the Fenton-like reaction and as modified agent of carbon-based electrodes in the heterogeneous electro-Fenton process. Even in both processes, the optimum pH for atrazine degradation was under acidicc conditions (pH ~ 3). In this work, it was possible to degrade ATZ under higher pH conditions (pH 4 and 6) without losing the catalytic efficiency. ATZ oxidation rates of the heterogeneous electro-Fenton process were higher than the Fenton-like reaction, which was attributed to continuous electro-regeneration of Fe^{2+}/Fe^{3+} species. Atrazine degradation by heterogeneous electro-Fenton process occurs by dealkylation of ethylamino side chain for producing desethyl-atrazine (DEA) and desethyl-deisoprophyl-atrazine (DEIA) as mainly degradation products. Therefore, in this work, the use of iron oxide-supported allophane is present as promissory catalysts in the heterogeneous Fenton process for degrading organic pollutant in high concentrations by an environmental friendly way. Further works are necessary to optimize the operation parameters.

4.6. Acknowledgments

This work was supported by a CONICYT Doctoral Scholarship as well as by a Scholarship for Implementation of Doctoral Theses 2010 (AT-24100139). FONDECYT (Projects 11070241 and 1100746) are gratefully acknowledged for their financial support.

4.7. References

Ahmad, R., Rahman, A. 2009. Sorption characteristics of Atrazine and Imazethapyr in Soils of New Zealand: Importance of Independently Determined Sorption Data. J. Agric. Food. Chem. 57, 10866-10875.

Ardakani, M., Akrami, Z., Kazemian, H., Zare, H.R. 2006. Electrocatalytic characteristics of uric acid oxidation at graphite-zeolite-modified electrode doped with iron (III). J. Electroanal. Chem. 586, 31-38.

Arnold, S.M., Hickey, W.J., Harris, R.F., 1995. Degradation of atrazine by Fenton's reagent: condition optimization and product quantification. Environ. Sci. Technol. 29, 2083–2089. Catal. Today 133–135, 600–605.

Balci, B., Oturan, N., Cherrier, R., Oturan, M. 2009. Degradation of atrazine in aqueous medium by electrocatalytically generated hydroxyl radicals. A kinetic and mechanistic study. Water Res. 43, 1924-1934.

Barr, T.L., Seal, S., Krezoski, S., Petering, D.H. 1996. X-ray Photoelectron Spectroscopic Study of the Possible Interactions of Biocells-with the Surfaces of Select Silicates. Surface and Interface analysis. 24, 99-112.

Barr, T.L., Seal, S., Wozniak, K., Klinowski, J. 1997. ESCA studies of the coordination state of aluminium in oxide environments. J. Chem. Soc., Faraday Trans., 93(1), 181 – 186.

Bergé-Lefranc, D., Eyraud, M., Schäf, O. 2008. Electrochemical determination of p-cresol concentration using zeolite-modified electrodes. C.R. Chimie. 11, 1063-1073.

Bobu, M., Yediler, A., Siminiceanu, I., Schulte-Hostede, S. 2008. Degradation studies of ciprooxacin on a pillared iron catalyst. Appl. Catal. B: Environ. 83, 15–23.

Calabi-Floody, M., Theng, B.K.G., Reyes, P., Mora, M.L. 2009. Natural nanoclays: applications and future trends – a Chilean perspective. Clay Miner. 44, 161–176.

Calabi-Floody, M., Bendal, J., Jara, A., Welland, M., Theng, B.K.G., Rumpel, C., Mora, M.L. 2011. Nanoclays from an Andisol: Extraction, properties and carbon stabilization. Geoderma 16, 159–167.

Carvalho, R.H., Lemos, F., Lemos, M.A.N.D.A, Cabral, J.M.S., Ramôa Ribeiro, F. 2006. Electrooxidation of phenol on zeolite/graphite composite electrodes Part 1. Electrochemical behavior over NaY zeolite. J. Mol. Catal. A: Chem.248, 48-52.

Chan, K.H., Chu, W., 2003. Modeling the reaction kinetics of Fenton´s process on the removal of atrazine. Chemosphere 51, 305–311.

Chan, K.H., Chu, W., 2005. Model applications and mechanism study on the degradation of atrazine by Fenton's system. J. Hazard. Mater. 118, 227–237.

Childs, C.W., Inque, K., Seyama, H., Soma, M., Theng, B.K.G, Yuan, G. 1997. X-ray photoelectron spectroscopic characterization of Silica Spring allophane. Clay Miner. 32, 565-572.

Choi, J-S., Yoon, S-S., Jang, S-H., Ahn, W-S. 2006. Phenol hydroxylation using Fe-MCM-41 catalysts. Catal. Today 111, 280−287.

Chorkendorff, I., Niemantsverdriet, J.W. 2003 in "Concepts of Modern Catalysis and Kinetiks. I", p.149. Wiley-VCH Verlag GmbH Co. KGaA, Weinheim.

Diamant, A., Pasternak, M., Banin. 2002. Characterization of Adsorbed Iron in Montmorillonite by Mossbauer SpectroscopyA. Clay. Clay. Miner. 30 (1982) 63-66

Díaz, P., Galindo, G., Escudey, M., 1990. Sintesis de aluminosilicatos semejantes a los existentes en suelos volcanicos. Bol. Soc. Chil. Quim. 35, 385–389.

Escudey, M., Galindo, G. 1983. Effect of iron oxide coatings in electrophoretic mobility and dispersion of allophane. J. Coll. Int. Sci. 93, 78-83.

Gallard, H., De Laat, J., 2000. Kinetic modelling of Fe(III)/H2O2 oxidation reactions in dilute aqueous solution using atrazine as a model organic compound. Water Res. 34, 3107–3116.

Garrido-Ramírez, E.G., Theng, B.K.G., Mora, M.L. 2010. Clays and oxide minerals as catalysts and nanocatalysts in Fenton-like reactions – A review. App. Clay Sci. 47, 182-192.

Garrido-Ramírez, E.G. Sivaiah, M.V. Barraült Joel., Valange, S. Theng, B.K., Ureta-Zañartu, M.S., Mora, M.L. 2011. Catalytic wet peroxide oxidation of phenol over iron or copper oxide-supported allophane clay materials: influence of catalyst SiO2/Al2O3 ratio. Micropor. Mesopor. Mat. Submitted. MICMAT-D-11-01077

Gligor, D., Maicaneanu, A., Walcarious, A. 2010. Iron-enriched natural zeolite modified carbon paste electrode for H2O2 detection. Electrochim. Acta. 55, 4050-4056.

Ghoneim, E., El-Desoky, H. 2010. Electrochemical determination of methocarbamol on a montmorillonite-Ca modified carbon paste electrode in formulation and human blood. Bioelectrochemistry 79 (2010) 241–247

Gómez, Y., Fernández, L., Borrás, C., Mostany, J., Scharifker, B. 2011. Characterization of a carbon paste electrode modified with tripolyphosphate-modified kaolinite clay for the detection of lead. Talanta. 85, 1357-1363.

Gracia, M., Marco, J.F., Gancedo, J.R., Exel, W., Meisel, M. 2000. A surface spectroscopic study of the corrosion of ultrathin 57Fe evaporated an Langmuir-Blodgett films in humid SO2 environments.Surf. Interf. Anal. 29, 82-91.

Hildebrandt, A., M. Guillamón, S. Lacorte, R. Tauler and D. Barceló. 2008. Impact of pesticides used in agriculture and vineyards to surface and groundwater quality (North Spain). Water Res. 42(13), 3315-3326

Hincapié-Pérez, M., Peñuela, Maldonado, M.I., Malato, O., Fernández-Ibáñez, Oller, I., Gernjak, W., Malato, S. 2006. Degradation of pesticides in water using solar advanced oxidation processes. Appl. Catal. B: Environ. 64, 272-281.

Jara, A.A., Goldberg, S., Mora, M.L. 2005. Studies of the surface charge of amorphous aluminosilicates using surface complexation models. J. Colloid Interface Sci. 292,160–170.

Jiang, H., Adams, C. 2006. Treatability of chloro-s-triazines by conventional drinking water treatment technologies. Water. Res. 40, 1657-1667.

Joo, S.H., Zhao, D. 2008. Destruction of lindane and atrazine using stabilized iron nanoparticles under aerobic and anaerobic conditions: Effects of catalyst and stabilizer. Chemosphere. 70, 418-425.

Kima, G., Jeong, W., Choe, S. 2008. Dechlorination of atrazine using zero-valent iron (Fe0) under neutral pH conditions. J. Hazard. Mater. 155, 502–506

Konstantinou, I.K., Albanis, T., Petrakis, D.E., Pomonis, P.J. 2000. Removal of herbicide from aqueous solutions by adsorption on Al-Pillared Clays, Fe-Al Pillared Clays and Mesoporous Alumina Aluminium Phosphates. Water. Res. 34(12), 3123-3136.

Lapworth, D. J. and D. C. Gooddy. 2006. Source and persistence of pesticides in a semi-confined chalk aquifer of southeast England. Environ. Pollut. 144(3), 1031-1044.

Li, Y.C., Bachas, L.G., Bhattacharyya, D., 2007. Selected chloro-organic detoxications by polychelate (poly(acrylic acid)) and citrate-based Fenton reaction at neutral pH environment. Ind. Eng. Chem. Res. 46, 7984–7992.

Malpass, G.R.P, Miwa, D.W., Machado, S.A.S., Olivi, P. Motheo, A.J. 2006. Oxidation of the pesticide at DSA electrodes. J. Hazard. Mater. B 137, 565.572.

McIntyre, N.S., Zetaruk, D.G. 1977. X-ray photoelectron spectroscopic studies of iron oxides. Anal. Chem. 49,1521-1529.

Mora, M. L. 1992. Síntesis, caracterización y reactividad de un suelo alofanico modelo. Departamento de Química. Chile, Universidad de Santiago de Chile.

Mora, M.L., Escudey, M., Galindo, G. 1994. Síntesis y caracterización de suelos alofanicos. Bol. Soc. Chil.Quim. 39, 237–243.

Nogueira, R. F. P., Trovó, A.G., d. Silva, M.R.A.,Villa, R.D., d. Oliveira, M.C. 2007. Fundamentos e Aplicacoes Ambientais dos Processos Fenton e Foto-Fenon. Quimica Nova. 30 (2), 400-408

Polcaro, A.M., Vacca, A., Mascia, M., Palmas, S. 2005. Oxidation at boron doped diamond electrodes: an effective method to mineralise triazines. Electrochim. Acta. 50, 1841-1847.

Tierney, D. P., B. R. Christensen, C. Dando, K. M. Marut, M. L. Homer, E. M. Janis and C. B. Orvin. 2008. Atrazine and Simazine Monitoring Data in Community Water Systems in the United States during 1993 to 2000. The Triazine Herbicides. San Diego, Elsevier**:** 439-449

Trasatti, S., Petrii, O.A. 1992. Real surface area measurements in electrochemistry, IUPAC, J. Electroanal. Chem., 327, 353-376.

Ureta-Zañartu, M.S., Mora, M.L., Diez, M.C., Berríos, C., Ojeda, J., Gutiérrez, C., 2002. Chlorophenol electrooxidation on iron oxide-covered aluminosilicates deposited on glassy carbon. J. Appl. Electrochem. 32, 1211–1218.

USEPA (2000) "http://www.epa.gov/pesticides/cumulative/common_mech_groups.htm#triazine.

Ventura, A., Jacquet, G., Bermond, A. Camel, V. 2002. Electrochemical generation of the Fenton`s reagent: application to atrazine degradation. Water Res. 36, 3517-3522.

Weber, J. B., Warre, R.L., Swaina, L.R., Yelverton, F.H. 2007. Physicochemical property effects of three herbicides and three soils on herbicide mobility in field lysimeters. Crop Protection 26, 299–311

5

General Discussions and Conclusions

5.1. General discussion

As was previously discussed, the use of solid catalyst as Fenton reagent in the heterogeneous Fenton process is a promissory alternative for overcome the drawbacks associated to conventional Fenton reaction. Clays or iron minerals are ubiquitous in the nature and therefore can be considered such as catalyst environmental friendly and the low cost. These characteristics offer the possibility to perform the heterogeneous Fenton processes for *in situ* remediation of contaminated soils, sediments and groundwater, beside their use as solid catalyst for organic pollutant degradation in wastewater streams. Some examples of organic pollutant degradation using clays or iron minerals as solid catalyst in the Fenton-like reaction were presented in the chapter II. In this chapter, was also discussed the use of solid catalyst in the nano-scale range. The use of nanocatalyst improve the efficiency catalytic by Fenton-like processes, due their large surface area, which implies a higher accessibility to site active for the substrate molecules than conventional homogeneous catalysts (Valdés-Solís et al., 2007). In addition, in the chapter II, iron oxide-supported allophane nanoparticles were proposed as solid catalyst in the Fenton-like reaction.

Allophane is clay minerals found mainly in soils derived from volcanic ash (Andisols). Allophane occurs as hollow in the nano-scale range (Parffit 2009) and in Andisols are in association with iron oxide, mainly ferrihydrite-like materials (Escudey and Galindo 1983). In Chile, allophane clays minerals are important due to Andisol cover about 60% (5.1 million ha) of Agricultural lands (Mora 1992; Calaby-Floody et al., 2009). For these reasons the properties of iron oxide-supported allophane have been widely studied (Mora et al., 1994; Mora and Canales, 1995; Jara et el., 2005: Jara et el., 2006), showing that the iron coating increase the acidity of the

surface sites of allophane nanoparticles. However, in the literature there is not evidence about the use of these compounds as solid catalyst in the heterogeneous Fenton processes. Similarly, the properties of allophane nanoparticles coated with copper oxide remains unexplored.

In the chapter III, is presented the first report based on experimental results, about the use of synthetic allophane with SiO_2/Al_2O_3 ratio of 1.0 (AlSi1) and 2.2 (AlSi2) as an efficient and stable iron or copper oxide-support for phenol oxidation by Fenton-like reaction. The structural and textural properties of parental allophane samples (AlSi1 and AlSi2) and their iron or copper oxide-supported counterparts were determined by X-ray diffractometry, N_2 adsorption-desorption at 77 K, electrophoretic mobility measurements, infrared spectroscopy, transmission and scanning microscopy and thermo-gravimetric analysis. The structure of AlSi1 sample was similar to Al rich soil allophane with a typical structure of imogolite but lacking its regular tubular organization (Parffit 2009). AlSi2 allohane showed a typical structure of hydrous feldspathoid with a large inter-spherule surface and therefore a high surface area. Hydrous felspathoid allophanes are composed of polymerized Si-tetrahedral, forming the framework of the allophane. In these compounds there is a wide substitution of Al for Si in the tetrahedral sites, and the remaining Al forms an uncompleted (fragmented) octahedral sheet (Avena and De Pauli 1996; Parffit 2009). As expected, the catalytic activity of the iron or copper oxide-supported allophane was markedly influenced by their SiO_2/Al_2O_3 ratio and by their respective structure. Iron or copper oxide-supported AlSi2 allophane with tail-like structure and high surface area were more active for phenol oxidation than their corresponding AlSi1 counterparts. The type of site active (iron or copper oxide) affected the efficiency catalytic for phenol oxidation by Fenton-like reaction. The copper-based allophane catalyst were far less efficient in oxidizing phenol than

their iron-supported counterparts, as was indicated by strong differences in terms of phenol conversion rates (induction period), TOC abatement values and stability of active phase.

In the chapter IV, we have studied the atrazine oxidation in a high concentration by heterogeneous Fenton process (Fenton-like reaction and electro-Fenton process) using an iron oxide-supported on allophane with SiO_2/Al_2O_3 of 2.2 as solid catalyst. We have characterized the iron-based allophane catalyst by X-ray photoelectron spectroscopy (XPS). The XPS results showed the presence of Fe^{3+} and Fe^{2+} species. As was previously reported (Mora et al., 1994; Jara et al., 2005) Fe^{3+} species are forming covalent bond with the allophane surface, with species such as Si-O-Fe and Al-O-Fe. Besides, previous Mösbauer analysis (Mora et al., 1994) showed the presence of Fe^{3+} in a ferrihydrite-like structure. However, Fe^{2+} species were not identified by Mösbauer spectroscopy at room temperature (300 K). These results suggest that Fe^{2+} species could be adsorbed or occluded in the mesopores of the allophane aggregates, and therefore, is possible that Fe^{2+} species do not pertain to the structure of aluminosilicate. In order to confirm this hypothesis is necessary to recorder a Mösbauer spectrum at cryogenic temperature.

The chapter IV shown that both processes, Fenton-like reaction and heterogeneous electro-Fenton were effective in oxidize atrazine under acidic conditions (pH ~ 3) in agreement with the optimum pH for the Fenton-based processes (Chan and Chu 2005; Gallard and De Laat 2000). However, in this work, we were able to oxidize atrazine at more initial neutral pH (pH ~6), achieving 68% ATZ decay after 24 h reaction in the Fenton-like reaction, while 76% ATZ decay was achieved in 8 h in the heterogeneous electro-Fenton process. The higher catalytic efficiency of the heterogeneous electro-Fenton process was attributed to continuous electro-regeneration of Fe^{3+}/Fe^{2+} species. It was demonstrated that ATZ degradation by heterogeneous electro-Fenton

process occurs mainly by dealkylation of ethylamino side chain for producing desethyl-atrazine (DEA) and deserhyl-deisopropyl-atrazine (DEA) as main degradation products.

5.2. General conclusions

In this work, the structural, textural and surface properties of allophane nanoparticles with SiO_2/Al_2O_3 ratio of 1.0 (AlSi1) and 2.2 (AlSi2) were studied by X-ray diffractometry, N_2 adsorption-desorption at 77 K, electrophoretic mobility measurements, infrared spectroscopy, transmission and scanning microscopy and thermo-gravimetric analysis. The structure of AlSi1 allophane was similar to Al-rich soil allophane, while AlSi2 structure was typical of hydrous feldsphatoid.

The catalytic properties of iron or copper oxide-supported allophane with different SiO_2/Al_2O_3 ratio by Fenton-like reaction were studied for phenol oxidation. The catalytic efficiency of these materials depended on their structural and surface properties, being the SiO_2/Al_2O_3 ratio the main factor that affected the catalytic activity. AlSi2 allophane as support of iron or copper oxide was effective in oxidize phenol, in aqueous medium, in agreement with its large surface area, tail-like structure and higher concentration of active site (iron or copper oxide).

The thermally treated iron oxide-supported allophane ($AlSi2Fe6_{T300}$) was the most active catalyst, achieving 63% TOC decay after 4 hours at 40ºC. This catalyst was stable in solution with a minimal Fe leached below 0.37 mg L^{-1} (0.52% of the initial iron content).

Copper oxide-supported allophane catalyst were less efficient in oxidizing phenol than their iron oxide-supporting counterparts, as was indicated by strong differences in terms of phenol conversion rates (induction period), TOC abatement values and stability of the active phase.

Atrazine oxidation in a high concentration (46 - 92 μM) was studied by heterogeneous Fenton reaction and electro-Fenton process using an iron oxide supported-allophane (AlSi2Fe6) as solid catalyst. Both processes were effective for atrazine oxidation under acidic conditions (pH ~ 3). However, it was possible to degrade ATZ at more neutral conditions (pH ~ 6), archiving 68% atrazine oxidation in the heterogeneous Fenton reaction and 76% in the electro-Fenton process.

The heterogeneous electro-Fenton process was more efficient in oxidizing atrazine than the Fenton-like reaction. The higher catalytic efficiency of heterogeneous electro-Fenton process was attributed to continuous electro-regeneration of Fe^{3+} /Fe^{2+} species. Atrazine degradation by heterogeneous electro-Fenton process occurs by dealkylation of ethylamino side chain for produce desethyl-atrazine and desethyl-desisopropyl atrazine as mainly degradation products.

5.3. References

Avena, M., De Pauli, C. 1996. Modeling the interfacial properties of an amorphous aluminosilicate dispersed in aqueous NaC1 solutions. Colloid. Surface. A. 118, 75-87.

Calabi-Floody, M., Theng, B.K.G., Reyes, P., Mora, M.L. 2009. Natural nanoclays: applications and future trends – a Chilean perspective. Clay Miner. 44, 161–176.

Chan, K.H., Chu, W., 2005. Model applications and mechanism study on the degradation of atrazine by Fenton's system. J. Hazard. Mater. 118, 227–237.

Escudey, M., Galindo, G. 1983. Effect of iron oxide coatings in electrophoretic mobility and dispersion of allophane. J. Coll. Int. Sci. 93, 78-83.

Gallard, H., De Laat, J., 2000. Kinetic modelling of Fe(III)/H2O2 oxidation reactions in dilute aqueous solution using atrazine as a model organic compound. Water Res. 34, 3107–3116.

Jara, A.A., Goldberg, S., Mora, M.L. 2005. Studies of the surface charge of amorphous aluminosilicates using surface complexation models. J. Colloid Interface Sci. 292,160–170.

Jara, A.A., Violante, A., Pigna, M., Mora, M.L. 2006. Mutual Interactions of Sulfate, Oxalate, Citrate, and Phosphate on Synthetic and Natural Allophanes. Soil Sci. Soc. Am. J. 70:337–346.

Mora, M. L. 1992. Síntesis, caracterización y reactividad de un suelo alofanico modelo. Departamento de Química. Chile, Universidad de Santiago de Chile.

Mora, M.L., Escudey, M., Galindo, G. 1994. Síntesis y caracterización de suelos alofanicos. Bol. Soc. Chil.Quim. 39, 237–243.

Mora, M.L and Canales, J. 1995. Interaction of humic substances with allophanic compounds. Commun. Soil. Sci. Plant. Anal.26, 2805-2817.

Parffit, R.L. 2009. Allophane and imogolite: role in soil biogeochemical processes. Clay Miner. 44, 135–155.

Valdés-Solís, T.P., Valle-Vigón, P., Sevilla, M., Fuertes, A.B., 2007a. Encapsulation of nanosized catalysts in the hollow core of a mesoporous carbon capsule. J. Catal. 251, 239–243.

6

Appendix

6.1. List of original papers of this thesis

Garrido-Ramírez, E.G., Theng, B.K.G., Mora, M.L. 2010. Clays and oxide minerals as catalysts and nanocatalysts in Fenton-like reactions – A review. Appl. Clay Sci. 47, 182−192.

Garrido-Ramírez, E.G. Sivaiah, M.V. Barraült Joel., Valange, S. Theng, B.K., Ureta-Zañartu, M.S., Mora, M.L. 2011. Catalytic wet peroxide oxidation of phenol over iron or copper oxide-supported allophane clay materials: influence of catalyst SiO2/Al2O3 ratio. Micropor. Mesopor. Mat. Submitted. MICMAT-D-11-01077

Garrido-Ramírez, E.G., Mora, M.L., Marco, J.F. Ureta-Zañartu, M.S. 2012. Oxidation of a high Concentration of Atrazine by Fenton-like reaction and heterogeneous electro-Fenton process using an iron-oxide supported- allophane. In preparation

6.2. List of papers in collaboration

E.G. Garrido**,** A. A. Jara and M.L. Mora; Natural Nanoclays: Physicochemical Characterization (2008) Journal of Science and Plant Nutrition. p. 280; Fasc. 3; Vol. 8; Serie. ISSN 0717-635X; Special Issue: ISMOM 2008 5th. International Symposium of Interactions of Soil Minerals with Organic

Menezes-Blackburn, D., Jorquera, M., Gianfreda, L., Rao, M., Ralf Greiner, R., Garrido, E, Mora, M.L. (2011). Activity stabilization of *Aspergillus niger* and *Escherichia coli* phytases immobilized on allophanic synthetic compounds and montmorillonite nanoclays. Bioresource Technol. 102 (2011) 9360−9367.

Silva-Weiss, A., Garrido, E., Ihl, M., Bifani V., Mora. M.L.Theng B.K. 2012. Chemical interactions, mechanical properties and structure of starch/cmc/montmorillonite nanocomposite films. In preparation.

Applied Clay Science 47 (2010) 182–192

Contents lists available at ScienceDirect

Applied Clay Science

journal homepage: www.elsevier.com/locate/clay

Review Article

Clays and oxide minerals as catalysts and nanocatalysts in Fenton-like reactions — A review

E.G. Garrido-Ramírez [a], B.K.G Theng [b,*], M.L. Mora [c]

[a] Programa de Doctorado en Ciencias de Recursos Naturales Universidad de La Frontera, Av. Francisco Salazar 01145, Casilla 54-D, Temuco, Chile
[b] Landcare Research, Private Bag 11052, Palmerston North 4442, New Zealand
[c] Scientific and Technological Bioresources Nucleus, Departamento de Ciencias Químicas, Universidad de La Frontera, Av. Francisco Salazar 01145, Casilla 54-D, Temuco, Chile

ARTICLE INFO

Article history:
Received 5 May 2009
Received in revised form 20 November 2009
Accepted 21 November 2009
Available online 29 November 2009

Keywords:
Allophane
Catalysts
Clays
Fenton-like reaction
Oxide minerals
Zeolites

ABSTRACT

Advanced oxidation processes (AOP), involving the generation of highly oxidizing radical species, have attracted much attention because of their potential in eliminating recalcitrant organic pollutants from different environmental matrices. Among the most investigated AOP is the Fenton reaction in which hydroxyl radicals ($HO^{\bullet}$) are generated through the catalytic reaction of Fe(II)/Fe(III) in the presence of hydrogen peroxide. The use of clays and iron-oxide minerals as catalysts of Fenton-like reactions is a promising alternative for the decontamination of soils, groundwaters, sediments, and industrial effluents. The low cost, abundance, and environmentally friendly nature of clay minerals and iron oxides are an added advantage. Additionally, the introduction of nanoparticles in heterogeneous catalytic processes has led to appreciable improvements in catalytic efficiency. Here we review the application of clays and iron-oxide minerals as supports or active catalysts in Fenton-like reactions, and summarize the latest advances in nanocatalyst development. We also evaluate the potential use of allophane nanoparticles, coated with iron oxides, as catalysts of Fenton-like reactions.

1. Introduction

The development of processes, such as advanced oxidation, for the efficient degradation of persistent organic pollutants in the environment has attracted a great deal of interest. Advanced oxidation processes involve the generation of reactive radicals, notably hydroxyl radicals ($HO^{\bullet}$) that are highly oxidative and capable of decomposing a wide range and variety of organic compounds (Ramírez et al., 2007a). Depending on the structure of the organic compound in question, different reactions may occur including hydrogen atom abstraction, electrophilic addition, electronic transfer, and radical–radical interactions (Nogueira et al., 2007).

Advanced oxidation processes (AOP) use a combination of strong oxidants such as ozone, oxygen, or hydrogen peroxide and catalysts (e.g., transition metals, iron), semiconductor solids together with sources of radiation or ultrasound (Primo et al., 2008a). Typical AOP include O_3/UV, H_2O_2/UV, TiO_2/UV, H_2O_2/O_3 (Pérez-Estrada et al., 2007; Popiel et al., 2008) and those based on the Fenton reaction. Initially developed by Fenton (1894) for the oxidation of tartaric acid, this reaction has been used for the decomposition and removal of hydrocarbons (Kong et al., 1998; Kanel et al., 2004; Ferrarese et al., 2008), organic dyes (Núñez et al., 2007; Cheng et al., 2008), antibiotics (Bobu et al., 2008), pesticides (Arnold et al., 1995; Balmer and Sulzberger, 1999; Gallard and De Laat, 2000; Saltmiras and Lemley, 2002; Ventura et al., 2002; Chan and Chu, 2005; Barreiro et al., 2007; Oller et al., 2007b), landfill leachates (Deng and Englehardt, 2006; Deng, 2007; Primo et al., 2008a,b), explosives (Liou and Lu, 2008), phenols (Barrault et al., 1998; Farjerwerg et al., 2000; Barrault et al., 2000b; Catrinescu et al., 2003; Carriazo et al., 2005b; Araña et al., 2007; El-Hamshary et al., 2007) as well as for microbial decontamination (Rincón and Pulgarin, 2007; Shah et al., 2007).

The Fenton process involves the reaction of Fe(II) with hydrogen peroxide, giving rise to hydroxyl radicals as shown in Eq. (1). This catalytic reaction is propagated by the reduction of Fe(III) to Fe(II) as shown in Eq. (2) with the generation of more radicals as depicted by Eqs. (3)–(5).

$$Fe^{2+} + H_2O_2 \rightarrow Fe^{3+} + OH^- + HO^{\bullet} \quad E_a = 39.5\ \text{kJ mol}^{-1} \quad k_1 = 76\ \text{M}^{-1}\text{s}^{-1} \tag{1}$$

$$Fe^{3+} + H_2O_2 \rightarrow Fe^{2+} + HO_2^{\bullet} + H^+ \quad E_a = 126\ \text{kJ mol}^{-1} \quad k_2 = 0.001\text{–}0.01\ \text{M}^{-1}\text{s}^{-1} \tag{2}$$

$$Fe^{2+} + HO_2^{\bullet} \rightarrow Fe^{3+} + HO_2^- \quad E_a = 42\ \text{kJ mol}^{-1} \quad k_3 = 1.3 \times 10^6\ \text{M}^{-1}\text{s}^{-1} \tag{3}$$

* Corresponding author. Tel.: +64 6 353 4945; fax: +64 6 353 4801.
E-mail address: thengb@landcareresearch.co.nz (B.K.G. Theng).

0169-1317/$ – see front matter © 2009 Elsevier B.V. All rights reserved.
doi:10.1016/j.clay.2009.11.044

$$Fe^{3+} + HO_2^{\bullet} \rightarrow Fe^{2+} + O_2 + H^+ \quad E_a = 33\ \text{kJ mol}^{-1} \quad k_4 = 1.2 \times 10^6\ M^{-1}s^{-1} \tag{4}$$

$$H_2O_2 + HO^{\bullet} \rightarrow HO_2^{\bullet} + H_2O \quad E_a = 14\ \text{kJ mol}^{-1} \quad k_5 = 2.7 \times 10^7\ M^{-1}s^{-1}. \tag{5}$$

Typical values of the activation energy (E_a), and apparent rate constant (k) for these reactions are taken from Lee and Yoon (2004) and Nogueira et al. (2007), respectively.

The generation of hydroxyl radicals in the Fenton reaction has been used in a variety of processes: (1) homogeneous Fenton process, involving iron(II) salts dissolved in an acid medium, (2), heterogeneous catalysis ('Fenton-like reaction'), (3) photo-reduction of Fe(III) to Fe(II) through the use of ultraviolet radiation ('photo-Fenton process') (Zeep et al., 1992; Feng et al.;, 2003a,b, 2004c, 2009; Farré et al., 2007; Malato et al., 2007; Schwingel de Oliveira et al., 2007; Oller et al., 2007a), (4) electro-oxidation and photo-electro-oxidation (Ventura et al., 2002; Andrade et al., 2007; Kurt et al., 2007; Sirés et al., 2007; Ting et al., 2007), and (5) nanocatalysis (Kwon et al., 2007; Valdés-Solís et al., 2007b; Joo and Zhao, 2008).

The homogeneous Fenton process has been widely investigated (Pignatello, 1992; Arnold et al., 1995; Lee et al., 2001; Chan and Chu, 2005; Barros et al., 2006; Deng and Englehardt, 2006; Deng, 2007; Li et al., 2007; Nogueira et al., 2007; Núñez et al., 2007; Schwingel de Oliveira et al., 2007; Siedlecka et al., 2007; Ferrarese et al., 2008). This simple process uses a conventional equipment and operates at ambient temperatures and pressures. The process, however, has some drawbacks due mainly to the formation of different Fe(III) complexes as solution pH changes.

The optimum pH for the homogeneous Fenton process is about 2.8 when the iron in solution occurs partly as Fe(III) and partly as Fe(III)$(OH)^{2+}$, representing the photo-active species. Below this pH, the hydroxyl radicals are scavenged by protons and the concentration of Fe(III)$(OH)^{2+}$ declines while above this pH, Fe(III) precipitates as an oxyhydroxide (Pignatello, 1992; Sum et al., 2005; Li et al., 2007; Martínez et al., 2007; Bobu et al., 2008). In order to maintain a pH of ~3, large amounts of acid (usually sulphuric acid) must be added to the reaction medium (Valdés-Solís et al., 2007b). Thus, it is impractical to apply the homogeneous Fenton process to *in situ* environmental remediation because (without pH adjustment) large amounts of ferric hydroxide sludges would be produced, creating disposal and other environmental problems (Catrinescu et al., 2003; Feng et al, 2004c; Hanna et al., 2008).

On the other hand, heterogeneous solid catalysts can mediate Fenton-like reactions over a wide range of pH values (Caudo et al., 2007; Cheng et al., 2008). This is because the Fe(III) species in such catalysts is "immobilized" within the structure and in the pore/interlayer space of the catalyst. As a result, the catalyst can maintain its ability to generate hydroxyl radicals from H_2O_2, and iron hydroxide precipitation is prevented (Catrinescu et al., 2003; Chen and Zhu, 2006; 2007). Besides showing limited leaching of iron ions, the catalysts can easily be recovered after the reaction, and remain active during successive operations (Centi et al., 2000; Sum et al., 2005; Kasiri et al., 2008).

A range of heterogeneous solid catalysts, including activated carbon impregnated with iron and copper oxide metals have been used to degrade recalcitrant organic compounds through the Fenton-like reaction (Georgi and Kopinke, 2005; Ramírez et al., 2007b). Some examples are Nafion film or Nafion (Fernandez et al., 1998, 1999; Gumy et al., 2005), resin-supported Fe(II) or Fe (III) (Cheng et al., 2004; Liou et al., 2005), iron-containing ashes (Flores et al., 2008), iron-coated pumice particles (Kitis and Kaplan, 2007), and iron-immobilized aluminates (Muthuvel and Swaminathan, 2008).

Clays and oxide minerals, either as such or as supports of iron and other metal species, can also serve as heterogeneous catalysts in the Fenton-like reaction (Halász et al., 1999; Barrault et al., 2000b; Chirchi and Ghorbel, 2002; Carriazo et al., 2005b; Baldrian et al., 2006; Matta et al., 2007; Bobu et al., 2008; Chen et al., 2008; Ortiz de la Plata et al., 2008). Indeed, these materials provide an attractive alternative for the decontamination of soils, underground waters, sediments, and industrial effluents because they are natural, abundant, inexpensive, and environmentally friendly (Watts et al., 1994, 2002; Watts and Dilly, 1996; Andreozzi et al., 2002a; Carriazo et al., 2005b; Aravindhan et al., 2006; Mecozzi et al., 2008). Examples of solid catalysts are natural and synthetic zeolites exchanged with iron or copper ions (Pulgarin et al., 1995; Farjerwerg and Debellefontaine, 1996; Larachi et al., 1998; Kušić et al., 2006; Chen et al., 2008; Kasiri et al., 2008), pillared interlayered clays (Barrault et al., 1998; Guélou et al., 2003; Li et al., 2006; Giordano et al., 2007; De León et al., 2008; Sanabria et al., 2008) and iron-oxide minerals (Lin and Gurol, 1998; Kwan and Voelker, 2002, 2003; Wu et al., 2006; Matta et al., 2007; Hanna et al., 2008; Liou and Lu, 2008).

However, these catalysts, especially those containing iron(III) oxides, need ultraviolet radiation to accelerate the reduction of Fe(III) to Fe(II). This is because the reaction, depicted in Eq. (2), is much slower than the decomposition of H_2O_2 in the presence of Fe(II) (Eq. (1)) as used in the photo-Fenton process (Kwan and Voelker, 2003; Nogueira et al., 2007). The photo-Fenton or photo-Fenton-like process is generally more efficient than its normal (non-irradiated) Fenton or Fenton-like counterpart but the operating cost of the former is quite high in terms of energy and UV-lamp consumption (Centi et al., 2000). Additionally, the photo-Fenton process requires that the whole catalyst be accessible to light.

Valdés-Solís et al. (2007a,b) have developed a new catalyst using nanosize particles with a high surface area that can accelerate the Fenton-like reaction without requiring UV radiation. These nanocatalysts are very reactive because the active sites are located on the surface. As such, they have a low diffusional resistance, and are easily accessible, to the substrate molecules. Nanocatalysis is but one of the many practical applications of nanotechnology which is concerned with the synthesis and functions of materials at the nanoscale range (<100 nm) (Mamalis, 2007; Miyazaki and Islam, 2007; Lines, 2008). An important feature of nanomaterials is that their surface properties can be very different from those shown by their macroscopic or bulk counterparts (Theng and Yuan, 2008). As the term suggests, 'nanocatalysis' uses nanoparticles and nanosize porous supports with controlled shapes and sizes (Bell, 2003).

This review describes the use of clays and iron-oxide minerals as supports or active catalysts in the Fenton-like reaction, and summarizes recent advances in the development of nanocatalysts with improved catalytic efficiency. We also evaluate the potential of allophane nanoparticles, coated with iron oxides, to serve as catalysts in the Fenton-like reaction.

2. Heterogeneous solid catalysts

A wide range of solid materials, such as transition metal-exchanged zeolites (Pulgarin et al., 1995; Farjerwerg and Debellefontaine, 1996; Larachi et al., 1998; Kušić et al., 2006; Chen et al., 2008; Kasiri et al., 2008), pillared interlayered clays containing iron or copper species (Barrault et al., 1998; Guélou et al., 2003; Li et al., 2006; Giordano et al., 2007; De León et al., 2008; Sanabria et al., 2008) and iron-oxide minerals (Lin and Gurol, 1998; Kwan and Voelker, 2002, 2003; Wu et al., 2006; Matta et al., 2007; Hanna et al., 2008; Liou and Lu, 2008) have been proposed as heterogeneous catalysts for the oxidative degradation of organic compounds through the Fenton-like reaction. By combining the efficiency of the homogeneous Fenton process with the advantages of heterogeneous catalysis, these materials show great promise for the treatment of highly recalcitrant organic pollutants.

Solid catalysts must fulfill a number of requirements, such as high activity in terms of pollutant removal, marginal leaching of active

cations, stability over a wide range of pH and temperature, and a high hydrogen peroxide conversion with minimum decomposition (Larachi et al., 1998). For practical applications, these materials should also be available at a reasonable cost.

2.1. Transition metal-exchanged zeolites

Zeolites are hydrated aluminosilicates with a cage-like structure. Their internal and external surface areas may extend to several hundred square meters per gram, while their cation exchange capacities are up to several milliequivalents per kilogram. At least 41 types of natural zeolites have been identified, and many others have been synthesized. Zeolites have an open porous structure capable of accommodating a wide variety of exchangeable cations, including iron (Kušić et al., 2006; Tekbas et al., 2008).

Zeolites are ideal catalysts because the dimension of their pores is similar to that of the reacting molecules (Neamtu et al., 2004b; Aravindhan et al., 2006; Tekbas et al., 2008). Thus, zeolites can function as both selective adsorbents and '*in situ*' oxidation catalysts (Doocey et al., 2004). The size and shape of the nanopores in synthetic zeolites can vary according to the experimental conditions as do their macroscopic properties (Ovejero et al., 2001b; Neamtu et al., 2004b; Tekbas et al., 2008). Being strongly bound to exchange sites within the pore structure, transition metals (e.g., iron, copper) are not prone to leach out or precipitate during the process (Neamtu et al., 2004b).

Zeolites containing transition metal ions have been shown to be efficient catalysts in the oxidation of a range of organic pollutants through the Fenton-like reaction (Ovejero et al., 2001b; Doocey et al., 2004; Makhotkina et al., 2006; Kuznestsova et al., 2008), the photo-Fenton process (Rios-Enriquez et al., 2004; Noorjahan et al., 2005; Kasiri et al., 2008; Muthuvel and Swaminathan, 2008; Tekbas et al., 2008), and the wet oxidation process using hydrogen peroxide (Larachi et al., 1998; Centi et al., 2000; Farjerwerg et al., 2000; Huu Phu et al., 2001; Ovejero et al., 2001a; Neamtu et al., 2004a,b; Zrnčević and Gomzi, 2005; Aravindhan et al., 2006).

Neamtu et al. (2004a) have proposed that Fe-exchanged zeolites degrade organic pollutants through the Fenton reaction (Eq. (1)) by generating $HO^{\bullet}$ radicals that can diffuse into the bulk solution. This implies that the pollutants are decomposed in the external medium as well as within the zeolite framework. Kušić et al. (2006) have proposed a similar mechanism for the degradation of phenol by Fe-ZSM-5 zeolite, while Noorjahan et al. (2005) concluded that the enhanced activity of a Fe(III)-HY zeolite system was due to the synergistic effect of pollutant adsorption and $HO^{\bullet}$ radical diffusion.

In common with the homogeneous Fenton process, the efficiency of heterogeneous Fenton-like catalysis is influenced by several operating parameters, such as iron concentration, type of iron catalyst, H_2O_2 concentration, iron catalyst/hydrogen peroxide ratio, temperature, pH and treatment time (Doocey et al., 2004; Kušić et al.., 2006). Data on the degradation of recalcitrant organic compounds through the Fenton reaction, using Fe- and Cu-exchanged zeolites, are summarized in Table 1.

These studies show that the catalytic efficiency and stability against leaching of Fe-exchanged zeolites are related to their iron content. For example, Doocey et al. (2004) found that the rate of hydrogen peroxide decomposition was higher for Fe-4A zeolite (3.4% w/w iron) than Fe-Beta zeolite (1.25% w/w iron). At the same time, the former was slightly more stable in the cation leaching test. The catalytic efficiency and stability of Fe-exchanged zeolites are also affected by pH and temperature. Using Fe-Beta and Fe-4A zeolites as catalysts, Doocey et al. (2004) observed optimal hydrogen peroxide decomposition at pH 3.5. Neamtu et al. (2004b) reported that the degradation of the Azo dye *Procion Marine H-EXL* by Fe-Y zeolite was higher at pH 3 (97%) than at pH 5 (53%) in 10 min of operation, while increasing the time of operation to 30 min resulted in 97% removal at pH 5. For the reaction at pH 3, this (initial) value did not change throughout the treatment. During the reaction at pH 5, however, the pH decreased to about 3.5. This might be because the dye molecules fragment into organic acids as the reaction proceeds. As a result, solution pH decreases and the degradation process is accelerated (Neamtu et al., 2004b). Similar results were obtained by Kasiri et al. (2008) for the photo-degradation of Acid Blue 74 using Fe-ZSM-5 zeolite. Thus, Fe-exchanged zeolites can effectively operate at near neutral pH as cation leaching is limited, and zeolite stability is maintained (Doocey et al., 2004; Neamtu et al., 2004a,b).

Although a rise in temperature increases catalytic efficiency, it also enhances cation leaching and decomposition of hydrogen peroxide to oxygen and water. Neamtu et al. (2004a) found an optimal temperature of 50 °C for the degradation of the azo dye C.I. Reactive Yellow 84 (RY84) by wet hydrogen peroxide oxidation using a Fe-exchanged Y zeolite catalyst.

The preparation of metal-exchanged zeolites also influences catalytic activity. Valkaj et al. (2007), for example, reported that the activity of a Cu-ZSM-5 catalyst prepared by direct hydrothermal synthesis (DHS) was higher than that of a catalyst obtained by the ion exchange (IE) method in terms of phenol oxidation and hydrogen peroxide decomposition. The stability of the DHS catalyst was also superior to that of the IE material because leaching of the active ingredient was relatively low in the former instance.

Using a Fe-exchanged zeolite, Centi et al. (2000) compared the catalytic efficiency of the homogeneous Fenton process with that of the (heterogeneous) Fenton-like reaction. The Fe-ZSM-5 catalyst was more efficient in degrading propionic acid (72%) than the homogeneous Fenton process (43%). The heterogeneous process was also less sensitive to changes in pH.

2.2. Pillared interlayered clays

Pillared interlayered clays (PILC) are low-cost, microporous solid catalysts with unique properties and structures (Li et al., 2006; Ramírez et al., 2007a; Mishra et al., 2008), formed by intercalation of metal polycations into swelling clay minerals, notably smectites. On heating at high temperatures (≈500 °C), the intercalated polycations are converted into the corresponding metal oxide clusters through dehydration and dehydroxylation. By propping the silicate layers apart, these oxides act as "pillars", creating interlayer meso- and micro-pores (Mishra et al., 1996; Kloprogge, 1998; Bergaya et al., 2006; Bobu et al., 2008; Pan et al., 2008). The intercalation of metal oxocations increases the basal spacing of the parent clays. The increase in basal spacing is higher for Fe-supported Al-PILC catalysts (Fe–Al-PILC) than for their Fe-PILC counterparts. Li et al. (2006) reported a basal spacing increment of 0.62 nm for Fe–Al-PILC and 0.51 nm for Fe-PILC with respect to the original bentonite clay, while Chen and Zhu (2007) reported an increment of 3.93 nm for Fe-PILC. Sanabria et al. (2008) found a basal spacing increment of 0.38 nm for Al–Fe-PILC, while Pan et al. (2008) observed an increment of 0.64 nm for Al-PILC prepared from Na-montmorillonite.

The surface area of PILC, determined by adsorption of N_2 gas at 77 K and applying the Brunauer–Emmett–Teller (BET) equation, is invariably much larger than the corresponding starting clay or clay mineral. For example, Pan et al. (2008) measured a surface area of 176 $m^2\,g^{-1}$ for Al-PILC as against 43 $m^2\,g^{-1}$ for the original Na-montmorillonite. Similarly, Li et al. (2006) obtained a BET surface area of 114.6 $m^2\,g^{-1}$ for Fe-PILC and 194.2 $m^2\,g^{-1}$ for Al–Fe-PILC as compared with 31.8 $m^2\,g^{-1}$ for the original bentonite clay. In addition, pillaring greatly increases the accessibility of interlayer catalytic sites to the reactant molecules (Kloprogge, 1998; Carriazo et al., 2003; Sanabria et al., 2008).

Pillared interlayered clays containing oxocations of copper (Cu-PILC) or iron (Fe-PILC) together with Al-PILC supporting iron and copper ions, have been widely used as catalysts for the degradation of recalcitrant organic compounds via Fenton-like reactions, photo-

Table 1
Catalytic degradation of organic compounds over iron- or copper-exchanged zeolites through different Fenton-like processes.

Compound	Catalyst/support	Process	Reference
Remazol Brilliant Orange 3C	Fe(III)-exchanged natural zeolite	Photo-Fenton	Tekbas et al. (2008)
Indigoid dye C.I. Acid Blue 74	Fe-ZSM-5 synthetic zeolite	Photo-Fenton	Kasiri et al. (2008)
Reactive Brilliant Blue KN-R	Fe-NaY and Fe-ZSM-5	Fenton-like reaction	Chen et al. (2008)
Azo dye Acid Violet 7	Fe(III) immobilized Al_2O_3 catalyst	Photo-Fenton	Muthuvel and Swaminathan (2008)
Azo dye Porción Marine H-EXL	Fe-exchanged Y zeolite	Wet hydrogen peroxide oxidation	Neamtu et al. (2004b)
Acid brown	Mn-exchanged Na-Y zeolite	Wet hydrogen peroxide oxidation	Aravindhan et al. (2006)
C.I. Reactive Yellow 84 (RY84)	Fe-Y zeolite	Wet hydrogen peroxide oxidation	Neamtu et al. (2004a)
Phenol	Fe-ZSM-5 zeolite	Wet hydrogen peroxide oxidation	Huu Phu et al. (2001)
Phenol model wastewater	Fe-ZSM-5	Fenton-like reaction and Photo-Fenton	Kušić et al. (2006)
Phenol	Cu-Y-5	Wet hydrogen peroxide oxidation	Zrnčević and Gomzi (2005)
Chlorinated phenols	Fe-Beta zeolite Fe-4A zeolite	Fenton-like reaction	Doocey et al. (2004)
Phenolic solutions	Fe-NaY, Fe-USY, and Fe-ZSM-5	Fenton-like reaction	Ovejero et al. (2001b)
Phenol	Fe(III)-HY catalyst	Photo-Fenton	Noorjahan et al. (2005)
Phenol	MFI zeolite	Wet hydrogen peroxide oxidation	Ovejero et al. (2001a)
Phenol	Fe-ZSM-5	Wet hydrogen peroxide oxidation	Farjerwerg et al. (2000)
Phenolic aqueous wastes	Fe-ZSM-5	Wet hydrogen peroxide oxidation	Farjerwerg and Debellefontaine (1996)
Phenolic aqueous wastes	Fe-ZSM-5	Wet hydrogen peroxide oxidation	Farjerwerg et al. (1997)
4-Nitrophenol	Fe-ZSM-5	Photo-Fenton	Pulgarin et al. (1995)
Phenol	Cu-ZSM-5	Wet hydrogen peroxide oxidation	Valkaj et al. (2007)
1,1-Dimethylhydrazine and ethanol	Fe-MF1 zeolite catalyst	Fenton-like reaction	Kuznestsova et al. (2008)
1,1-Dimethylhydrazine	Fe-ZSM-5 zeolite	Fenton-like reaction	Makhotkina et al. (2006)
Carboxylic acids	Fe-ZSM-5	Wet hydrogen peroxide oxidation	Centi et al. (2000)
Acetic acid	Cu–NaY zeolite	Wet hydrogen peroxide oxidation	Larachi et al. (1998)
2,4-xylidine	Fe(III)-zeolite Y	Fenton-like reaction	Rios-Enriquez et al. (2004)

Fenton reactions, and wet hydrogen peroxide oxidation (Table 2). Pillared interlayered clay catalysts are also very stable, showing minimal leaching of interlayer metal species to the external solution (Caudo et al., 2007; Chen and Zhu, 2007; Giordano et al., 2007; Ramírez et al., 2007a; Bobu et al., 2008; Caudo et al., 2008; Pan et al., 2008; Sanabria et al., 2008). These materials can therefore be used repeatedly with little loss of catalytic activity, while problems associated with water contamination by soluble metals and waste disposal are avoided. The relatively short periods of operation are an added advantage of using PILCs catalysts.

In investigating the wet acid oxidation by H_2O_2 of *p*-coumaric acid and *p*-hydroxybenzoic acid using Cu-PILC with different Cu loadings (0.5, 1.0 and 2.0% Cu), Caudo et al. (2008), for example, found that 76–82% of total organic carbon (TOC) was removed within 4 h of operation. Similarly, Sanabria et al. (2008) observed 100% removal of phenol in 2 h of operation by a Fenton-like reaction, using Fe-PILC in

Table 2
Pillared interlayered clays (PILC) as heterogeneous catalysts for the decomposition of various organic compounds via Fenton-like reactions.

Compound	Catalyst/support	Clay	Process	Reference
Azo dye X-3B	Fe-PILC Al–Fe-PILC	Bentonite	Photo-Fenton	Li et al. (2006)
Methylene blue	Fe-PILC	Natural montmorillonite	Photo-Fenton	De León et al. (2008)
Orange II	Hydroxyl-Fe-PILC	Bentonite	Photo-Fenton	Chen and Zhu (2006)
Acid Light Yellow G	Fe-PILC (catalyst)	Natural bentonite	Photo-Fenton	Chen and Zhu (2007)
Azo dye Orange II solution	Al-PILC impregnated with Fe	Natural saponite	Fenton-like reaction	Ramírez et al. (2007a)
Ciprofloxacin (fluoroquinolones)	Fe-PILC nanocomposite	Laponite (synthetic hectorite)	Photo-Fenton	Bobu et al. (2008)
Phenol	Mixed (Al–Fe)-PILC	Commercial Greek bentonite	Catalytic wet oxidation with H_2O_2	Barrault et al. (2000a)
Phenol	Al–Cu-PILC Al–Fe-PILC	Commercial Greek bentonite	Catalytic wet oxidation with H_2O_2	Barrault et al. (2000b)
Phenol	Al- or mixed Al–Fe-complexes PILC	Commercial Greek bentonite	Catalytic wet oxidation with H_2O_2	Guélou et al. (2003)
Phenol	Fe-PILC	Laponite	Photo-Fenton	Iurascu et al. (2009)
4-Nitrophenol	Fe(III)-exchanged PILC	Montmorillonite	Fenton-like reaction	Chirchi and Ghorbel (2002)
Phenol	Al–Cu-, Al–Fe- and Fe-PILC	Natural sodium bentonite and natural sodium montmorillonite	Catalytic wet oxidation with H_2O_2	Carriazo et al. (2003)
Phenol	Fe-exchanged Al-PILC	Synthetic beidellite	Catalytic wet oxidation with H_2O_2	Catrinescu et al. (2003)
Phenol	Al-, Al–Fe- and Al–Ce–Fe-PILC	Natural Colombian bentonite	Catalytic wet oxidation with H_2O_2	Carriazo et al. (2005a)
Phenol	Al–Fe-PILC Al–Ce–Fe-PILC	Natural Colombian bentonite	Fenton-like reaction	Carriazo et al. (2005b)
Phenol	Al–Fe-PILC	Natural bentonite	Catalytic wet oxidation with H_2O_2	Sanabria et al. (2008)
Benzene	Al-PILC as supports for Cu, V, Fe	Natural sodium montmorillonite	Fenton-like reaction	Pan et al. (2008)
p-Coumaric acid and *p*-hydroxybenzoic acid olive oil mill wastewater	Cu-PILC Fe-PILC	Commercial bentonite	Catalytic wet oxidation with H_2O_2	Caudo et al. (2007)
Polyphenols olive oil mill wastewater	Cu-based zeolite Cu-PILC	Zeolite and commercial bentonite	Catalytic wet oxidation with H_2O_2	Giordano et al. (2007)
Wastewater from agro-food production	Cu-PILC	Commercial bentonite	Catalytic wet oxidation with H_2O_2	Caudo et al. (2008)

an aqueous medium, while Giordano et al. (2007) were able to remove 97% of polyphenols from olive oil mill wastewater within 3 h, using Cu-PILC in a wet oxidation process with H_2O_2. Although the optimal pH for the Fenton and photo-Fenton processes is around 3 (Ramírez et al., 2007a; Bobu et al., 2008; Sanabria et al., 2008), Fe-PILC are active over a wide range of pH (De León et al., 2008), and offer the potential to operate at near neutral pH without significant loss of activity (Chen and Zhu, 2007; Bobu et al., 2008; Caudo et al., 2008).

As already remarked on, this is because the Fe(III) species is largely "immobilized" in the interlayer space of the clay mineral. As such, the iron in PILC is stable against changes in solution pH and shows only limited leaching. Further, the strong surface acidity of some Fe-PILC allows catalytic activity to be maintained over a wide range of pH values (Chen and Zhu, 2006, 2007; De León et al., 2008). In using Fe-PILC as heterogeneous catalysts, H_2O_2 is often added to the solution at near neutral pH. As the reaction proceeds, however, the solution pH decreases due to the formation of acidic intermediates (e.g., acetic acid, oxalic acid). These acids can capture any Fe ions that are released from the catalyst, giving rise to soluble complexes and promoting a homogeneous Fenton process. The concentration of Fe in solution is proportional to that of the pollutant. When the acidic intermediates are mineralized (oxidized) to CO_2 and H_2O, the Fe ions can be re-adsorbed to the PILC surface, forming an Fe(III) cycle (Bobu et al., 2008).

2.3. Iron-oxide minerals

The ability and potential of iron-oxide minerals to catalyze the oxidation of organic compounds through the Fenton-like reaction have been well documented (Lin and Gurol, 1998; Huang et al., 2001; Kwan and Voelker, 2002, 2003; Baldrian et al., 2006; Wu et al., 2006; Matta et al., 2007; Hanna et al., 2008; Liou and Lu, 2008; Ortiz de la Plata et al., 2008). The iron-oxide minerals that have been investigated include goethite (Kong et al., 1998; Lin and Gurol, 1998; Huang et al., 2001; Kwan and Voelker, 2003; Wu et al., 2006; Liou and Lu, 2008), hematite (Huang et al., 2001; Matta et al., 2007), magnetite (Kong et al., 1998), ferrihydrite (Huang et al., 2001; Kwan and Voelker, 2002; Barreiro et al., 2007), pyrite (Matta et al., 2007) and lepidocrocite (Matta et al., 2007).

Iron oxides, used for wastewater decontamination, can be recovered and reused because they are practically insoluble in water. Since iron minerals are widespread in the soil environment, they can also be used for the *in situ* remediation of soils and groundwaters through the Fenton-like reaction in the presence of H_2O_2 (Kanel et al., 2004; Yeh et al., 2008). Furthermore, the operation does not require strict control of pH as is the case in the homogeneous Fenton process (Andreozzi et al., 2002a). Several authors, for example have reported that the iron/hydrogen peroxide system can catalyze the oxidation of pollutants at pH values between 3 and 7 through a Fenton-like reaction (Table 3). The process apparently involves hydroxyl radicals, generated by decomposition of hydrogen peroxide on the surface of iron-oxide particles through a chain reaction mechanism (Lin and Gurol, 1998; Huang et al., 2001; Kwan and Voelker, 2003) although Andreozzi et al. (2002a) have suggested that the oxidation of organic compounds can occur through a non-radical mechanism (Table 4).

According to the radical mechanism proposed by Lin and Gurol (1998), the reaction is initiated by the formation of an inner-sphere complex between hydrogen peroxide (H_2O_2) and ≡Fe(III)–OH groups at the oxide surface (Table 4, Eq. (2.1)). The surface complex may be regarded as a ground-state (Eq. (2.2) (mediating a reversible electronic transfer from ligand to metal. The electronically excited state can be deactivated through dissociation of the peroxide radical ("successor complex"), as shown by Eq. (2.3). Being very active, the peroxide radical can immediately react with other compounds. Therefore, the reverse reaction of Eq. (2.3) may be assumed to be negligible ($K_3 >> K_{3a}$). The reduced iron can react with either hydrogen peroxide or oxygen, as shown by reactions 2.4 and 2.4a. Reaction 2.4a, however, is slower than reaction 2.4. The hydrogen and peroxide radicals produced can react with Fe(II) and Fe(III), exposed on surface sites, according to reactions 2.6 and 2.7. These free radicals can also react with H_2O_2 (reactions 2.8 and 2.9). Finally, the radicals can react with themselves, terminating the reactions (2.10 and 2.11).

On the other hand, Andreozzi et al. (2002a) have suggested a non-radical mechanism for the degradation of 3,4-dihydroxybenzoic acid as shown by Eqs. (2.22) and (2.23) (Table 4) where (*) denotes the active sites on the catalyst and C_I is their concentration (mol dm^{-3}). The adsorbed substrate (S) and hydrogen peroxide react on the catalyst surface, giving rise to reaction products and the regeneration of active sites (Eq. (2.24)).

The efficiency of iron-oxide minerals in catalyzing the decomposition of the organic pollutants through the Fenton-like reaction is influenced by several parameters, such as hydrogen peroxide concentration, type and surface area of the iron mineral, solution pH (and ionic strength), and pollutant characteristics (Matta et al., 2007; Yeh et al., 2008). Kwan and Voelker (2003) have described a method for determining the rate of formation of hydroxyl radicals ($V_{OH\bullet}$) in iron oxide/hydrogen peroxide systems. $V_{OH\bullet}$ is proportional to the product of the concentrations of surface area of the iron oxide and hydrogen peroxide, with a different coefficient of proportionality for each iron oxide.

Since the concentration of hydrogen peroxide is directly related to the amount of hydroxyl radicals produced in the catalytic reaction, this parameter influences degradation efficiency. In investigating the oxidation of dimethyl sulphoxide (DMSO) by hydrogen peroxide with goethite as catalyst, Wu et al. (2006) found that when the H_2O_2 concentration was increased from 2.5 to 10 g/L, more hydroxyl radicals were generated, and the rate of degradation increased. However, when the dosage of H_2O_2 was further increased from 10 to 15 g/L, the rate of decomposition declined. This was ascribed to scavenging of H_2O_2 by hydroxyl radicals resulting in the formation of hydroperoxide radicals that were much less active and did not contribute to the oxidation of DMSO.

As regards mineral type, Fe(III) oxides are catalytically less active than their Fe(II) counterparts (Kwan and Voelker, 2003). In evaluating the activity of different iron minerals in catalyzing the degradation of 2,4,6-trinitrotoluene (TNT) through a Fenton-like reaction in aqueous solution at pH 3, Matta et al. (2007) found that iron(III) oxides (hematite, goethite, lepidocrocite, and ferrihydrite) were less effective than Fe(II) minerals, such as magnetite and pyrite.

The surface area of iron-oxide minerals is also an important factor influencing the degradation of organic pollutants by the Fenton-like reaction. Hanna et al. (2008), for example, observed that the efficiency of four quartz–iron-oxide mixtures in degrading methyl red (MR) at pH 5 decreased in the order quartz–goethite (Q_4)>quartz/amorphous iron(III) oxide (Q_1)>quartz–maghemite (Q_2)>quartz–magnetite (Q_3). This was also the order by which the surface area of the mineral mixtures decreased: Q_4 (148 m^2 g^{-1})>Q_1 (121 m^2 g^{-1})>Q_2 (11.5 m^2 g^{-1})>Q_3 (8.6 m^2 g^{-1}).

Other factors influencing the degradation of organic compounds by iron oxides are medium pH and chemical properties of the pollutant. At acid pH values, the degradation process is mainly due to dissolution of iron oxides in solution, promoting the homogeneous Fenton-like reaction. Liou and Lu (2008) studied the degradation of explosives (2,4,6-trinitrophenol and ammonium picrate) by hydrogen peroxide at pH 2.8, using goethite as catalyst. Here again, the underlying mechanism involves dissolution of goethite and the generation of ferrous ions which react with H_2O_2 to produce HO•, according to the homogeneous Fenton process. In studying the oxidation of atrazine using ferrihydrite as catalyst, Barreiro et al. (2007) found that the rate of oxidation strongly depended on pH. A high degradation rate was observed at pH 3–4 when ferrihydrite dissolution strongly increased. The increase in oxidation rate at low pH was attributed to the

Table 3
Oxidation of various organic compounds catalyzed by iron-oxide minerals through Fenton-like processes.

Compound	Catalyst	Process	Reference
Bromophenol Blue, Chicago Sky Blue, Cu Phthalocyanine, Eosin Yellowish, Evans Blue, Naphthol Blue Black, Phenol Red, Poly B-411, Reactive Orange 16	Magnetic mixed iron oxides ($MO–Fe_2O_3$); M = Fe, Co, Cu, Mn	Fenton-like reaction	Baldrian et al. (2006)
Methyl red (MR)	Quartz/amorphous iron(III) oxide, quartz/maghemite, quartz/magnetite, and quartz/goethite	Fenton-like reaction	Hanna et al. (2008)
2,4,6-Trinitrophenol and ammonium picrate	Goethite	Fenton-like reaction	Liou and Lu (2008)
2,4,6-Trinitrotoluene	Ferrihydrite, hematite, goethite, lepidocrocite, magnetite and pyrite	Fenton-like reaction	Matta et al. (2007)
2-Chlorophenol	Ferrihydrite, goethite and hematite	Fenton-like reaction	Huang et al. (2001)
2-Chlorophenol	Goethite	Fenton-like reaction	Lu et al. (2002)
Benzoic acid	[gamma]-FeOOH	Fenton-like reaction	Chou and Huang (1999)
3,4-Dihydroxybenzoic acid	Goethite	Hydrogen peroxide in aqueous slurry	Andreozzi et al. (2002a)
Petroleum-contaminated soils (diesel and kerosene)	Goethite and magnetite	Fenton-like reaction	Kong et al. (1998)
Aromatic hydrocarbons and chloroethylenes	Goethite	Fenton-like reaction	Yeh et al. (2008)
Atrazine	Ferrihydrite	Fenton-like reaction	Barreiro et al. (2007)
Aromatic substrates	Goethite	Hydrogen peroxide in aqueous slurry	Andreozzi et al. (2002b)
Dimethyl sulphoxide	Goethite	Fenton-like reaction (aqueous solution)	Wu et al. (2006)

enhanced solubility of iron (III) species at acid pH, promoting the homogeneous Fenton reaction. Fe(III) can also be solubilized by forming complexes with organic acid intermediates produced during pollutant degradation (Feng et al., 2006; Martínez et al., 2007; Bobu et al., 2008).

At near neutral pH values, the solubility of iron-oxide minerals decreases, and hence the degradation of organic compounds (on the catalyst surface) is mediated by the heterogeneous Fenton reaction which controls the efficiency of the process. Under these conditions, the electrostatic interactions between the catalyst surface and the organic compounds become important. Kwan and Voelker (2004) investigated the effect of electrostatic interaction between catalyst (goethite) surface and several probe molecules (formic acid, nitrobenzene and 2-chlorophenol) on their oxidization by H_2O_2. At pH 4, formic acid was negatively charged and interacted with the positively charged iron-oxide surface where HO. species were generated. As a result, the oxidation rate of formic acid increased by a factor of 50 relative to that of the neutral molecule. This observation provides strong support for the hypothesis that surface-adsorbed organic compounds are readily accessible to oxidation by HO. radicals.

Hanna et al. (2008) evaluated the catalytic efficiency of four iron oxide-quartz mixtures in degrading methyl red (MR) at pH 5 and 7. The high catalytic activity at pH 5 was ascribed to electrostatic interactions between the carboxylate group of MR (pKa = 5.1) and the partially protonated oxide surface (PZC > 6). Since the soluble iron concentration at both pH values was below the limit of detection, adsorption of MR to the solid oxide surface had a determining influence on the degradation of MR through the heterogeneous Fenton reaction. Wu et al. (2006) found that the goethite-catalyzed degradation of dimethyl sulphoxide (DMSO) decreased in the order: pH 5 > pH 3 > pH 7 ≈ pH 10. They suggested that electrostatic interactions between the partial negative charge on the oxygen atom of DMSO and the partially protonated goethite surface at pH 5 favoured degradation.

Table 4
Mechanisms proposed for the oxidation of organic compounds on the surface of iron-oxide catalysts through a Fenton-like reaction.

1. Radical mechanism proposed by Lin and Gurol (1998)

$$\equiv Fe(III)-OH + H_2O_2 \Leftrightarrow (H_2O_2)_s \quad (2.1)$$
$$(H_2O_2)_s \Leftrightarrow (\equiv Fe(II)^*O_2H) + H_2O \quad (2.2)$$
$$(\equiv Fe(II)^*O_2H) \Leftrightarrow Fe(II) + HO_2^* \quad (2.3)$$
$$\equiv Fe(II) + H_2O_2 \xrightarrow{K_4} \equiv Fe(III)-OH + {}^*OH + H_2O \quad (2.4)$$
$$Fe(II) + O_2 \xrightarrow{K_{4a}} Fe(III)-OH + HO_2^* \quad (2.4a)$$
$$HO_2^* \Leftrightarrow H^+ + O_2^{*-} \quad pKa = 4.8 \quad (2.5)$$
$$\equiv Fe(III)-OH + HO_2^* / O_2^{*-} \xrightarrow{K_6} \equiv Fe(II) + H_2O / OH^- + O_2 \quad (2.6)$$
$${}^*OH + \equiv Fe(II) \xrightarrow{K_7} \equiv Fe(III)-OH \quad (2.7)$$
$${}^*OH + (H_2O_2)_s \xrightarrow{K_8} Fe(III)-OH + HO_2^* + H_2O \quad (2.8)$$
$$(H_2O_2)_s + HO_2^* / O_2^{*-} \xrightarrow{K_9} \equiv Fe(III)-OH + H_2O / OH^- + {}^*OH + O_2 \quad (2.9)$$
$$HO_2^* + HO_2^* \xrightarrow{K_{10}} (H_2O_2)_s + O_2 \quad (2.10)$$
$${}^*OH + HO_2^* / O_2^{*-} \xrightarrow{K_{11}} H_2O_2 + O_2 \quad (2.11)$$

2. Radical mechanism proposed by Kwan and Voelker (2003)

$$\equiv Fe(III) + H_2O_2 \rightarrow \equiv Fe(HO_2)^{2+} + H^+ \quad (2.12)$$
$$\equiv Fe(HO_2)^{2+} \rightarrow \equiv Fe(II) + HO_2^* \quad (2.13)$$
$$\equiv Fe(II) + H_2O_2 \rightarrow Fe(III) + {}^*OH + OH^- \quad (2.14)$$
$${}^*OH + H_2O_2 \rightarrow H_2O + HO_2^* \quad (2.15)$$
$$\equiv Fe(II) + O_2^{*-} \rightarrow \equiv Fe(III) + O_2 \quad (2.16)$$
$$\equiv Fe(III) + HO_2^* \rightarrow \equiv Fe(II) + HO_2^- \quad (2.17)$$
$$\equiv Fe(II) + HO_2^- \rightarrow \equiv Fe(III) + HO_2^* \quad (2.18)$$

3. Non-radical mechanism proposed by Andreozzi et al. (2002a) *for the oxidation of 3,4-dihydroxybenzoic acid in a goethite/H_2O_2 system*

$$\equiv Fe(III)-OH \text{ (catalytically active sites on goethite)} \quad (2.19)$$
$$\equiv Fe(III)-OH + H^+ \rightarrow \equiv Fe(III)-OH_2^+ \quad (2.20)$$
$$\equiv Fe(III)-OH \rightarrow Fe(III)-O^- + H^+ \quad (2.21)$$
$$H_2O_2 + (*) \xleftrightarrow{K_h} H_2O_2^* \qquad K_h = \frac{[H_2O_2^*]}{H_2O_2C_l} \quad (2.22)$$
$$S + (*) \xrightarrow{K_1} S^* \quad (2.23)$$
$$S + H_2O_2^* \xrightarrow{K_2} products + 2(*) \quad (2.24)$$

2.4. Nanocatalysts

An important feature of nanoparticles is that their surface properties can deviate markedly from those of their macroscopic (bulk) counterparts (Theng and Yuan, 2008). In terms of catalysis, the activity and selectivity of nanocatalysts are strongly dependent on their size, shape, and surface structure, as well as on their bulk composition (Bell, 2003; Perez, 2007). The synthesis, development, and practical applications of nanoparticulate catalysts have been described by Bell (2003), Perez (2007), Bach et al. (2008), and Dhakshinamoorthy and Pitchumani (2008). Examples of the use of nanocatalysts in the degradation of recalcitrant organic compounds are given in Table 5. Liu (2006) have proposed that nanoparticles are potentially useful for remediating polluted sites because they can reach or penetrate into zones that are inaccessible to microsize solid catalysts.

The application of nanoparticles as catalysts of the Fenton-like and photo-Fenton reactions has been described by several investigators (Feng et al., 2004a,b, 2006; Valdés-Solís et al., 2007a,b; Zelmanov and Semiat, 2008). In comparison with their microsize counterparts, nanoparticles show a higher catalytic activity because of their large

Table 5
Nanocatalysts used in the degradation of various organic compounds.

Compound	Nanocatalyst	Process	Reference
Orange II	Composite of iron-oxide and silicate nanoparticles (Fe-nanocomposite)	Photo-Fenton reaction	Feng et al. (2003a)
Orange II	Fe^{3+}-doped TiO_2 and bentonite clay-based Fe nanocatalyst	Photo-Fenton reaction	Feng et al. (2004a)
Orange II	Bentonite clay-based Fe-nanocomposite	Photo-Fenton reaction	Feng et al. (2004b)
Trichloroethene	Pd-on-Au	Aqueous-phase hydrodechlorination	Nutt et al. (2006)
Butachlor	Immobilized TiO_2 nanoparticles	Photocatalysis in aqueous solution	Mahmoodi et al. (2007)
Nonylphenyl poly (oxyethylene) ethers (NPE-10)	Au-doped nano-TiO_2	Photo-degradation	Du et al. (2008)
Orange G	Iron–nickel bimetallic nanoparticles	Degradation in aqueous solution	Bokare et al. (2008)
Phenol	Chain-like Ru nanoparticle arrays	Hydrogenation in aqueous media	Lu et al. (2008)
Lindane and atrazine	Fe–Pd bimetallic nanoparticles	Aerobic and anaerobic degradation	Joo and Zhao (2008)
Cango red	Selenium nanoparticles	Photocatalytic decolorization	Yang et al. (2008)

specific surface where catalytically active sites are exposed (Nurmi et al., 2005). The advantage of using nanoparticles as catalysts for Fenton-like reactions would more than offset the disadvantage (associated with the use of iron(III) catalysts) of requiring ultraviolet radiation to accelerate the reaction.

In investigating the catalytic degradation of ethylene glycol and phenol by iron(III) oxide nanoparticles in the absence of ultraviolet radiation, Zelmanov and Semiat (2008) found that the rate of degradation was 2–4 and 35 times higher, respectively, than the values reported in the literature using Fenton's reagent/H_2O_2/UV. Kwon et al. (2007) evaluated two iron-oxide catalysts for the oxidation of carbon monoxide and methane at low temperatures. One of the materials (NANOCAT®) had an average particle size of 3 nm and a specific surface area of 250 $m^2\,g^{-1}$, while the other material (Fe_2O_3PVS) had an average particle size of 300 nm and a surface area of 4 $m^2\,g^{-1}$. Although both catalysts were effective, the nanocatalyst showed superior activity because of its high surface area. Using a nanocasting technique, Valdés-Solís et al. (2007b) obtained $MnFe_2O_4$ nanoparticles as heterogeneous catalysts for the Fenton-like reaction. These solid nanocatalysts were active over a wide range of pH values (6–13) and H_2O_2 concentrations (0.005–3 M).

3. Iron-oxide-coated allophane nanocatalysts in Fenton-like reactions

Allophane is the main component of the clay fraction of soils derived from volcanic ash and weathered pumice (Andisols) which are widespread in southern Chile. Iron oxides of short-range order, notably ferrihydrite, are also widespread in Andisols although their concentration rarely exceeds 10% (Galindo, 1974). These constituents often occur as coatings of clay mineral particles.

Allophane may be defined as "a group of clay-size minerals with short-range order which contain silica, alumina, and water in chemical combination" (Parfitt, 1990). Allophanes occur as hollow spherules with an external diameter between 3.5 and 5.5 nm and a wall thickness of 0.7–1.0 nm. Defects in the wall structure give rise to perforations of about 0.3 nm in diameter permitting water molecules to enter the inner-spherule void (Henmi and Wada, 1976; Wada and Wada, 1977; Hall et al., 1985; Brigatti et al., 2006). Parfitt (1990) has distinguished three types of allophane with different structural features: (a) Al-rich type, also referred to as 'proto-imogolite' or 'imogolite-like' allophane, with an Al/Si ratio of ~2, (b) Si-rich type, sometimes referred to as 'halloysite-like' allophane, with an Al/Si ratio of ~1, and (c) stream-deposit allophane with Al/Si ratios ranging from 0.9 to 1.8. As the name suggests, type (c) allophane does not occur in soil. The specific surface area of allophane, determined by adsorption of polar liquids (ethylene glycol, ethylene glycol monoethyl ether), ranges from 300 to 600 $m^2\,g^{-1}$, and from 145 to 170 $m^2\,g^{-1}$ when measured by adsorption of nitrogen gas and applying the BET equation (Díaz et al., 1990).

Montarges-Pelletier et al. (2005) have synthesized allophanes with a wide range of Al/Si ratios (0.19–1.96) in order to assess the effect of composition on texture. Transmission electron microscopy (TEM) shows differences in aggregate size and density. Aggregates of allophanes with a relatively low Al/Si ratio are less dense than those with high Al/Si ratios, probably because the former samples have a low isoelectric point and surface charge. The shape of the nitrogen adsorption–desorption isotherms also varies with Al/Si ratio. Samples with an Al/Si ratio <0.5 have high adsorption volumes at P/P_o ~1, suggesting the presence of relatively large mesopores and a wide pore-size distribution. Samples with an Al/Si ratio of 0.5–0.8 show marked hysteresis between the adsorption and desorption branches, indicative of a narrow pore-size distribution. Samples with an Al/Si ratio of 0.8–1.3 show high microporosity, low adsorbed nitrogen volume, and limited mesoporosity. Samples with an Al/Si ratio >1.3 have a low nitrogen adsorption capacity.

Díaz et al. (1990) were able to synthesize allophane-like aluminosilicates by both coprecipitation of sodium silicate and aluminium chloride and hydrolysis of tetraethylortosilicate and terbutoxyde of aluminium. Besides being faster, the coprecipitation method gave materials with similar surface charge characteristics to those shown by natural allophanes. Mora et al. (1994) and Jara et al. (2005) also used the coprecipitation approach to prepare synthetic allophane-like materials which they then coated with iron oxides, using a wet impregnating technique. They proposed that the iron oxide (coat) was attached to the allophane surface through Si–O–Fe and Al–O–Fe bonds.

The ^{57}Fe Mössbauer spectrum at 300 K of iron-oxide-coated synthetic allophane, is shown in Fig. 1. The presence of a broad paramagnetic doublet with a quadrupole splitting (Δ) of 0.86 mm s^{-1}, a line width (γ) of 0.51 mm s^{-1}, and an isomer shift (δ) of 0.36 mm s^{-1} is typical of high-spin ferric iron in octahedral coordination (to O and OH ligands), corresponding to a ferrihydrite-like material (Childs and Johnston, 1980; Mora et al., 1994; Jara et al., 2005). Fig. 2 shows

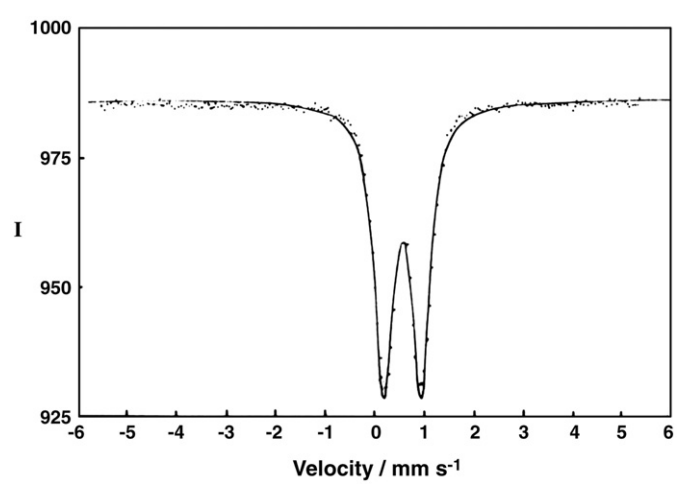

Fig. 1. ^{57}Fe Mössbauer spectrum (at 300 K) of synthetic allophane coated with iron oxide (adapted from Mora et al., 1994).

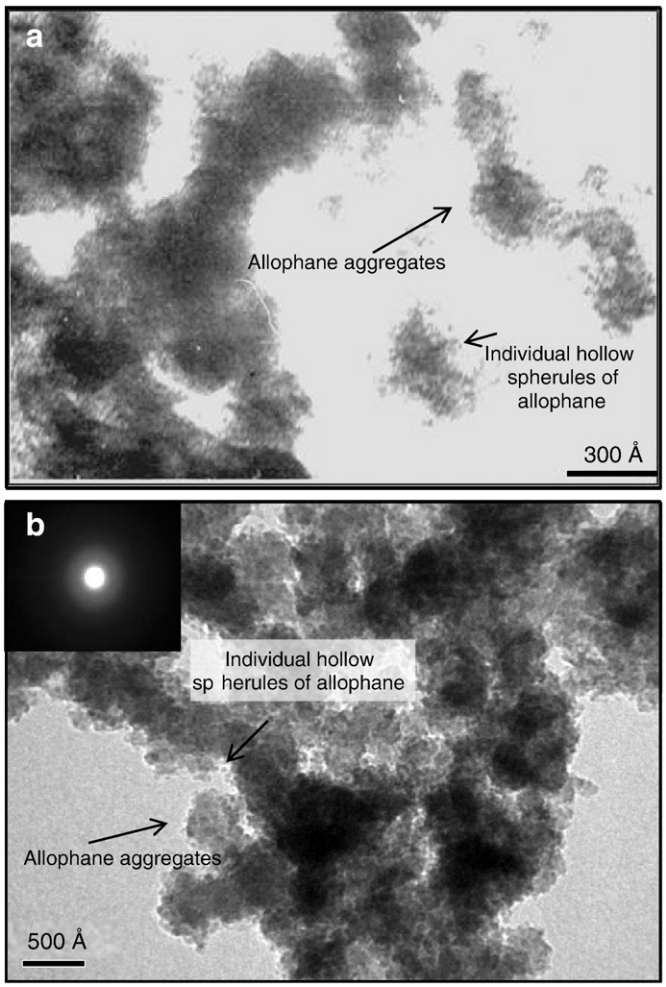

Fig. 2. Transmission electron micrographs of synthetic allophane. Top (a): adapted from Mora et al. (1994); bottom (b): unpublished data.

transmission electron micrographs of the same iron-oxide-coated synthetic allophane. Individual hollow allophane spherules with an outer diameter of about 5 nm can be seen to form 30–50 nm aggregates that, in turn, coalesce into globular clusters, similar to what Hall et al. (1985) have found with naturally occurring (soil) allophanes. The point of zero charge (PZC) of the samples was determined using the method described by Parks (1967), while the isoelectric point (IEP) was assessed by electrophoretic mobility measurements. The measured values of ~4.2 for the PZC and ~8.5 for the IEP, were consistent with the presence of an iron-oxide coating over allophane-like particles, causing an overall increase in surface acidity.

The nanosize clay fraction separated from an Andisol (Piedras Negras series) in southern Chile, has an Al/Si ratio of 0.24 and a BET nitrogen surface area of 124 $m^2\ g^{-1}$ (unpublished results). The shape of the nitrogen adsorption–desorption curves of this natural nanoclay was very similar to that reported by Montarges-Pelletier et al. (2005) for a synthetic allophane-like material with an Al/Si ratio <0.5, indicating a high volume of mesopores, and a wide distribution of pore sizes. The nanoclay has a PZC of 3.8 and an IEP of 7.0. These values are similar to those shown by an iron-oxide-coated allophane-like material reported by Mora et al. (Mora, 1992; Mora et al., 1994; Jara et al., 2005).

The potential use of allophane nanoparticles and allophanic soils for pollution control has been described by several investigators (Diez et al., 1999, 2005; Vidal et al., 2001; Navia et al., 2003, 2005; Yuan and Wu, 2007). Allophane is also potentially useful as a catalyst carrier, deodorizer, humidity-controlling agent, membrane for separating CO_2, and support for enzyme immobilization (Suzuki et al., 2000; Ohashi et al., 2002; Abidin et al., 2007a,b; Calabi Floody et al., 2009). Little information, however, is available about the ability of iron-oxide-coated allophane nanoparticles to catalyze the decomposition of organic compounds through Fenton-like reactions.

Ureta-Zañartu et al. (2002) studied the electro-oxidation of chlorophenols using electrodes of glassy carbon (GC) covered with synthetic iron-oxide-coated aluminosilicates (AlSiFe-GC) with three different Si/Al ratios and isoelectric points of 3.2, 7.2 and 8.2. The catalytic activity of all three AlSiFe-GC electrodes was similar, indicating that the basicity of AlSiFe did not affect the electro-oxidation process. Subsequently, Pizarro et al. (2005) evaluated the catalytic potential of iron oxides, separated from volcanic soils, using the gas-shift reaction of iron in water. More recently, Cea (2006) investigated the decomposition of pentachlorophenol (PCP), 2,4,6-trichlorophenol (2,4,6-TCF) and 2,4-dichlorophenol (2,4-DCF) catalyzed by the clay fraction of an Andisol under ultraviolet radiation. The reaction followed first-order kinetics, the rate of photolysis being dependent on the degree of chlorine substitution, and decreasing in the order: PCP>2,4,6-TCF>2,4-DCF.

The stability of iron-oxide-coated allophane as a heterogeneous catalyst in Fenton-like reactions has not been previously investigated. Our research group has looked into the dissolution of synthetic allophane and its iron-oxide-coated counterpart between pH 4 and pH 7. The preliminary data (unpublished) for synthetic allophane showed that 8.6 mg Al and 16 mg Si per gram allophane were dissolved at pH 4.5. The corresponding values for iron-oxide-coated allophane were 1.2 mg Al/g and 3.3 mg Si/g. Dissolution decreased dramatically (<1 mg/g) at near neutral pH, and became negligible at pH>7. Similarly, the stability of iron-rich minerals (as heterogeneous catalysts) is strongly dependent on solution pH. As already mentioned, the solubility of such minerals increases at low pH. On other hand, the iron species incorporated into pillared interlayered clays (PILCs) is relatively resistant to (acid) leaching, and appears to be more stable than its counterpart in zeolites or oxide minerals. This observation may be ascribed to strong binding (coordination) of the iron species to the interlayer surface of the clay mineral (De León et al., 2008). By the same token, octahedrally coordinated iron within the layer structure of clay minerals is more stable against leaching than exchangeable iron in the interlayer space (Cheng et al., 2008).

4. Conclusions

Clays and iron-oxide minerals possess structural and surface charge characteristics that are conducive to their use as supports of catalytically active (Fe, Cu) phases, or as solid heterogeneous catalysts for the Fenton-like reaction. These minerals can operate over a wide range of pH and temperature, are easy to separate, and retain activity during successive treatments. The catalytic efficiency of solid catalysts in decomposing organic pollutants through the heterogeneous Fenton-like reaction is influenced by the following factors: concentration and type of catalyst, surface area of catalyst, hydrogen peroxide concentration, medium temperature, medium pH, and pollutant structure.

The use of nanocatalysts is a promising alternative to conventional catalysis. Because of their large surface area and low diffusional resistance, nanoparticles are more efficient than conventional heterogeneous catalysts. The ability of nanocatalysts to operate in the absence of ultraviolet radiation is an added advantage. Iron-oxide-coated allophane nanoparticles can catalyze the degradation of persistent organic pollutants through the Fenton-like reaction, and are useful for treating industrial effluents. The Fenton-like reaction may also be used for *in situ* remediation of contaminated soil, sediment, and groundwater because nanosize clays and iron oxides are ubiquitous in the natural environment.

References

Abidin, Z., Matsue, N., Henmi, T., 2007a. Differential formation of allophane and imogolite: experimental and molecular orbital study. J. Comput.-Aided Mater. Des. 14, 15–18.

Abidin, Z., Matsue, N., Henmi, T., 2007b. Nanometer-scale chemical modification of nano-ball allophane. Clays Clay Miner. 55, 443–449.

Andrade, L.S., Ruotolo, L.A.M., Rocha-Filho, R.C., Bocchi, N., Biaggio, S.R., Iniesta, J., García-Garcia, V., Montiel, V., 2007. On the performance of Fe and Fe, F doped Ti–Pt/PbO_2 electrodes in the electrooxidation of the Blue Reactive 19 dye in simulated textile wastewater. Chemosphere 66, 2035–2043.

Andreozzi, R., Caprio, V., Marotta, R., 2002a. Oxidation of 3, 4-dihydroxybenzoic acid by means of hydrogen peroxide in aqueous goethite slurry. Water Res. 36, 2761–2768.

Andreozzi, R., D'Apuzzo, A., Marotta, R., 2002b. Oxidation of aromatic substrates in water/goethite slurry by means of hydrogen peroxide. Water Res. 36, 4691–4698.

Araña, J., Pulido, M.P., Rodríguez, L.V.M., Peña, A.A., Doña, R.J.M., González, D.O., Pérez, P.J., 2007. Photocatalytyc degradation of phenol and phenolic compounds part I. Adsorption and FTIR study. J. Hazard. Mater. 146, 520–528.

Aravindhan, R., Fathima, N.N., Rao, J.R., Nair, B.U., 2006. Wet oxidation of acid brown dye by hydrogen peroxide using heterogeneous catalyst Mn-salen-Y zeolite: a potential catalyst. J. Hazard. Mater. 138, 152–159.

Arnold, S.M., Hickey, W.J., Harris, R.F., 1995. Degradation of atrazine by Fenton's reagent: condition optimization and product quantification. Environ. Sci. Technol. 29, 2083–2089.

Bach, A., Zelmanov, G., Semiat, R., 2008. Cold catalytic recovery of loaded activated carbon using iron oxide-based nanoparticles. Water Res. 42, 163–168.

Baldrian, P., Merhautová, V., Gabriel, J., Nerud, F., Stopka, P., Hrubý, M., Benes, M.J., 2006. Decolorization of synthetic dyes by hydrogen peroxide with heterogeneous catalysis by mixed iron oxides. Appl. Catal. B: Environ. 66, 258–264.

Balmer, M.E., Sulzberger, B., 1999. Atrazine degradation in irradiated iron/oxalate systems: effects of pH and oxalate. Environ. Sci. Technol. 33, 2418–2424.

Barrault, J., Abdellaoui, M., Bouchoule, C., Majesté, A., Tatibouët, J.M., Louloudi, A., Papayannakos, N., Gangas, N.H., 2000a. Catalytic wet peroxide oxidation over mixed (Al–Fe) pillared clays. Appl. Catal. B: Environ. 27, L225–L230.

Barrault, J., Bouchoule, C., Echachoui, K., Frini-Srasra, N., Trabelsi, M., Bergaya, F., 1998. Catalytic wet peroxide oxidation (CWPO) of phenol over mixed (AlCu)-pillared clays. Appl. Catal. B: Environ. 15, 269–274.

Barrault, J., Tatibouët, J.M., Papayannakos, N., 2000b. Catalytic wet peroxide oxidation of phenol over pillared clays containing iron or copper species. C.R. Acad. Sci. Paris, Sér. II C, Chem. 3, 777–783.

Barreiro, J.C., Capelato, M.D., Martin-Neto, L., Hansen, H.C.B., 2007. Oxidative decomposition of atrazine by a Fenton-like reaction in a H_2O_2/ferrihydrite system. Water Res. 41, 55–62.

Barros, A.L., Pizzolato, T.M., Carissimi, E., Schneider, I.A.H., 2006. Decolorizing dye wastewater from the agate industry with Fenton oxidation process. Miner. Eng. 19, 87–90.

Bell, A.T., 2003. The impact of nanoscience on heterogeneous catalysis. Science 299, 1688–1691.

Bergaya, F., Aouad, A., Mandalia, T., 2006. Pillared clays and clay minerals. In: Bergaya, F., Theng, B.K.G., Lagaly, G. (Eds.), Handbook of Clay Science. Elsevier, Amsterdam, pp. 393–421.

Bobu, M., Yediler, A., Siminiceanu, I., Schulte-Hostede, S., 2008. Degradation studies of ciprofloxacin on a pillared iron catalyst. Appl. Catal. B: Environ. 83, 15–23.

Bokare, A.D., Chikate, R.C., Rode, V., Paknikar, M., 2008. Iron–nickel bimetallic nanoparticles for reductive degradation of azo dye Orange G in aqueous solution. Appl. Catal. B: Environ. 79, 270–278.

Brigatti, M.F., Galan, F., Theng, B.K.G., 2006. Structures and mineralogy of clay minerals. In: Bergaya, F., Theng, B.K.G., Lagaly, G. (Eds.), Handbook of Clay Science. Elsevier, Amsterdam, pp. 19–86.

Calabi Floody, M., Theng, B.K.G., Reyes, P., Mora, M.L., 2009. Natural nanoclays: applications and future trends — a Chilean perspective. Clay Miner. 44, 161–176.

Carriazo, J., Guélou, E., Barrault, J., Tatibouët, J.M., Molina, R., Moreno, S., 2005a. Synthesis of pillared clays containing Al. Al–Fe or Al–Ce–Fe from a bentonite: characterization and catalytic activity. Catal. Today 107–108, 126–132.

Carriazo, J., Guélou, E., Barrault, J., Tatibouët, J.M., Molina, R., Moreno, S., 2005b. Catalytic wet peroxide oxidation of phenol by pillared clays containing Al–Ce–Fe. Water Res. 39, 3891–3899.

Carriazo, J.G., Guelou, E., Barrault, J., Tatibouët, J.M., Moreno, S., 2003. Catalytic wet peroxide oxidation of phenol over Al–Cu or Al–Fe modified clays. Appl. Clay Sci. 22, 303–308.

Catrinescu, C., Teodosiu, M., Macoveanu, M., Miehe-Brendlé, J., Le Dred, R., 2003. Catalytic wet peroxide oxidation of phenol over Fe-exchanged pillared beidellite. Water Res. 37, 1154–1160.

Caudo, S., Centi, G., Genovese, C., Perathoner, S., 2007. Copper- and iron-pillared clay catalysts for the WHPCO of model and real wastewater streams from olive oil milling production. Appl. Catal. B: Environ. 70, 437–446.

Caudo, S., Centi, G., Genovese, C., Perathoner, S., 2008. Copper-pillared clays (Cu-PILC) for agro-food wastewater purification with H_2O_2. Micropor. Mesopor. Mater. 107, 46–57.

Cea, M., 2006. Mecanismos fisicoquímicos involucrados en la retención de compuestos organoclorados en un suelo alofánico. Doctor en Ciencias de Recursos Naturales, Universidad de La Frontera, Chile.

Centi, G., Perathoner, S., Torre, T., Verduna, M.G., 2000. Catalytic wet oxidation with H_2O_2 of carboxylic acids on homogeneous and heterogeneous Fenton-type catalysts. Catal. Today 55, 61–69.

Chan, K.H., Chu, W., 2005. Model applications and mechanism study on the degradation of atrazine by Fenton's system. J. Hazard. Mater. 118, 227–237.

Chen, A., Ma, X., Sun, H., 2008. Decolorization of KN-R catalyzed by Fe-containing Y and ZSM-5 zeolites. J. Hazard. Mater. 156, 568–575.

Chen, J., Zhu, L., 2006. Catalytic degradation of Orange II by UV-Fenton with hydroxyl-Fe-pillared bentonite in water. Chemosphere 65, 1249–1255.

Chen, J., Zhu, L., 2007. Heterogeneous UV-Fenton catalytic degradation of dyestuff in water with hydroxyl-Fe pillared bentonite. Catal. Today 146, 463–470.

Cheng, M., Ma, W., Li, J., Huang, Y., Zhao, J., Wen, Y., Xu, Y., 2004. Visible-light-assisted degradation of dye pollutants over Fe(III)-loaded resin in the presence of H_2O_2 at neutral pH values. Environ. Sci. Technol. 38, 1569–1575.

Cheng, M., Song, W., Ma, W., Chen, C., Zhao, J., Lin, J., Zhu, H., 2008. Catalytic activity of iron species in layered clays for photodegradation of organic dyes under visible irradiation. Appl. Catal. B: Environ. 77, 355–363.

Childs, C.W., Johnston, J.H., 1980. Mössbauer spectra of proto-ferrihydrite at 77 K and 295 K, and a reappraisal of the possible presence of akaganéite in New Zealand soils. Aust. J. Soil Res. 18, 245–250.

Chirchi, L., Ghorbel, A., 2002. Use of various Fe-modified montmorillonite samples for 4-nitrophenol degradation by H_2O_2. Appl. Clay Sci. 21, 271–276.

Chou, S., Huang, C., 1999. Application of a supported iron oxyhydroxide catalyst in oxidation of benzoic acid by hydrogen peroxide. Chemosphere 38, 2719–2731.

De León, M.A., Castiglioni, J., Bussi, J., Sergio, M., 2008. Catalytic activity of an iron-pillared montmorillonitic clay mineral in heterogeneous photo-Fenton process. Catal. Today 133–135, 600–605.

Deng, Y., 2007. Physical and oxidative removal of organics during Fenton treatment of mature municipal landfill leachate. J. Hazard. Mater. 146, 334–340.

Deng, Y., Englehardt, J.D., 2006. Treatment of landfill leachate by the Fenton process. Water Res. 40, 3683–3694.

Dhakshinamoorthy, A., Pitchumani, K., 2008. Clay entrapped nickel nanoparticles as efficient and recyclable catalysts for hydrogenation of olefins. Tetrahedron Lett. 49, 1818–1823.

Díaz, P., Galindo, G., Escudey, M., 1990. Sintesis de aluminosilicatos semejantes a los existentes en suelos volcanicos. Bol. Soc. Chil. Quim. 35, 385–389.

Diez, M.C., Mora, M.L., Videla, S., 1999. Adsorption of phenolic compounds and color from bleached kraft mill effluent using allophanic compounds. Water Res. 33, 125–130.

Diez, M.C., Quiroz, A., Ureta-Zañartu, S., Vidal, G., Mora, M.L., Gallardo, F., Navia, R., 2005. Soil retention capacity of phenols from biologically pre-treated kraft mill wastewater. Water Air Soil Pollut. 163, 325–339.

Doocey, D.J., Sharratt, P.N., Cundy, C.S., Plaisted, R.J., 2004. Zeolite-mediated advanced oxidation of model chlorinated phenolic aqueous waste part 2: solid phase catalysis. Process Saf. Environ. Prot. 82, 359–364.

Du, Z., Feng, C., Li, Q., Zhao, Y., Tai, X., 2008. Photodegradation of NPE-10 surfactant by Au-doped nano-TiO_2. Colloids Surf. A Physicochem. Eng. Asp. 315, 254–258.

El-Hamshary, H., El-Sigeny, S., Abou Taleb, M.F., El-Kelesh, N.A., 2007. Removal of phenolic compounds using (2-hydroxyethyl methacrylate/acrylamidopyridine) hydrogel prepared by gamma radiation. Sep. Purif. Technol. 57, 329–337.

Farjerwerg, K., Castan, T., Foussard, J.-N., Perrard, A., Debellefontaine, H., 2000. Dependency on some operating parameters during wet oxidation of phenol by hydrogen peroxide with Fe-ZSM-5 zeolite. Environ. Technol. 21, 337–344.

Farjerwerg, K., Debellefontaine, H., 1996. Wet oxidation of phenol by hydrogen peroxide using heterogeneous catalysis Fe-ZSM-5: a promising catalyst. Appl. Catal. B Environ. 10, L229–L235.

Farjerwerg, K., Foussard, J.-N., Perrard, A., Debellefontaine, H., 1997. Wet oxidation of phenol by hydrogen peroxide: the key role of pH on the catalytic behaviour of Fe-ZSM-5. Water Sci. Technol. 35, 103–110.

Farré, M.J., Doménech, X., Peral, J., 2007. Combined photo-Fenton and biological treatment for Diuron and Linuron removal from water containing humic acid. J. Hazard. Mater. 147, 167–174.

Feng, J., Hu, X., Yue, P.L., Zhu, H.Y., Lu, G.Q., 2003a. Degradation of azo-dye Orange II by a photoassisted Fenton reaction using a novel composite of iron oxide and silicate nanoparticles as a catalyst. Ind. Eng. Chem. Res. 42, 2058–2066.

Feng, J., Hu, X., Yue, P.L., Zhu, H.Y., Lu, G.Q., 2003b. A novel clay-based Fe-nanocomposite and its photo-catalytic activity in photo-assisted degradation of Orange II. Chem. Eng. Sci. 58, 679–685.

Feng, J., Hu, X., Yue, P.L., 2004a. Novel bentonite clay-based Fe-nanocomposite as a heterogeneous catalyst for photo-Fenton discoloration and mineralization of Orange II. Environ. Sci. Technol. 38, 269–275.

Feng, J., Hu, X., Yue, P.L., 2004b. Discoloration and mineralization of Orange II using different heterogeneous catalysts containing Fe: a comparative study. Environ. Sci. Technol. 38, 5773–5778.

Feng, J., Hu, X., Yue, P.L., 2006. Effect of initial solution pH on the degradation of Orange II using clay-based Fe nanocomposites as heterogeneous photo-Fenton catalyst. Water Res. 40, 641–646.

Feng, J., Hu, X., Yue, P.L., Qiao, S., 2009. Photo-Fenton degradation of high concentration Orange II (2 mM) using catalysts containing Fe: a comparative study. Sep. Purif. Technol. 67, 213–217.

Feng, J., Wong, R.S.K., Hu, X., Yue, P.L., 2004c. Discoloration and mineralization of Orange II by using Fe^{3+}-doped TiO_2 and bentonite clay-based Fe nanocatalysts. Catal. Today 98, 441–446.

Fenton, H.J.H., 1894. Oxidation of tartaric acid in the presence of iron. Chem. Soc. J. Lond. 65, 899–910.

Fernandez, J., Bandara, J., Lopez, A., Albers, P., Kiwi, J., 1998. Efficient photo-assisted Fenton catalysis mediated by Fe ions on Nafion membranes active in the abatement of non-biodegradable azo-dye. Chem. Commun. 1493–1494.

Fernandez, J., Bandara, J., Lopez, A., Buffet, Ph., Kiwi, J., 1999. Photoassisted Fenton degradation of nonbiodegradable azo dye (Orange II) in Fe-free solution mediated by cation transfer membranes. Langmuir 15, 185–192.

Ferrarese, E., Andreottola, G., Oprea, I.A., 2008. Remediation of PAH-contaminated sediments by chemical oxidation. J. Hazard. Mater. 152, 128–139.

Flores, Y., Flores, R., Gallegos, A.A., 2008. Heterogeneous catalysis in the Fenton-type system reactive black 5/H_2O_2. J. Mol. Catal. A. 281, 184–191.

Galindo, G., 1974. Electric charges, sorption of phosphate and cation exchange equilibria in Chilean Dystrandepts. Ph.D Thesis, University of California Riverside.

Gallard, H., De Laat, J., 2000. Kinetic modelling of Fe(III)/H_2O_2 oxidation reactions in dilute aqueous solution using atrazine as a model organic compound. Water Res. 34, 3107–3116.

Georgi, A., Kopinke, F.-D., 2005. Interaction of adsorption and catalytic reactions in water decontamination processes part I. Oxidation of organic contaminants with hydrogen peroxide catalyzed by activated carbon. Appl. Catal. B Environ. 58, 9–18.

Giordano, G., Perathoner, S., Centi, G., De Rosa, S., Granato, T., Katovic, A., Siciliano, A., Tagarelli, A., Tripicchio, F., 2007. Wet hydrogen peroxide catalytic oxidation of olive oil mill wastewaters using Cu-zeolite and Cu-pillared clay catalysts. Catal. Today 124, 240–246.

Guélou, E., Barrault, J., Fournier, J., Tatibouët, J.-M., 2003. Active iron species in the catalytic wet peroxide oxidation of phenol over pillared clays containing iron. Appl. Catal. B Environ. 44, 1–8.

Gumy, D., Fernández-Ibáñez, P., Malato, S., Pulgarin, C., Enea, O., Kiwi, J., 2005. Supported Fe/C and Fe/Nafion/C catalysts for the photo-Fenton degradation of Orange II under solar irradiation. Catal. Today 101, 375–382.

Halász, J., Hegedüs, M., Kun, É., Méhn, D., Kiricsi, I., 1999. Destruction of chlorobenzenes by catalytic oxidation over transition metal containing ZSM-5 and Y (FAU) zeolites. Stud. Surf. Sci. Catal. 125, 793–800.

Hall, P.L., Churchman, G.J., Theng, B.K.G., 1985. Size distribution of allophone unit particles in aqueous suspensions. Clays Clay Miner. 33, 345–349.

Hanna, K., Kone, T., Medjahdi, G., 2008. Synthesis of the mixed oxides of iron and quartz and their catalytic activities for the Fenton-like oxidation. Catal. Commun. 9, 955–959.

Henmi, T., Wada, K., 1976. Morphology and composition of allophane. Am. Mineral. 61, 379–390.

Huang, H.-H., Lu, M.-C., Chen, J.-N., 2001. Catalytic decomposition of hydrogen peroxide and 2-chlorophenol with iron oxides. Water Res. 35, 2291–2299.

Huu Phu, N., Kim Hoa, T.T., Van Tan, N., Vinh Thang, H., Le Ha, P., 2001. Characterization and activity of Fe-ZSM-5 catalysts for the total oxidation of phenol in aqueous solutions. Appl. Catal. B Environ. 4, 267–275.

Iurascu, B., Siminiceanu, I., Vione, D., Vicente, M.A., Gil, A., 2009. Phenol degradation in water through a heterogeneous photo-Fenton process catalyzed by Fe-treated laponite. Water Res. 43, 1313–1322.

Jara, A.A., Goldberg, S., Mora, M.L., 2005. Studies of the surface charge of amorphous aluminosilicates using surface complexation models. J. Colloid Interface Sci. 292, 160–170.

Joo, S.H., Zhao, D., 2008. Destruction of lindane and atrazine using stabilized iron nanoparticles under aerobic and anaerobic conditions: effects of catalyst and stabilizer. Chemosphere 70, 418–425.

Kanel, S.R., Neppolian, B., Jung, H., Choi, H., 2004. Comparative removal of polycyclic aromatic hydrocarbons using iron oxide and hydrogen peroxide in soil slurries. Environ. Eng. Sci. 21, 741–751.

Kasiri, M.B., Aleboyeh, H., Aleboyeh, A., 2008. Degradation of Acid Blue 74 using Fe-ZSM5 zeolite as a heterogeneous photo-Fenton catalyst. Appl. Catal. B Environ. 84, 9–15.

Kitis, M., Kaplan, S.S., 2007. Advanced oxidation of natural organic matter using hydrogen peroxide and iron-coated pumice particles. Chemosphere 68, 1846–1853.

Kloprogge, J.T., 1998. Synthesis of smectites and porous pillared clay catalysts: a review. J. Porous Mater. 5, 5–41.

Kong, S.-H., Watts, R.J., Choi, J.-H., 1998. Treatment of petroleum-contaminated soils using iron mineral catalyzed hydrogen peroxide. Chemosphere 37, 1473–1482.

Kurt, U., Apaydin, O., Gonullu, M.T., 2007. Reduction of COD in wastewater from an organized tannery industrial region by electro-Fenton process. J. Hazard. Mater. 143, 33–40.

Kušić, H., Koprivanac, N., Selanec, I., 2006. Fe-exchanged zeolite as the effective heterogeneous Fenton-type catalyst for the organic pollutant minimization: UV irradiation assistance. Chemosphere 65, 65–73.

Kuznestsova, E.V.P., Vanina, M.P., Preis, S., 2008. The activation of heterogeneous Fenton-type catalyst Fe-MFI. Catal. Commun. 9, 381–385.

Kwan, W.P., Voelker, B.M., 2002. Decomposition of hydrogen peroxide and organic compounds in the presence of dissolved iron and ferrihydrite. Environ. Sci. Technol. 36, 1467–1476.

Kwan, W.P., Voelker, B.M., 2003. Rates of hydroxyl radical generation and organic compound oxidation in mineral-catalyzed Fenton-like systems. Environ. Sci. Technol. 37, 1150–1158.

Kwan, W.P., Voelker, B.M., 2004. Influence of electrostatics on the oxidation rates of organic compounds in heterogeneous Fenton systems. Environ. Sci. Technol. 38, 3425–3431.

Kwon, S.C., Fan, M., Wheelock, T.D., Saha, B., 2007. Nano- and micro-iron oxide catalysts for controlling the emission of carbon monoxide and methane. Sep. Purif. Technol. 58, 40–48.

Larachi, F., Lévesque, S., Sayari, A., 1998. Wet oxidation of acetic acid by H_2O_2 catalyzed by transition metal-exchanged NaY zeolites. J. Chem. Technol. Biotechnol. 73, 127–130.

Lee, B.D., Iso, M., Hosomo, M., 2001. Prediction of Fenton oxidation positions in polycyclic aromatic hydrocarbons by Frontier electron density. Chemosphere 42, 431–435.

Li, Y., Lu, Y., Zhu, X., 2006. Photo-Fenton discoloration of the azo dye X-3B over pillared bentonites containing iron. J. Hazard. Mater. 132, 196–201.

Lee, C., Yoon, J., 2004. Temperature dependence of hydroxyl radical formation in the $h\nu$/Fe^{3+}/H_2O_2 and Fe^{3+}/H_2O_2 systems. Chemosphere 56, 923–924.

Li, Y.C., Bachas, L.G., Bhattacharyya, D., 2007. Selected chloro-organic detoxifications by polychelate (poly(acrylic acid)) and citrate-based Fenton reaction at neutral pH environment. Ind. Eng. Chem. Res. 46, 7984–7992.

Lin, S.-S., Gurol, M.D., 1998. Catalytic decomposition of hydrogen peroxide on iron oxide: kinetics, mechanism, and implications. Environ. Sci. Technol. 32, 1417–1423.

Lines, M.G., 2008. Nanomaterials for practical functional uses. J. Alloys Compd. 449, 242–245.

Liou, M.-J., Lu, M.-C., 2008. Catalytic degradation of explosives with goethite and hydrogen peroxide. J. Hazard. Mater. 151, 540–546.

Liou, R.-M., Chen, S.-H., Hung, M.-Y., Hsu, C.-S., Lai, J.-Y., 2005. Fe (III) supported on resin as effective catalyst for the heterogeneous oxidation of phenol in aqueous solution. Chemosphere 59, 117–125.

Liu, W.-T., 2006. Nanoparticles and their biological and environmental applications. J. Biosci. Bioeng. 102, 1–7.

Lu, F., Liu, J., Xu, J., 2008. Synthesis of chain-like Ru nanoparticle arrays and its catalytic activity for hydrogenation of phenol in aqueous media. Mater. Chem. Phys. 108, 369–374.

Lu, M.-C., Chen, J.-N., Huang, H.-H., 2002. Role of goethite dissolution in the oxidation of 2-chlorophenol with hydrogen peroxide. Chemosphere 46, 131–136.

Mahmoodi, N.M., Arami, M., Limaee, N.Y., Gharanjig, K., Nourmohammadian, F., 2007. Nanophotocatalysis using immobilized titanium dioxide nanoparticle: degradation and mineralization of water containing organic pollutant: case study of Butachlor. Mater. Res. Bull. 42, 797–806.

Makhotkina, O.A., Kuznetsova, E.V., Preis, S.V., 2006. Catalytic detoxification of 1, 1-dimethylhydrazine aqueous solutions in heterogeneous Fenton system. Appl. Catal. B: Environ. 68, 85–91.

Malato, S., Blanco, J., Maldonado, M.I., Oller, I., Gernjak, W., Pérez-Estrada, L., 2007. Coupling solar photo-Fenton and biotreatment at industrial scale: main results of a demonstration plant. J. Hazard. Mater. 146, 440–446.

Mamalis, A.G., 2007. Recent advances in nanotechnology. J. Mater. Process. Technol. 181, 52–58.

Martínez, F., Calleja, G., Melero, J.A., Molina, R., 2007. Iron species incorporated over different silica supports for the heterogeneous photo-Fenton oxidation of phenol. Appl. Catal. B Environ. 70, 452–460.

Matta, R., Hanna, K., Chiron, S., 2007. Fenton-like oxidation of 2, 4, 6-trinitrotoluene using different iron minerals. Sci. Total Environ. 385, 242–251.

Mecozzi, R., Di Palma, L., De Filippis, P., 2008. Effect of modified Fenton treatment on the thermal behavior of contaminated harbor sediments. Chemosphere 71, 843–852.

Mishra, T., Parida, K.M., Rao, S.B., 1996. Transition metal oxide pillared clay: 1. A comparative study of textural and acidic properties of Fe(III) pillared montmorillonite and pillared acid activated montmorillonite. J. Colloid Interface Sci. 183, 176–183.

Mishra, T., Mohapatra, P., Parida, K.M., 2008. Synthesis, characterisation and catalytic evaluation of iron-manganese mixed oxide pillared clay for VOC decomposition reaction. Appl. Catal. B Environ. 79, 279–285.

Miyazaki, K., Islam, N., 2007. Nanotechnology systems of innovation — an analysis of industry and academia research activities. Technovation 27, 661–675.

Montarges-Pelletier, E., Bogenez, S., Pelletier, M., Razafitianamaharavo, A., Ghanbaja, J., Lartiges, B., Michot, L., 2005. Synthetic allophane-like particles: textural properties. Colloids Surf., A Physicochem. Eng. Asp. 255, 1–10.

Mora, M.L., Escudey, M., Galindo, G., 1994. Sintesis y caracterización de suelos alofanicos. Bol. Soc. Chil.Quim. 39, 237–243.

Mora, M.L., 1992. Sintesis, caracterización y reactividad de un suelo alofanico modelo. Universidad de Santiago de Chile, Departamento de Química.

Muthuvel, I., Swaminathan, M., 2008. Highly solar active Fe(III) immobilised alumina for the degradation of Acid Violet 7. Sol. Energy Mater. Sol. Cells 92, 857–863.

Navia, R., Fuentes, B., Lorber, K.E., Mora, M.L., Diez, M.C., 2005. In-series columns adsorption performance of Kraft mill wastewater pollutants onto volcanic soil. Chemosphere 60, 870–878.

Navia, R., Levet, L., Mora, M.L., Vidal, G., Diez, M.C., 2003. Allophanic soil adsorption system as a bleached kraft mill aerobic effluent post-treatment. Water Air Soil Pollut. 148, 323–333.

Neamtu, M., Catrinescu, C., Kettrup, A., 2004a. Effect of dealumination of iron(III)-exchanged Y zeolites on oxidation of Reactive Yellow 84 azo dye in the presence of hydrogen peroxide. Appl. Catal. B Environ. 51, 149–157.

Neamtu, M., Zaharia, C., Catrinescu, C., Yediler, A., Macoveanu, M., Kettrup, A., 2004b. Fe-exchanged Y zeolite as catalyst for wet peroxide oxidation of reactive azo dye Procion Marine H-EXL. Appl. Catal. B Environ. 48, 287–294.

Nogueira, R.F.P., Trovó, A.G., da Silva, M.R.A., Villa, R.D., de Oliveira, M.C., 2007. Fundamentos e aplicações ambientais dos processos Fenton e foto-Fenton. Quim. Nova. 30, 400–408.

Noorjahan, M., Kumari, V.D., Subrahmanyam, M., Panda, L., 2005. Immobilized Fe(III)-HY: an efficient and stable photo-Fenton catalyst. Appl. Catal. B Environ. 57, 291–298.

Núñez, L., García-Hortal, J.A., Torrades, F., 2007. Study of kinetic parameters related to the decolourization and mineralization of reactive dyes from textile dyeing using Fenton and photo-Fenton processes. Dyes Pigm. 75, 647–652.

Nurmi, J., Tratnyek, P.G., Sarathy, V., Baer, D.R., Amonette, J.E., Pecher, K., Wang, C., Linehan, J.C., Matson, D.W., Penn, R.L., Driessen, M.D., 2005. Characterization and properties of metallic iron nanoparticle: spectroscopy, electrochemistry, and kinetics. Environ. Sci. Technol. 39, 1221–1230.

Nutt, M.O., Heck, K.N., Alvarez, P., Wong, M.S., 2006. Improved Pd-on-Au bimetallic nanoparticle catalysts for aqueous-phase trichloroethene hydrodechlorination. Appl. Catal. B Environ. 69, 115–125.

Ohashi, F., Wada, S.-I., Suzuki, M., Maeda, M., Tomura, S., 2002. Synthetic allophane from high-concentration solutions: nanoengineering of the porous solid. Clay Miner. 37, 451–456.

Oller, L., Malato, S., Sánchez-Pérez, J.A., Gernjak, W., Maldonado, M.L., Pérez-Estrada, L.A., Pulgarín, C., 2007a. A combined solar photocatalytic-biological field system for the mineralization of an industrial pollutant at pilot scale. Catal. Today 122, 150–159.
Oller, I., Malato, S., Sánchez-Pérez, J.A., Maldonado, M.L., Gassó, R., 2007b. Detoxification of wastewater containing five common pesticides by solar AOPs-biological coupled system. Catal. Today 129, 69–78.
Ortiz de la Plata, G.B., Alfano, O.M., Cassano, A.E., 2008. Optical properties of goethite catalyst for heterogeneous photo-Fenton reactions. Comparison with a titanium dioxide catalyst. Chem. Eng. J. 137, 396–410.
Ovejero, G., Sotelo, J.L., Martínez, F., Gordo, L., 2001a. Novel heterogeneous catalysts in the wet peroxide oxidation of phenol. Water Sci. Technol. 44, 153–160.
Ovejero, G., Sotelo, J.L., Martínez, F., Melero, J.A., Gordo, L., 2001b. Wet peroxide oxidation of phenolic solutions over different iron-containing zeolitic materials. Ind. Eng. Chem. Res. 40, 3921–3928.
Pan, J., Wang, C., Guo, S., Li, J., Yang, Z., 2008. Cu supported over Al-pillared interlayer clays catalysts for direct hydroxylation of benzene to phenol. Catal. Commun. 9, 176–181.
Parfitt, R.L., 1990. Allophane in New Zealand — a review. Aust. J. Soil Res. 28, 343–360.
Parks, G.A., 1967. Aqueous surface chemistry of oxides and complex oxide minerals. Isoelectric point and zero point of charge. Adv. Chem. Ser. 67, 121–160.
Pérez-Estrada, L.A., Malato, S., Agüera, A., Fernández-Alba, A.R., 2007. Degradation of dipyrone and its main intermediates by solar AOPs identification of intermediate products and toxicity assessment. Catal. Today 129, 207–214.
Perez, J.M., 2007. Iron oxide nanoparticles hidden talent. Nature Nanotech. 2, 535–536.
Pignatello, J.J., 1992. Dark and photoassisted Fe^{3+}-catalyzed degradation of chlorophenoxy herbicides by hydrogen peroxide. Environ. Sci. Technol. 26, 944–951.
Pizarro, C., Escudey, M., Moya, S.A., Fabris, J.D., 2005. Iron oxides from volcanic soils as potential catalysts in the water gas shift reaction. J. AIP Conf. Proceedings 756, 56–59.
Popiel, S., Witkiewicz, Z., Chrzanowski, M., 2008. Sulfur mustard destruction using ozone, UV, hydrogen peroxide and their combination. J. Hazard. Mater. 153, 37–43.
Primo, O., Rivero, M.J., Ortiz, I., 2008a. Photo-Fenton process as an efficient alternative to the treatment of landfill leachates. J. Hazard. Mater. 153, 834–842.
Primo, O., Rueda, A., Rivero, M.J., Ortiz, I., 2008b. An integrated process, Fenton reaction ultrafiltration, for the treatment of landfill leachate: pilot plant operation and analysis. Ind. Eng. Chem. Res. 47, 946–952.
Pulgarin, C., Peringer, P., Albers, P., Kiwi, J., 1995. Effect of Fe-ZSM-5 zeolite on the photochemical and biochemical degradation of 4-nitrophenol. J. Mol. Catal. A Chem. 95, 61–74.
Ramírez, J.H., Costa, C.A., Madeira, L.M., Mata, G., Vicente, M.A., Rojas-Cervantes, M.L., López-Peinado, A.J., Martín-Aranda, R.M., 2007a. Fenton-like oxidation of Orange II solutions using heterogeneous catalysts based on saponite clay. Appl. Catal. B Environ. 71, 44–56.
Ramírez, J.H., Maldonado-Hódar, F.J., Pérez-Cadenas, A.F., Moreno-Castilla, C., Costa, C.A., Madeira, L.M., 2007b. Azo-dye Orange II degradation by heterogeneous Fenton-like reaction using carbon-Fe catalysts. Appl. Catal. B Environ. 75, 312–323.
Rincón, A.-G., Pulgarin, C., 2007. Fe^{3+} and TiO_2 solar-light-assisted inactivation of *E. coli* at field scale. Implications in solar disinfection at low temperature of large quantities of water. Catal. Today 122, 128–136.
Rios-Enriquez, M., Shahin, N., Durán-de-Bazúa, C., Lang, J., Oliveros, E., Bossmann, S.H., Braun, A.M., 2004. Optimization of the heterogeneous Fenton-oxidation of the model pollutant 2, 4-xylidine using the optimal experimental design methodology. Sol. Energy 77, 491–501.
Saltmiras, D.A., Lemley, A.T., 2002. Atrazine degradation by anodic Fenton treatment. Water Res. 36, 5113–5119.
Sanabria, N., Álvarez, A., Molina, R., Moreno, S., 2008. Synthesis of pillared bentonite starting from the Al–Fe polymeric precursor in solid state, and its catalytic evaluation in the phenol oxidation reaction. Catal. Today 133–135, 530–533.
Schwingel de Oliveira, I., Viana, L., Verona, C., Vargas, F.V.L., Nunes, A.C.M., Pires, M., 2007. Alkydic resin wastewaters treatment by Fenton and photo-Fenton processes. J. Hazard. Mater. 146, 564–568.
Shah, S., Dzikovski, B., Shah, V., 2007. Development of a new approach for microbial decontamination of water using modified Fenton's reaction. Environ. Pollut. 148, 674–678.
Siedlecka, E.M., Wieckowska, A., Stepnowski, P., 2007. Influence of inorganic ions on MTBE degradation by Fenton's reagent. J. Hazard. Mater. 147, 497–502.
Sirés, I., Centellas, F., Garrido, J.A., Rodríguez, R.M., Arias, C., Cabot, P.-L., Brillas, E., 2007. Mineralization of clofibric acid by electrochemical advanced oxidation processes using a boron-doped diamond anode and Fe^{2+} and UVA light as catalysts. Appl. Catal. B Environ. 72, 373–381.
Sum, O.S.N., Feng, J., Hu, X., Yue, P.L., 2005. Photo-assisted Fenton mineralization of an azo-dye black 1 using a modified laponite clay-based Fe nanocomposite as a heterogeneous catalyst. Top. Catal. 33, 233–242.
Suzuki, M., Ohashi, F., Inukai, K., Maeda, M., Tomura, S., Mizota, T., 2000. Hydration enthalpies of inorganic porous materials with different structures. Mineral. J. 22, 1–10.
Tekbas, M., Yatmaz, H.C., Bektas, N., 2008. Heterogeneous photo-Fenton oxidation of reactive azo dye solutions using iron exchanged zeolite as a catalyst. Micropor. Mesopor. Mater. 115, 594–602.
Theng, B.K.G., Yuan, G., 2008. Nanopaticles in the soil environment. Elements 4, 395–399.
Ting, W.-P., Huang, Y.-H., Lu, M.-C., 2007. Catalytic treatment of petrochemical wastewater by electroassisted Fenton technologies. React. Kinet. Catal. Lett. 92, 41–48.
Ureta-Zañartu, M.S., Mora, M.L., Diez, M.C., Berríos, C., Ojeda, J., Gutiérrez, C., 2002. Chlorophenol electrooxidation on iron oxide-covered aluminosilicates deposited on glassy carbon. J. Appl. Electrochem. 32, 1211–1218.
Valdés-Solís, T.P., Valle-Vigón, P., Sevilla, M., Fuertes, A.B., 2007a. Encapsulation of nanosized catalysts in the hollow core of a mesoporous carbon capsule. J. Catal. 251, 239–243.
Valdés-Solís, T.P., Valle-Vigón, P., Álvarez, S., Marbán, G., Fuertes, A.B., 2007b. Manganese ferrite nanoparticles synthesized through a nanocasting route as a highly active Fenton catalyst. Catal. Commun. 8, 2037–2042.
Valkaj, K.M., Katović, A., Zrnčević, S., 2007. Investigation of the catalytic wet peroxide oxidation of phenol over different types of Cu/ZSM-5 catalyst. J. Hazard. Mater. 144, 663–667.
Ventura, A., Jacquet, G., Bermond, A., Camel, V., 2002. Electrochemical generation of the Fenton's reagent: application to atrazine degradation. Water Res. 36, 3517–3522.
Vidal, G., Navia, R., Levet, L., Mora, M.L., Diez, M.C., 2001. Kraft mill anaerobic color enhancement by a fixed-bed adsorption system. Biotechnol. Lett. 23, 861–865.
Wada, S.-I., Wada, K., 1977. Density and structure of allophane. Clay Miner. 12, 289–298.
Watts, R.J., Dilly, S.E., 1996. Evaluation of iron catalysts for the Fenton-like remediation of diesel-contaminated soils. J. Hazard. Mater. 51, 209–224.
Watts, R.J., Kong, S., Dippre, M., Barnes, W.T., 1994. Oxidation of sorbed hexachlorobenzene in soils using catalyzed hydrogen peroxide. J. Hazard. Mater. 39, 33–47.
Watts, R.J., Stanton, P.C., Howsawkeng, J., Teel, A.L., 2002. Mineralization of a sorbed polycyclic aromatic hydrocarbon in two soils using catalyzed hydrogen peroxide. Water Res. 36, 4283–4292.
Wu, J.J., Muruganandham, M., Yang, J.S., Lin, S.S., 2006. Oxidation of DMSO on goethite catalyst in the presence of H_2O_2 at neutral pH. Catal. Commun. 7, 901–906.
Yang, L.B., Shen, Y.H., Xie, A.J., Liang, J.J., Zhang, B.C., 2008. Synthesis of Se nanoparticles by using TSA ion and its photocatalytic application for decolorization of cango red under UV irradiation. Mater. Res. Bull. 43, 572–585.
Yeh, C.K.-J., Hsu, C.-Y., Chiu, C.-H., Huang, K.-L., 2008. Reaction efficiencies and rate constants for the goethite-catalyzed Fenton-like reaction of NAPL-form aromatic hydrocarbons and chloroethylenes. J. Hazard. Mater. 151, 562–569.
Yuan, G., Wu, L., 2007. Allophane nanoclay for the removal of phosphorus in water and wastewater. Sci. Technol. Adv. Mater. 8, 60–62.
Zelmanov, G., Semiat, R., 2008. Iron(3) oxide-based nanoparticles as catalysts in advanced organic aqueous oxidation. Water Res. 42, 492–498.
Zeep, R.G., Faust, B.C., Hoigne, J., 1992. Hydroxyl radical formation in aqueous reactions (pH 3–8) of iron(II) with hydrogen peroxide: the photo-Fenton reaction. Environ. Sci. Technol. 26, 313–319.
Zrnčević, S., Gomzi, Z., 2005. CWPO: an environmental solution for pollutant removal from wastewater. Ind. Eng. Chem. Res. 44, 6110–6114.